Effects of low frequency electromagnetic fields on biological systems : experimental results and theoretical models

by Timothy Allen Mohr

A thesis submitted in partial fulfillment of the requirements for the degree of Doctor of Philosophy
Electrical Engineering
Montana State University

Abstract:
This thesis attempts to broaden the understanding of low frequency electromagnetic field effects on biological systems. Special emphasis is placed on the "cyclotron resonance" theory of interaction, in which DC and AC magnetic fields combine to induce resonant motion of biological ions.

A brief review of the body of experimental evidence for low frequency electromagnetic field effects is presented. Several of these experiments have demonstrated the ability of cyclotron resonance tuned magnetic fields to enhance bone growth. A practical application of this result was implemented in the form of a microprocessor-based device to control magnetic fields at a human bone fracture site. A description of the design and operation of the device is included.

Experiments involving cyclotron resonant magnetic fields were performed on two new biological systems: yeast and plants: Applied fields produced no net effect on yeast metabolism as measured by CO2 evolution. Growth rates of bean plants were enhanced by Ca2+ tuned cyclotron resonant fields. The effect was more pronounced at temperatures significantly lower than the optimal growth temperature.

A review of current models of electromagnetic field interaction with living organisms is included. The theories are evaluated from several new perspectives. An attempt is made to provide a physical basis for the existence of low frequency resonant ion motion in the face of high frequency thermal collisions. Finally, a new model of interaction incorporating these findings is postulated. The model involves possible synchronous displacement of many ions at binding sites along a membrane surface. It is hypothesized that the cooperative displacement may alter the electrostatic environment of the membrane sufficiently to create changes in the gating characteristics of membrane ion channels.

EFFECTS OF LOW FREQUENCY ELECTROMAGNETIC FIELDS ON BIOLOGICAL SYSTEMS: EXPERIMENTAL RESULTS AND THEORETICAL MODELS

by

Timothy Allen Mohr

A thesis submitted in partial fulfillment
of the requirements for the degree

of

Doctor of Philosophy

in

Electrical Engineering

MONTANA STATE UNIVERSITY
Bozeman, Montana

May 1991

APPROVAL

of a thesis submitted by

Timothy Allen Mohr

This thesis has been read by each member of the thesis committee and has been found to be satisfactory regarding content, English usage, format, citations, bibliographic style, and consistency, and is ready for submission to the College of Graduate Studies.

May 9, 1991
Date

Bruce R. McLeod
Chairperson, Graduate Committee

Approved for the Major Department

May 9, 1991
Date

Head, Major Department

Approved for the College of Graduate Studies

May 9, 1991
Date

Harvey J. Parsons
Graduate Dean

STATEMENT OF PERMISSION TO USE

In presenting this thesis in partial fulfillment of the requirements for a doctoral degree at Montana State University, I agree that the Library shall make it available to borrowers under rules of the Library. I further agree that copying of this thesis is allowable only for scholarly purposes, consistent with "fair use" as prescribed in the U.S. Copyright Law. Requests for extensive copying or reproduction of this thesis should be referred to University Microfilms International, 300 North Zeeb Road, Ann Arbor, Michigan 48106, to whom I have granted "the exclusive right to reproduce and distribute copies of the dissertation in and from microfilm and the right to reproduce and distribute by abstract in any format."

Signature 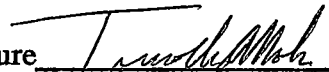

Date 5/9/91

ACKNOWLEDGEMENTS

I wish to thank Dr. Bruce McLeod for his enthusiasm, interest and guidance in the work that led to this thesis. There are numerous times when he has provided just the help I needed to continue. Dr. Stephen D. Smith and his wife Mary Jane have also encouraged me in many ways. Their generosity toward both me and my family did not go unappreciated. I would also like to thank Dr. Roy Johnson for his help and encouragement, especially during my period of readjustment to graduate school after a long break from academics.

Several people from VLC Inc. in Bozeman, Montana provided valuable input in the design of the bone healing device described in this thesis. Lee Cannon, Gabe Kohn and Brian Robertus provided much help in the design and practical implementation of the device. Thanks also go to the people from IatroMed Inc. who provided financial support for the work.

My deepest thanks go to my wife Becky, and children Beth, Michelle and Katharine, who have loved me from long ago, and whose love is growing deeper with time. I also thank my dad and mom, Duane and Katharine Mohr, for their interest, encouragement, generosity and love during this time. From them I learned my first lessons about God, who has packed his universe full of wonders just waiting to be discovered.

TABLE OF CONTENTS

TABLE OF CONTENTS- Continued

TABLE OF CONTENTS- Continued

TABLE OF CONTENTS- Continued

LIST OF TABLES

LIST OF FIGURES

LIST OF FIGURES - Continued

ABSTRACT

This thesis attempts to broaden the understanding of low frequency electromagnetic field effects on biological systems. Special emphasis is placed on the "cyclotron resonance" theory of interaction, in which DC and AC magnetic fields combine to induce resonant motion of biological ions.

A brief review of the body of experimental evidence for low frequency electromagnetic field effects is presented. Several of these experiments have demonstrated the ability of cyclotron resonance tuned magnetic fields to enhance bone growth. A practical application of this result was implemented in the form of a microprocessor-based device to control magnetic fields at a human bone fracture site. A description of the design and operation of the device is included.

Experiments involving cyclotron resonant magnetic fields were performed on two new biological systems: yeast and plants. Applied fields produced no net effect on yeast metabolism as measured by CO_2 evolution. Growth rates of bean plants were enhanced by Ca^{2+} tuned cyclotron resonant fields. The effect was more pronounced at temperatures significantly lower than the optimal growth temperature.

A review of current models of electromagnetic field interaction with living organisms is included. The theories are evaluated from several new perspectives. An attempt is made to provide a physical basis for the existence of low frequency resonant ion motion in the face of high frequency thermal collisions. Finally, a new model of interaction incorporating these findings is postulated. The model involves possible synchronous displacement of many ions at binding sites along a membrane surface. It is hypothesized that the cooperative displacement may alter the electrostatic environment of the membrane sufficiently to create changes in the gating characteristics of membrane ion channels.

CHAPTER 1

INTRODUCTION

Historical Background

Electromagnetic forces are an integral part of the processes of all living organisms. Inside our own bodies, these forces are employed to accomplish countless tasks. These tasks can be as basic as individual cell regulation or as complex as human thought. Perhaps it is not surprising, then, that electromagnetic energy of all kinds has long been known to affect the processes of living organisms.

This thesis is concerned with a particular class of electromagnetic energy, consisting of Extremely-Low-Frequency (ELF), weak electromagnetic fields. For purposes of this thesis, this class includes electromagnetic fields with frequencies less than 300 Hz at energy levels far below those required to break chemical bonds and thus produce electrical ions. Fields to be considered in this thesis are limited to magnitudes of not more than 1000 Volts/meter (V/m) for electric fields and not more than 50 Gauss (g) for magnetic fields. To gain a perspective on these magnitudes, it is of interest to calculate the energies stored in these fields and compare them with bonding energies and mean thermal kinetic energies at physiological temperatures. For example, the energy stored in a static magnetic field can be calculated according to [Zahn,1979]:

$$W = \frac{B^2}{2\mu} \tag{1.1}$$

where W is the stored energy density in joules/m^3, B is the magnetic field magnitude in Tesla, and μ is the magnetic permeability of the material ($4\pi x10^{-7}$ Henry/meter for free space and for most biological materials). For a 1 gauss (10^{-4} Tesla), magnetic field the stored energy density is $4x10^{-3}$ joule/m^3. If such a field were applied to a large biological molecule occupying a cylindrical volume of 50 angstroms length and 10 angstroms radius, the total magnetic energy in the volume would be only $6.3x10^{-29}$ joules or $3.9x10^{-10}$ electron-volts (eV). For comparison, Table 1 shows bonding energies for some common chemical bonds, and the mean kinetic energy of particles due to random thermal motion at 37°C.

Table 1. Energies of various chemical bonds.

Bond Type	Energy (eV)
Covalent	2.2-4.8
Van der Waals	.04-.08
Hydrogen	.13-.30
Ionic	.2
Mean thermal kinetic energy	.027

The miniscule energy content of the electromagnetic fields creates some severe difficulties in attempting to propose mechanisms by which the fields might affect organisms. The most obvious way in which electromagnetic energy can affect organisms is by heating the tissue. However, in the case of fields of this magnitude thermal effects can be ruled out from the outset. A comparison of the energy content of the fields with thermal kinetic energy at physiological temperatures demonstrates this point dramatically. It is well known that thermal kinetic energy in systems of particles manifests itself in random particle motion [Halliday and Resnick,1962]. To affect the system in a coherent way, it is necessary to either overpower this noise (as in the case of chemical bond-forming), or to employ other means to sidestep the noise problem. A first glance at the huge energy disparity between weak electromagnetic fields and thermal forces leaves one at a loss to explain any biological effects from these fields at all. Nevertheless a brief but quickly broadening history of experiments has shown some dramatic effects on widely varying biological systems. This thesis is an attempt to broaden the knowledge of the interaction of ELF fields with living organisms on three fronts. First, the thesis will describe experimental results obtained by applying ELF fields to several new systems. Second, the thesis will contain an analysis of current hypotheses for interaction mechanisms of ELF fields with organisms. Third, new ideas for a possible interaction mechanism will be proposed.

The Cyclotron Resonance Theory

Several theories attempting to explain the observed effects of ELF fields have

been advanced. Reviews and evaluations of the theories are included in Chapter 6. One theory, which has served as a hypothesis spawning several successful experiments, is related to the physical resonance phenomenon that a cyclotron uses to accelerate charged particles. This "cyclotron resonance" theory is central to much of the work described in this thesis. It is therefore natural to describe the basis of the theory at the outset.

Electrically charged particles (ions) experience a force when in the presence of an electromagnetic field. This force, called the Lorentz force, can be formulated mathematically as:

$$\bar{F} = q(\bar{E} + \bar{v}\times\bar{B}) \tag{1.2}$$

where $\bar{F}$ is the vector Lorentz force, q is the charge on the particle (coulombs), $\bar{E}$ is the electric field (Volts/m), $\bar{v}$ is the particle velocity (m/sec), and $\bar{B}$ is the magnetic field (Tesla). Focusing on the case where the electric field is zero, and the magnetic field is constant, it is clear from (1.2) that the force on an ion due to such a DC magnetic field is always directed perpendicularly to the velocity of the ion. A consequence of this feature is that the magnetic field always tends to "bend" the ion motion into a curved path. The nature of this curved path can be determined by examining the differential equations associated with the ion motion. Assuming that the magnetic field is directed along the z axis (in Cartesian coordinates), the three component equations of motion are:

$$\begin{aligned} \dot{v}_x &= \frac{qv_yB}{m} \\ \dot{v}_y &= -\frac{qv_xB}{m} \\ \dot{v}_z &= 0 \end{aligned} \tag{1.3}$$

where v_x, v_y and v_z represent the velocities in the x, y and z directions, and the superscript dots represent derivatives with respect to time. Differentiating the first equation with respect to time and substituting the second equation into the result gives a single differential equation in v_x.

$$\ddot{v}_x + \omega_c^2 v_x = 0 \tag{1.4}$$

where

$$\omega_c = \frac{qB}{m} \tag{1.5}$$

The solutions to (1.4) are given in general by:

$$\begin{aligned} v_x &= A\sin(\omega t) + B\cos(\omega t) \\ v_y &= \frac{\dot{v}_x}{\omega} = A\cos(\omega t) - B\sin(\omega t) \end{aligned} \tag{1.6}$$

Assuming an initial velocity of v_0 in the x direction:

$$\bar{v}(t=0) = v_0\hat{x} \tag{1.7}$$

Equations (1.6) reduce to the following vector velocity in the xy-plane:

$$\bar{v} = v_0[\cos(\omega_c t)\hat{x} - \sin(\omega_c t)\hat{y}] \tag{1.8}$$

and the velocity expression can be integrated to give the instantaneous position vector:

$$\bar{p} = \frac{v_0}{\omega_c}[\sin(\omega_c t)\hat{x} + \cos(\omega_c t)\hat{y}] \tag{1.9}$$

where the constants of integration are neglected. Equation (1.9) is nothing more than the parametric representation of a circle in the xy-plane with radius v_o/ω_c. The circular motion has the associated radian frequency defined previously in (1.5). In terms of frequency in cycles per second, (1.5) can be expressed as:

$$f = \frac{qB}{2\pi m} \tag{1.10}$$

The above analysis reveals that if an ion is exposed to a constant magnetic field and has an initial velocity perpendicular to that field, it will execute a circular motion with radian frequency ω_c and radius v_o/ω_c. The critical facts about this circular motion are that the frequency of orbit is constant and independent of the velocity of the ion or the radius of the motion. The well defined frequency of orbit under these conditions leaves ions open to resonant effects on the ion motion if additional electromagnetic energy is applied at precisely the cyclotron resonance frequency or one of its harmonics [Liboff,1985; Liboff and McLeod,1988]. Durney [Durney et al.,1988] has described such resonant effects in an attempt to provide a physical basis for some of the observed biological effects of low frequency electromagnetic fields. The particle accelerator known as the cyclotron [Zahn,1979] uses electric fields applied at this frequency to accelerate ions to very large velocities.

Several experiments [Smith et al.,1991; Liboff et al,1987; Deibert et al.,1991; Smith et al.,1987] have shown dramatic resonant biological effects caused by applied magnetic fields in which the DC field amplitude and the AC field frequency bear the relationship described by Equation (1.10). Much of the experimental and theoretical

work described in this thesis employs this "cyclotron resonance" hypothesis as a basis. Therefore Equation (1.10) will appear many times throughout these pages. The experimental evidence linking cyclotron resonant magnetic fields to biological effects is convincing. The exact method by which these fields affect biological systems is unknown. This thesis contains some new experimental evidence for a magnetic cyclotron resonant biological effect, as well as some new ideas concerning the possible mechanism by which the fields interact with living organisms.

Organization of Remaining Chapters

The remaining pages will be organized into six chapters. Chapter 2 is a survey of the history of experimental results obtained by applying ELF fields to living organisms. The experimental procedures and results will be described. At the end of the chapter, a summary of the major features of the results will be included. These features are important as a basis for evaluating and constructing any model attempting to explain the method of interaction of ELF fields and organisms. Chapter 3 documents the design of a device intended as the first practical application of the experimental findings that have been obtained using cyclotron resonant magnetic fields. Previous experiments [Smith et al.,1991; Deibert et al.,1991] have demonstrated a rather dramatic stimulation of bone growth both in vitro and in vivo, when magnetic fields tuned to cyclotron resonance conditions for Ca^{2+} or Mg^{2+} are applied to the tissue. Consequently, a considerable amount of effort was directed toward developing a portable battery-powered device which would apply the desired ELF fields to a human bone fracture site.

A description of the device and its operation is included in the chapter. Chapter 4 describes the new experiments which formed part of the work on which this thesis is based. The chapter describes the work done with application of cyclotron resonant magnetic fields to liquid yeast cultures and to plants in early growth stages. The resonant fields were applied with a view toward affecting metabolic rates or growth rates in the target systems. The chapter contains a careful description of the experimental equipment and methods, as well as a complete synopsis of the experimental results. Chapter 5 consists of a brief summary of some of the recent discoveries regarding the processes of living cells. A particular emphasis is placed on the role of ionic flux and the mechanisms by which cells regulate that flux. The concepts are valuable as background information for use in the understanding and evaluation of theoretical models attempting to explain the effects of low frequency electromagnetic fields on biological systems. Chapter 6 changes the focus from experimental considerations to theoretical ones. The chapter is a survey of the various theories that have been advanced as models for the mechanism of interaction of ELF fields with organisms. Each theory is analyzed as to its ability to explain the major experimental features obtained to date, and its adherence to the physical realities of the biological systems. Chapter 7 begins by continuing the evaluation of proposed interaction models by presenting a new analysis that calls into question the assumption, inherent to several of the proposed models, that effects on cell systems are sensitive to the direction of the applied magnetic fields. In addition, Chapter 7 presents several ideas which attempt to explain how a form of ionic resonance might be maintained in the face of numerous thermal collisions of an ion with

surrounding particles. Such thermal collisions form one of the major objections to the hypothesis that an extremely low frequency resonant ion motion can be maintained in a biological atmosphere. Following the development of these ideas, an attempt is made to incorporate them into a description of the beginnings of a new model attempting to provide a rational basis for the observed experimental effects of cyclotron resonant magnetic fields. Chapter 8 contains conclusions and a description of possible future work that might shed new light on the methods by which living cells are affected by electromagnetic fields.

CHAPTER 2

REVIEW OF EXPERIMENTAL LITERATURE

Introduction

The purpose of this chapter is to provide a summary of a broad range of experiments that have been performed in order to investigate ELF electromagnetic field effects on biosystems. The experiments chronicled here form a strikingly diverse evidence base for such effects. In this review, the main features of the experiments are summarized. Table 2 in Appendix A further summarizes important characteristics and results of the experiments. In reviewing each experiment, an attempt is made not only to describe the experiment and its results, but to emphasize important conclusions that can be drawn. The conclusions will become important as a means for formulating and evaluating theories regarding the mechanism by which ELF field interactions take place. The experiment reviews are grouped according to the biological system used in each.

Bone Growth

Several experiments have chronicled the effectiveness of ELF fields in enhancing bone growth. A description of some of these experiments follows.

Bassett: Canine Fibular Osteotomies

Bassett et al. [1974] reported that pulsed magnetic fields could enhance bone repair rate in canines that had undergone fibular osteotomies. The experiments were inspired by the finding [Bassett,1971] that 100 V/cm capacitively coupled electric fields increased the repair rate of fibular osteotomies in rabbits. Capacitively coupled electric fields are created when a voltage is applied across two metallic plates placed on either side of the limb undergoing treatment. Under these conditions, the volume between the plates experiences an electric field directed perpendicularly to the plates. Previous attempts to stimulate bone repair involved small electric currents from surgically implanted electrodes [Bassett,1971]. One clear advantage of capacitively coupled fields over the electrode current method was that no surgical implants were required. Human application of capacitively coupled electric fields posed difficulties due to the distance required between capacitor plates to accommodate human limb dimensions. Required spacing dictated that external voltages larger than 100 volts would be required to generate sufficient internal electric fields to be effective in bone growth stimulation. These high voltages were viewed as a possible hazard, and thus a means of inductively coupling fields to the fracture site were also explored. The experiment involved canines that had undergone fibular osteotomies. The leg of each animal was fitted with a rectangular coil pair which was driven with current pulses in two different patterns. The first pattern employed pulses 1 msec in duration at a 1 Hz repetition rate, and an estimated amplitude of 2 mV/cm in the bone. The second pattern employed pulses 150 μsec in duration at a 65 Hz repetition rate, and an estimated amplitude of 20 mV/cm in

the bone. Animals exposed to the first waveform (1 Hz repetition rate) showed no statistically significant increase in bone load bearing capability compared to controls after 28 days of continuous field exposure. The limb contralateral from the exposed limb served as the control for each experimental trial. The second pulse pattern (65 Hz repetition rate), produced a significant ($p < .07$), increase in load bearing capability of the exposed side versus the control side. These results revealed the important point that not all frequency and power level combinations were effective in stimulating a biological result.

Smith: Embryonic Chick Bone

One of the earliest experiments designed to test the cyclotron resonance model of ELF interaction with cells was performed by Smith et al. [1991] and involved chick bone growth in vitro. Eight day old chick femurs were floated in a culture medium in the separate wells of culture plates. They were exposed to a combination of DC and AC magnetic fields which were designed to match the cyclotron resonance conditions for various unhydrated ions. Magnetic fields were generated in the culture dishes by passing an electric current through a pair of wire coils in Helmholtz configuration around the dishes. The Helmholtz coil configuration consists of two parallel, coaxially aligned coils separated by a distance equal to the radius of each coil. The DC magnetic field was maintained at .209 gauss, and the AC field was maintained at .4 gauss peak-to-peak. The frequency of the AC field was varied in different runs to reflect the different resonant frequencies for Ca^{2+}, K^{+}, Mg^{2+}, and Na^{+} ions. Results varied depending on the ion tuning. Fields tuned to the Ca^{2+} resonant conditions stimulated a 15% length and 22%

diameter increase of experimental over control bones after continuous exposure for 7 days. Fields tuned to the K^+ ion induced a 10% decrease in bone length. Fields tuned to Mg^{2+} produced roughly the same results as Ca^{2+} tuned fields. Comparison with results of bone growth studies using pulsed magnetic fields gave rise to the idea that a possible explanation for the pulsed field effects might lie in the cyclotron resonance theory. Pulsed waveforms can be viewed as a sum of sinusoidal Fourier components with a fundamental frequency equal to the pulse repetition rate. Given a local geomagnetic (DC) field in the area of the experiment, it is entirely possible that one of the frequencies comprising this spectrum could match the resonant frequency (given by Equation 1.10), for an ion important in the healing process.

Smith also calls attention to the extremely small magnitude of the fields employed in this experiment. Noting that the energy content of the fields is miniscule compared to the thermal energy of the molecules involved, Smith suggests that a biosystem must be in a state where a very small amount of energy at a very particular frequency can trigger a response out of proportion to the energy content of the signal.

Deibert: Rabbit Fibular Ostectomies

The effect of magnetic fields tuned to ion cyclotron resonance conditions on the healing of rabbit fibular ostectomies has been documented by Deibert et al. [1991]. One centimeter was removed from the fibula of 54 live, adult rabbits. The rabbits were then allowed to roam free in cages with no applied fields (controls), or with magnetic fields adhering to cyclotron resonance conditions for Ca^{2+} or Mg^{2+} ions. The AC magnetic field was held at .3 gauss peak-to-peak. The magnetic fields were generated by

Helmholtz coils situated around each cage so that the rabbit's whole body was exposed to the desired fields. In various test runs, the duty cycle of the applied fields was varied from .5 hours per day to 24 hours per day. The exposure period lasted for 28 days, after which the fibula were examined for size, stiffness, and histological qualities.

Rabbits exposed to Ca^{2+} cyclotron resonance conditions for .5 hours per day showed a 175% increase ($p<.05$), in stiffness of the fibula compared to control animals. Exposure for three hours per day increased the stiffness 169% ($p<.05$). The maximum stiffness gain was for a 24 hour per day exposure which yielded a 299% stiffness increase ($p<.01$). Rabbits exposed to Mg^{2+} cyclotron resonance conditions for .5 hours per day did not show a significant increase in stiffness of fibula. Three hour per day exposure with Mg^{2+} fields did result in a 175% stiffness increase ($p<.01$), and 24 hour per day exposure yielded a 137% increase ($p<.01$).

The resonant fields also had an effect on the callus diameter at the healing site. Calcium tuned fields induced significant ($p<.05$) increases in callus diameter for all three duty cycles. Magnesium tuning yielded significant callus diameter increases for .5 hour per day and 24 hour per day duty cycles ($p<.05$), but the increase for the 3 hour per day duty cycle was not significant.

Fabellar (sesamoid bone) diameter changes were also noted as a result of field application. Calcium resonance tuning yielded significant fabellar diameter increases ($p<.01$), for the 3 hour per day and 24 hour per day regimes, but insignificant results for the .5 hour per day duty cycle. Magnesium tuning yielded a dramatic 54% increase ($p<.001$) in fabellar diameter for the .5 hour per day tuning. The 3 hour per day and 24

hour per day duty cycles also increased the fabellar diameter significantly ($p<.05$).

Animal weights were recorded and compared to determine if the whole body exposure induced any gross changes in animal characteristics measurable as a weight difference. No significant weight differences between experimental and control groups were found.

The authors conclude that in general the calcium tuned fields dramatically increased bone stiffness and had a relatively minor effect on bone growth. The magnesium tuned fields, by contrast, had a greater influence on generalized growth and a lesser effect on increasing bone stiffness.

The authors go on to give ideas concerning the mechanism of interaction of the cyclotron resonant fields with biosystems. The hypothesis, first proposed by Liboff et al. [1985], that the field-ion interaction takes place within a membrane ion channel is espoused. Several membrane channels are known to have a helical shape or to be composed of helical protein subunits [Unwin,1986]. Since the motion of an ion in classical cyclotron resonance theory is helical in shape [Liboff,1985], it is argued that the Lorentz forces may reinforce the helical motion already observed in ion motion through a membrane channel.

Luben: In Vitro Bone Cells

Further investigation into the effect of low frequency pulsed magnetic fields on bone tissue was undertaken by Luben et al. [1982]. The purpose of the experiments was to shed further light on the mechanism by which pulsed magnetic fields stimulated bone growth. Previous experiments had employed pulsed magnetic fields of 20 gauss

magnitude with a square wave shape. Such pulsed fields were calculated to give current densities of approximately 1 $\mu A/cm^2$ with correspondent electric fields of 1 to 10 mV/cm in extracellular fluids. Actual transmembrane current density is up to 3 orders of magnitude below the value in the extracellular fluid, so that the current densities resulting from the pulsed magnetic field waveform are up to 6 orders of magnitude less than the typical membrane depolarization threshold current of 1 mA/cm^2. The authors concluded that a strong amplification mechanism is required to explain the results observed.

The experiments were performed on 3 day old mouse cranial bones in vitro. The cells were exposed to two different pulsed magnetic field regimes produced by 10 cm x 10 cm wire coils spaced 6.3 cm apart. The first regime consisted of square pulses of 325 μsec duration at a 72 Hz repetition rate. The second regime employed bursts of 4 kHz pulses, lasting for 5 msec, and repeated at a 15 Hz rate. Cell cultures were exposed to fields for a 72 hour period. Experimental assays included accumulation of cyclic adenosine monophosphate (cAMP), adenylate cyclase enzyme activity, and collagen synthesis. Cyclic adenosine monophosphate is a messenger molecule that acts as a chemical signal between the cell membrane and cytoplasmic enzymes, and is a second messenger for many hormone effects. Adenylate cyclase is an enzyme located in the cell membrane which catalyzes the conversion of ATP to cAMP. The cAMP accumulation was stimulated by either bovine parathyroid hormone (PTH), or osteoclast activating factor (OAF).

One of the dramatic influences of the pulsed fields in these experiments was a 90% decrease in the cAMP accumulation, which was apparently due to decreased PTH

activation in the cell membranes. A decreased activation by PTH of adenylate cyclase activity in the membranes was also observed, though the total cyclase activity remained unchanged. The authors conclude that the inhibition may be due to effects on cell surface receptors. The pulsed fields also blocked the inhibition of collagen synthesis by PTH. However it did not block collagen synthesis effects of another hormone (1,25 dihydroxyvitamin D3), that has a cytoplasmic receptor rather than a membrane receptor. This evidence also points to the membrane as a probable interaction site.

The authors explain that the PTH hormone is osteolytic. Therefore, blocking of its effects should increase the rate of bone formation, and perhaps account for the bone growth stimulation seen in other experiments. The authors also note that activation of adenylate cyclase by PTH is accompanied by an influx of Ca^{2+} ions. They suggest that the pulsed fields could have an effect on the binding and release of Ca^{2+} to sites on the polyanionic glycoprotein sheet at the membrane surface.

Brain Tissue

Due to the low frequency spontaneous electric fields that occur in brain tissue, some of the early attempts at affecting biological systems with externally applied ELF fields involved brain tissue. Some of the experiments are reviewed in this section.

Bawin: Cat Brain Rhythms

In this experiment [Bawin et al.,1973], an attempt was made to affect the naturally occurring electroencephalogram (EEG) voltage patterns seen in live cat brains

using a weak microwave signal modulated at low frequencies. Electrodes were implanted in the brains of 12 adult female cats to monitor EEG patterns. The cats were put in a copper screened isolation booth and conditioned by negative reinforcement (electric shock) to exhibit certain brain wave patterns within 2.5 seconds after a light flash. The operant response was the appearance of the desired brain wave pattern within the allotted time period after the flash. The conditioned wave patterns involved increased amplitude and sharply defined peak frequencies between 1 and 16 Hz in the brain wave spectrum. Experimental cats were irradiated with an electric field created between two aluminum plates. A 147 MHz carrier frequency was 90% amplitude modulated at selected frequencies less than 16 Hz. It was found that cats irradiated with the modulated microwave energy showed a greatly lengthened extinction time for the conditioned response. A spectral analysis of the wave patterns in the irradiated cats revealed a grouping of the wave frequencies around the applied modulation frequency. The authors noted that the fields appeared to be acting as reinforcers of already existing brain wave patterns. No new brain wave activity was observed. They suggest that the EEG patterns might be due to slow undulations of membrane potentials of groups of brain cells. They suggest further that the applied fields might be too weak to dominate these patterns, but strong enough to reinforce existing patterns.

Kaczmarek: Ionic Flux from Cortex

Partially as a result of the success of very weak electric fields in affecting the cat brain rhythms in Bawin's experiment, Kaczmarek and Adey [1974] applied low

frequency electric fields through implanted agar electrodes to live cat brain cortexes. The measured experimental parameters were efflux of radioactive gamma aminobutyric acid ([3H]GABA) and $^{45}Ca^{2+}$ from the cortical surface. Gamma aminobutyric acid is an inhibitory neurotransmitter in nerve tissue. The implanted electrodes allowed fields of 50 mV/cm to be applied directly to the tissue. The waveform applied involved a pulse train with a frequency of 200 pulses/sec and a pulse duration of 1 msec. Scintillation counts after irradiation periods of 10 to 20 minutes revealed 20 to 30% increases in both [3H]GABA and $^{45}Ca^{2+}$ efflux from the cortical tissue. The authors state their uncertainty concerning the mechanism of interaction of the fields with the tissue. For a typical synaptic terminal dimension of .5μm, the applied electric field would create a potential of only 25 μV across the terminal. Compared to normal transmembrane potentials of 50 mV, this potential seems astonishingly small. The authors suggest that the high sensitivity to the fields might be due to cooperative interactions among the membrane's components.

Bawin: Chick Brain Ca^{2+} Efflux and Modulated RF Fields

Bawin et al. [1975] performed experiments to further characterize the physical processes by which weak modulated microwave fields affected brain tissue. They hypothesized that amplitude modulated microwaves modified cat brain waves by inducing weak electric forces in the brain that modified the excitability of the tissue. Looking for physiological evidence for this idea, the group chose to expose chick brain tissue to the microwave fields in vitro, and monitor efflux of $^{45}Ca^{2+}$ from the tissue with scintillation

counts. A variation in Ca^{2+} efflux would indicate a field effect at a cellular level, most likely during the process of ion transport across the cell membranes. Chick forebrains were removed, cultured and loaded with radioactive $^{45}Ca^{2+}$. Following this they were exposed for a 20 minute period to 147 MHz fields amplitude modulated at 80 to 90%. As in the cat brain wave experiments, the fields were generated by parallel metallic plates. The signal power of the applied signal was kept between 1 and 2 mW/cm^2. A series of modulation frequencies between 0 and 35 Hz were tested. After the 20 minute exposure period, scintillation counts from exposed brain tissue were compared with counts from matched tissue that remained unexposed to the fields. Comparison of the counts revealed certain frequencies that caused enhanced Ca^{2+} efflux. In particular the results revealed an effective frequency bandwidth of several Hz centered around a peak effect of 10-20% at 16 Hz. Addition of cyanide poison (.4 mM NaCN) to the cultured chick brains resulted in no change in the efflux patterns. The authors conclude that the cause of the enhanced efflux is independent of any ongoing metabolic processes. The fields were also tested on chick muscle tissue with no apparent effects. The authors speculate that the interaction site for the applied fields might be the border zone between the cell membranes and the extracellular macromolecular material. They suggest that the binding of the Ca^{2+} to the neuronal membrane may be affected by the modulation of the radio frequency energy, as it induces a corresponding extracellular electric field.

Bawin: Ca^{2+} Efflux and ELF Fields

Success of the earlier modulated RF experiments at altering Ca^{2+} efflux from brain cells raised several questions. One of the most prominent of the questions was

whether the RF energy was necessary to produce the result, or whether the effect could be observed using ELF electric fields alone. Additional experiments [Bawin and Adey,1976], were performed to answer this question. The experimental procedure was identical to the previous modulated RF experiments except for the difference in applied fields. Whereas the earlier experiment utilized amplitude modulated RF signals in a transmission line exposure chamber, these experiments were performed with an electric field generated by applying a low frequency voltage across two parallel metal plates. Voltages of 5 to 100 volts were applied across the plates which were spaced 50 cm apart. Estimated field strength inside the tissue was on the order of 10^{-5} V/m. After labeling with radioactive $^{45}Ca^{2+}$ the chick brain samples were exposed to the experimental fields for 20 minutes. Results showed signal amplitude and frequency windows which were effective in decreasing $^{45}Ca^{2+}$ efflux from the brain tissue. Effective combinations included 10 V/m at 6 and 16 Hz, and 56 V/m at 6 and 16 Hz. In addition to chick brain tests, samples of chick striated muscle tissue (gastrocnemius muscle), and samples of cat brain cortex tissue were subjected to the same experimental procedures. Results showed all field combinations to be ineffective at altering Ca^{2+} efflux in the muscle tissue. Cat cortex tissue exhibited the same characteristics as the chick brain tissue, except that only 56 V/m intensities were effective. Neither 10 V/m nor 100 V/m produced statistically significant results. The authors suggest a similar mechanism in the two different brain tissues, with a slightly higher threshold required for the cat tissue.

One of the surprising results of these experiments was the apparent effectiveness of extremely weak internal fields (10^{-5} V/m). The authors make an attempt to establish

a rational basis for these effects by comparing these field magnitudes to the calculated thermal noise threshold for the tissue. The Boltzmann equation for the thermal noise voltage in a resistive system with a defined frequency bandwidth is given by:

$$V_{RMS} = \sqrt{4kTBR} \tag{2.1}$$

where V_{RMS} is the RMS noise voltage, k is Boltzmann's constant (1.38×10^{-23} joule/molecule-°K), T is temperature in °K and R is the resistance of the pathway. According to the authors, brain tissue exhibits a typical resistivity of 300 ohm-cm and a signal bandwidth of 100 Hz. The RMS noise voltage resulting from these values is on the order of 10^{-6} V/m. It would appear that the narrow signal bandwidth is a crucial requirement for coupling of weak electric fields to the biosystem.

Bawin: Ionic Factors in Chick

Brain Ca^{2+} Efflux

Bawin et al. [1978] extended their Ca^{2+} efflux studies to include varying concentrations of Ca^{2+} in the culture medium, and the effect of lanthanum (La^{3+}) and hydrogen (H^{+}) ions on the results. The experiment was designed to test the theory that the cell-field interaction takes place at the cell surface molecules, affecting binding of Ca^{2+} to the molecules. Lanthanum is known to block Ca^{2+} flux across excitable membranes by competing for surface binding sites. According to the authors, when lanthanum is present it is located close to the membrane in the extracellular space. Lanthanum is not found in cell cytoplasm, and apparently is not able to cross the cell membrane. Experimental parameters were similar to the previous studies. Chick

cerebral hemispheres were cultured and loaded with $^{45}Ca^{2+}$. The culture medium contained various concentrations of extracellular Ca^{2+}. The concentrations ranged from 0 to 4.16 mM. Radio frequency (450 MHz) fields amplitude modulated at 16 Hz to a 90% modulation depth were applied for a 20 minute exposure period. Field strength was .75 mW/cm^2, which created an electric field in air of 53 V/m. The induced tissue gradient was measured by a microdiode array to be 50-100 mV/cm in the brain tissue itself. Varying the extracellular Ca^{2+} concentration as described above did not affect either the control efflux or the field-induced 10 to 20% efflux increase. More experimental runs were performed in which HCO_3^- was omitted from the extracellular culture medium. This resulted in a 10% decrease in Ca^{2+} efflux which remained unaffected by field stimulation. Lowering the pH of the medium to 6.8 by addition of .1 mM H^+ had no sizable effect on the Ca^{2+} release. However when stimulated with fields, the efflux appeared slightly larger than unstimulated efflux, though no significance levels are given.

The authors interpret the experimental evidence as supportive of the theory that extracellular Ca^{2+} binding sites are the target for ELF field effects. They point out that H^+ is a competitor with Ca^{2+} for these binding sites. Displacement of Ca^{2+} from the binding sites by field stimulation followed by attachment of H^+ to these sites could explain the experimental phenomenon observed. The authors summarize their explanation as follows.

> "Thus it is possible that weak extracellular gradients play a role in the regulation of cell excitability by modulation of calcium binding at electroresponsive sites in the membrane."

Blackman: Chick Brain Ca^{2+} Efflux

Blackman et al. [1979] extended the studies concerning Ca^{2+} efflux from brain tissue exposed to low frequency modulated radio frequency energy. As in Bawin's studies, chick brain hemispheres were removed and placed in culture. $^{45}Ca^{2+}$ was again used to trace Ca^{2+} efflux from the tissue via scintillation counts. A rectangular transmission line (Crawford Cell), was employed as a field exposure chamber. The transmission line supported a TEM mode propagating wave, with 147 MHz used as the carrier frequency. Two different experimental series were performed. In the power density series, the modulation frequency was fixed at 16 Hz, and power densities of .5, .75, 1.0, 1.5, and 2.0 mW/cm^2 were applied. In the frequency series, power density was fixed at .75 mW/cm^2, and modulation frequencies employed were 0, 3, 9, 16, and 30 Hz. In all experiments the samples were exposed to the fields for 20 minutes, after which time scintillation counts were performed to estimate Ca^{2+} efflux. Results of the frequency series showed a significant enhancement of Ca^{2+} efflux at 16 Hz modulation ($p<.02$). The largest increase represented a 24% difference of exposed tissues compared with controls. Results of the power density series demonstrated a remarkably narrow power density window required for the biological effect. A significant ($p<.01$), increase in Ca^{2+} efflux was observed at a density of .75 mW/cm^2, but no effect was observed at any other density, including .5 mW/cm^2 and 1.0 mW/cm^2. These studies were important as a confirmation of the work of Bawin et al., and because of the description of a new variable, power density, as being critical in the Ca^{2+} efflux enhancement by modulated RF fields in brain tissue.

Sheppard: Chick Brain Ca^{2+} Efflux

with 450 MHz Carrier

Further confirmation of the Ca^{2+} experiments of Bawin and Blackman was provided by Sheppard et al. [1979]. Once again, Ca^{2+} efflux was measured from chick brain hemispheres after a 20 minute exposure to modulated RF fields. In this experiment, a 450 MHz carrier frequency was used. Amplitude modulation was at 16 Hz. Modulation depth was 90%. The application of fields resulted in approximate 10% increases ($p<.05$), in Ca^{2+} efflux. Two power density windows were observed. Effective power densities were .1 and 1 mW/cm^2. Ineffective power densities were .05, 2, and 5 mW/cm^2.

The authors offer some opinions concerning the nature of the interaction of the fields with the brain cells. They point out that the ELF fields are unlikely to have an effect on ions internal to cells. Due to the large concentration gradient for the Ca^{2+} ion in these cells (10^{-8} M inside the cell and 2.5 mM outside), a large amount of energy would be required to enhance Ca^{2+} efflux by directly moving ions against this gradient. A further fact making an internal effect unlikely is that due to the electrical polarity and conductivity of the cell membrane and cytoplasm, applied electric fields are much weaker inside the cell than outside. Citing the pH dependence, lanthanum, and hydrogen ion effects described by Bawin [Bawin et al.,1978], the authors agree that alteration of Ca^{2+} binding to the polyanionic sheet at the external membrane surface is a likely mechanism for the observed effects. They suggest that cooperative behavior of multiple molecules within a restricted frequency bandwidth is required to overcome noise due to thermal

agitation:

> "Cooperative interactions are essential to an explanation of weak-field effects, for only an organized ensemble of sensitive elements could respond with chemically significant energies to an initial stimulus of far lower energy."

The authors suggest that the applied electric fields create a corresponding polarization field oscillating at the same frequency at the membrane surface. This polarization field couples to bound ions in the region.

Blackman: Effect of Modulation Frequency on Ca^{2+} Efflux

Further extending the Ca^{2+} efflux experiments, Blackman et al. [1980a] attempted to answer two questions regarding the effect seen in chick brain tissue. The first was whether or not the number of samples changed the width of the effective power density window. The second was whether the modulation frequency affected the power density window. Once again, a 147 MHz carrier was modulated to 95% at 9 and 16 Hz frequencies. Chick brain tissue was prepared as before. Twenty minute field exposures were employed. The number of sample test tubes in the chamber was varied from 4 to 10 to test the effect of sample number on the results. Power densities tested were .11, .55, .83, 1.11, 1.38, and 1.66 mW/cm^2. Counts of the radioactive $^{45}Ca^{2+}$ after the exposure period revealed highly significant ($p<.0001$) increased Ca^{2+} efflux at .83 mW/cm^2 for the 4-tube sample. The 10-tube sample exhibited the same effect at .83 mW/cm^2, and in addition showed significant ($p<.05$), enhanced efflux at .55 and 1.11

mW/cm^2. Thus the effect of increasing the sample number appeared to be a broadening of the effective power density window. Tests were also run for the 10-tube samples at a 9 Hz modulation frequency. The results appeared virtually identical to those obtained with 16 Hz modulation. The authors state that the cause of the broadening of the power density window with an increase in sample number is unknown. They suggest that field distortions due to the close spacing of the samples may be a contributing factor.

Blackman: Ca^{2+} Efflux and 50 MHz Carrier

To further determine the effect of carrier frequency on the Ca^{2+} efflux effects seen in chick brain tissue, Blackman et al. [1980b] experimented with a 50 MHz carrier frequency. All experimental parameters were identical to the tests run with a 147 MHz carrier [Blackman et al.,1979], except the carrier frequency. A 16 Hz modulation frequency was used, and .37, .72, 1.44, 1.67, 2.17, 3.64, and 4.32 mW/cm^2 power densities were tested. Significant ($p<.02$), enhanced efflux was found at the 1.44, 1.67, and 3.64 mW/cm^2 power densities. These results were compared to those obtained using carrier frequencies of 147 MHz [Blackman et al.,1979], and 450 MHz [Sheppard et al.,1979]. The 147 MHz carrier had given power density windows at .55 and 1.38 mW/cm^2. The 450 MHz carrier had given power density windows at .1 and 1 mW/cm^2. The authors point out that the results can be interpreted as dependent on the electric field intensity in the sample. The higher carrier frequencies penetrate better into the tissue and thus require a smaller power density to achieve the same internal field strength. They also reiterate that temperature effects seem to be completely ruled out in these

experiments, by calculating that the energy dose delivered during the 20 minute exposure period was enough to cause only a 10^{-4} °C rise in temperature.

Blackman: Ca^{2+} Efflux at

Extremely Low Frequencies

The successful string of experiments employing modulated RF signals in enhancing Ca^{2+} efflux from chick brain tissue prompted further experiments [Blackman et al.,1982], using only low frequency fields without an RF carrier. Electric fields at 1 to 30 Hz frequencies were directly applied via transmission line to the chick brain tissue prepared as in previous experiments. Field magnitudes were 1 to 70 V/m. Both electric and magnetic fields were present. The magnitude of the magnetic field was proportional to the electric field in the transmission line setup. Its magnitude ranged from .033 mgauss to 2.33 mgauss. Results for a 16 Hz applied frequency showed enhanced Ca^{2+} efflux from 5 to 7.5 V/m applied electric field, with a center at 6 V/m. Another effective window appeared at 35 to 50 V/m, centered at 40 V/m. No efflux change occurred at other power densities in the 1 to 70 V/m range. No efflux changes were observed at 40 V/m for 1 or 30 Hz applied frequencies. The results confirm that low frequency fields without RF carriers can affect Ca^{2+} efflux in chick brain tissue, as reported by Bawin and Adey [1976]. Bawin's experiments revealed a decreased efflux when low frequencies were applied which differed from the enhanced efflux seen in these experiments. It is important to note that both field amplitude and frequency windows were observed in this experiment. The amplitude windows were interpreted as further evidence that a heating effect was not the cause of the results seen, since the two effective amplitude windows

were separated by an ineffective range. If heating were the cause of the efflux changes, one would expect the effect to increase in proportion to the temperature increase.

Blackman: Role for Magnetic Field in Ca^{2+} Efflux

Two motivations prompted this further investigation [Blackman et al.,1985] into low frequency field effects on Ca^{2+} efflux from chick brain tissue. The first was to find a reason why the low frequency effects observed by Bawin and Adey [1976] caused decreased Ca^{2+} efflux while their own experiments [Blackman et al.,1982] had shown an increased efflux. The second motivation was to investigate the role of the local geomagnetic field (LGF), on the results. The authors note that one main difference between the low frequency experiments of Bawin and Blackman was that Bawin used an electric field created by a capacitive effect between parallel metallic plates while Blackman's setup involved a transmission line that supported both electric and magnetic fields. To investigate whether the magnetic field contributed to the sign change between the two experiments, the 50 ohm load was removed from the transmission line. Removing the 50 ohm load reduced the magnetic field from 59.5 nT to approximately 15 pT, a decrease of more than three orders of magnitude. All other experimental parameters were identical to the previous tests. With the electric field only, no Ca^{2+} efflux shifts were observed at 6, 10, or 40 V/m external field strength at a frequency of 16 Hz. With both electric and magnetic fields present, significant Ca^{2+} efflux enhancement was observed at 6 and 40 V/m. The authors concluded that the magnetic field component was necessary to produce the Ca^{2+} shifts observed in the previous

experiments.

To investigate the role of the geomagnetic field in the Ca^{2+} efflux results, careful control of the local DC magnetic field was maintained by adjusting the electrical current through a pair of Helmholtz coils positioned symmetrically around the experimental chamber. A gaussmeter was used to monitor the net magnetic field due to the vector sum of the geomagnetic and coil fields along the axis of the transmission line chamber. With no coil current the geomagnetic field component along the chamber axis was .38 gauss. The first series of tests were run with an applied frequency of 15 Hz. At this frequency, with a .38 gauss local DC magnetic field, Ca^{2+} efflux was significantly enhanced as in previous experiments. When the local magnetic field was adjusted to .19 gauss, however, the efflux effect disappeared. Another series of tests were run using a 30 Hz AC frequency. At this frequency, local DC magnetic fields of .38, .505, and .830 gauss were ineffective at enhancing Ca^{2+} efflux, while .255 and .76 gauss were effective. The authors interpret the results as suggesting a pattern relating the effective frequencies to the net DC magnetic field (geomagnetic plus coil fields), described by:

$$F \alpha (2n+1)B \tag{2.2}$$

Liboff [1985] has pointed out that these results can be interpreted as consistent with cyclotron resonance conditions for the K^+ ion.

Blackman: Ca^{2+} Efflux

Frequency Series

Blackman et al., in an effort to shed light on underlying mechanisms of interaction, extended their experiments concerning Ca^{2+} efflux from chick brain tissue to

include frequencies from 15 Hz to 510 Hz in 15 Hz steps [Blackman et al.,1988a]. The experimental procedure was identical to the experiments described above. The local geomagnetic field was .38 gauss. Applied fields measured .6 mgauss RMS for the AC magnetic, and 15 V/m RMS for the electric field.

Results indicated highly significant ($p<.01$) enhanced Ca^{2+} efflux at odd multiples of the 15 Hz fundamental frequency through harmonic number 21 (315 Hz), with the exception of 165 Hz (harmonic 11), which yielded a null result. Slightly less significant ($p<.05$), enhanced efflux was found at harmonics 4, 6, 12, and 27 (60, 90, 180, and 405 Hz).

The authors offer a speculative interpretation of the results as possibly representing three different types of interaction based on magnetic resonance phenomenon and a Lorentz force model such as the cyclotron resonance model advocated by Liboff [1985].

Merritt: Rat Brain Ca^{2+} Efflux

The object of these experiments [Merritt et al.,1982] was to test $^{45}Ca^{2+}$ binding in rat brain tissue exposed to pulsed electromagnetic fields. As in the experiments of Bawin and Blackman, a high frequency carrier (1 GHz or 2.45 GHz), was amplitude modulated by a low frequency (16 Hz) pulsed waveform. The modulation pulses were 20 msec in duration. Power densities tried were 1 mW/cm^2 and 10 mW/cm^2. Tissue exposure to the fields lasted 20 minutes. Rather than allowing the cells to assimilate $^{45}Ca^{2+}$ themselves during a loading period (as did Bawin and Blackman), the Ca^{2+} was loaded directly into the cells via injection.

No significant Ca^{2+} efflux changes were observed in the course of these experiments. The authors do not conclude that previous reports regarding Ca^{2+} efflux effects are unfounded. Rather, they point out that the differences in this experiment, most notably the pulsed waveform as opposed to a sinusoidal one, might cause the difference in results. A Fourier analysis of a pulsed waveform reveals a spectrum of harmonic frequencies at various amplitudes. Thus the pulsed waveforms are qualitatively different from pure sinusoidal ones. Since the biological responses of the system to these harmonics are unknown, pulsed waveforms can make it difficult to ascertain the response of a system to a single frequency. Though an attempt was made to reproduce effective frequency and power density windows from Blackman's experiments, there is no guarantee that the experimental parameters did indeed fall within the required windows for this system.

Lin-Liu: Synaptosome Ca^{2+} Efflux

These experiments [Lin-Liu and Adey,1982] were designed specifically to test the hypothesis that Ca^{2+} efflux effects seen in previous experiments were due to stimulated release of Ca^{2+} from binding sites on the membrane surface. Synaptosome preparations are nerve terminals derived from homogenized brain tissue. As such, they are a good representation of synaptic membranes. They are not, however, collections of whole cells. Therefore this system is a good choice for determining whether the Ca^{2+} efflux is affected at membrane surface sites or whether intracellular metabolic processes are involved.

The exposure chamber was a Crawford cell waveguide device, similar to that

employed by Blackman in his experiments. Applied fields consisted of a 450 MHz carrier amplitude modulated at 75% by a low frequency sinusoidal signal. Modulation frequencies tried were 0, 16, and 60 Hz. Power density of the signal was .5 mW/cm^2. This power density created a measured 43 V/m electric field in the air surrounding the samples. The samples were exposed to the fields for a 10 minute period.

No Ca^{2+} efflux effects were observed for modulation frequencies of 0 and 60 Hz. The 16 Hz modulation frequency increased the rate of Ca^{2+} efflux by 38%. The results demonstrated that whole cells were not necessary to produce the Ca^{2+} efflux alterations observed in several previous experiments. The membrane surface is therefore hypothesized as the site for ELF field-cell interactions. Synaptic membranes have a sheet of negatively charged sites on their surfaces. The authors suggest that negatively charged phosphate groups on the membrane surface might be the major Ca^{2+} binding sites at which applied ELF fields can affect Ca^{2+} flux from the membrane.

Shelton: Pulsed Microwave in Rat Brain Tissue

An attempt to expand the experiments of Bawin to pulsed microwave in rat brain tissue was made by Shelton and Merritt [1981]. Rat brain tissue in vitro was exposed for 20 minutes to microwave energy with a 1 GHz carrier frequency, modulated by 10 msec pulses at a 16 or 32 Hz rate. Power densities tried were .5, 1, 2 and 15 mW/cm^2.

No significant alterations in Ca^{2+} efflux from the rat brain tissue were observed. The authors decline comparison of these results to Bawin's work due to the different carrier frequency and modulation scheme employed. The difference in the spectrum of

frequencies generated is cited as evidence that pulsed fields may not necessarily yield results identical to sinusoidally amplitude modulated fields.

Dixey: Noradrenaline Release in Nerve Cells

Dixey and Rein [1982], attempted to establish a model biological system that would facilitate investigation into the interaction mechanisms of ELF fields with cells. With this goal in mind, a clonal cell line maintained in tissue culture conditions was selected. One advantage of clonal cells is that the system has only one cell type. An advantage of cultured cell samples is that the geometry of the cell sample can be controlled so that field strengths and current densities are known.

PC12 nerve cells cloned from rat cells were grown in culture for the experiments. Two parallel wire coils were used to generate the fields applied to experimental cells. To control the induced electric field and thus eddy current magnitudes in the cell culture medium, the medium was constrained to an annular region symmetrical about the coil axis. Calculated electric fields in the annulus reached a magnitude of .038 V/m, while corresponding eddy currents were expected to reach .025 A/m^2. Voltage pulses were applied to the coils to create the desired fields. Pulse widths were .6 msec, with a 500 Hz overall frequency. The inductance of the coils smoothed the current (and thus magnetic field) waveform somewhat. The cells were exposed to fields for a 2 hour period, after which they were tested for release of radioactive H-noradrenaline.

The fields stimulated H-noradrenaline release from the cells significantly ($p<.001$). The overall increase was 27.5%. Addition of Mg^{2+} to the culture medium

inhibited the effect of the fields on noradrenaline release. Since Mg^{2+} is known to be a Ca^{2+} antagonist in several biological systems, the authors suggest that the field effect is due to Ca^{2+} ion flux alteration. The fields are unlikely to directly impose Ca^{2+} entry into the cell, since electric field magnitudes are 10^{-2} V/m as opposed to known nerve action potentials of 10^{3} V/m. The authors also favor the theory that the interaction of fields with cells takes place at ion binding sites on the cell surface.

Human Lymphocytes

Low frequency electromagnetic fields have been observed to alter various properties of lymphocyte cells in vitro. Some of the experiments performed with lymphocytes are outlined below.

Conti: Human Lymphocyte Mitogenic Stimulation

Certain mitogenic lectins stimulate mitosis in human lymphocyte cells. A first step in mitogenic stimulation is a rapid initial Ca^{2+} influx. Ca^{2+} is required for DNA synthesis in the cell during the 18-72 hour period following stimulation. Thus mitogenic stimulation of lymphocytes was adopted [Conti et al.,1983], as an experimental system to test the hypothesis that low frequency electromagnetic fields have their effect by influencing Ca^{2+} flux across the cell membranes.

The mitogenic lectins employed in this experiment were phytohaemagglutinin (PHA), concanavalin A (ConA), and pokeweed mitogen (PWM). Incorporation of radioactive thymidine into the cells was used as a measure of DNA synthesis which in

turn indicated mitogenic stimulation. A wire coil pair was used to generate magnetic (and induced electric) fields in the cell cultures. Coils were driven with 1, 3, 50, or 200 Hz voltage pulses. Calculated magnetic fields were 23-65 gauss. Calculated electric fields were .1-1 V/m, and calculated eddy current densities were on the order of 10 mA/m^2.

The first experimental runs involved field exposure for the full 72 hour incubation period after introduction of the mitogenic lectin. For these tests, the 1 Hz pulses reduced the PHA mitogenic effect ($p<.01$), while ConA and PWM stimulation was unaffected. The 3 Hz pulse regime produced significant decreases in mitogenic stimulation of all three lectins. 50 Hz pulses resulted in decreased mitogenic stimulation by PHA and ConA, while the PWM stimulation was unaffected. 200 Hz pulses resulted in a decrease in stimulation by PHA only.

To uncover further clues about the mechanism of interaction of the electromagnetic fields with the cells, more test runs were made with field exposure during various parts of the 72 hour incubation period. Since 3 Hz pulses produced the most consistent changes in mitogenic stimulation in the previous test runs, this frequency was chosen exclusively for the remaining tests. Exposure during the first 12 hours of the incubation period resulted in decreased mitogenic stimulation by PHA and ConA, but not by PWM. Exposure during the last 48 hours of the incubation period also resulted in decreased PHA and ConA stimulation, but had no effect on PWM stimulation. Exposure during the last 6 hours of the incubation period did not affect mitogenic stimulation by any of the lectins.

The authors interpret these results by concluding that the electromagnetic fields do not appear to interfere with the binding of the mitogens to the cell membrane, since exposure during the last 48 hours (when all lectin binding is complete), was still effective in altering mitogenic stimulation. They also conclude that the electromagnetic fields have no direct effect on thymidine incorporation since exposure during the last 6 hours had no effect on the results. These facts point to the conclusion that the thymidine incorporation decrease observed as a result of the applied fields is due to a decrease in DNA synthesis in the cells or a reduction in the number of cells reproducing.

Conti: Role for Ca^{2+} in

Lymphocyte Mitogenic Stimulation

Conti et al. [1985] continued their investigation into the mitogenic lectin stimulation of human lymphocytes by measuring Ca^{2+} associated with the cells during the stimulation period. The experimental setup was identical to the previous experiment, except that radioactive $^{45}Ca^{2+}$ was added to the culture medium to allow measurement of cell-associated Ca^{2+} via scintillation counts. Magnetic field pulses of 60 gauss magnitude and 3 Hz frequency were used in these experiments. Exposure was for the full 72 hour incubation period after addition of the mitogenic lectin. Lectins used were phytohemagglutinin (PHA), and phorbol-myristate-acetate (PMA).

Both PHA and PMA stimulated Ca^{2+} uptake by the lymphocyte cells. The application of electromagnetic fields decreased this Ca^{2+} uptake compared to controls ($p<.01$). Verapamil, a calcium channel blocking agent, also decreased both thymidine incorporation and Ca^{2+} uptake by the lymphocytes. The effects of the electromagnetic

fields and Verapamil were additive.

The authors conclude that the electromagnetic fields reduce cell blastogenesis by decreasing Ca^{2+} flux across the cell membranes. The additive effects of Verapamil and electromagnetic fields might indicate different targets for the two agents.

Liboff: Ca^{2+} Incorporation by Human Lymphocytes

These experiments [Liboff et al.,1987] were designed to investigate the effect of magnetic fields tuned to $^{45}Ca^{2+}$ cyclotron resonance conditions on $^{45}Ca^{2+}$ uptake by human lymphocyte cells in vitro.

Three Helmholtz coil pairs were used to create the desired magnetic fields for these experiments. A vertical pair eliminated the vertical component of the geomagnetic field. One horizontal pair was used to adjust the horizontal DC magnetic field component to .209 gauss. Another horizontal pair was used to apply an AC magnetic field collinear to the DC magnetic field. Various AC frequencies surrounding the resonant frequency of 14.27 Hz for $^{45}Ca^{2+}$ and various AC amplitudes were tested. Cell culture solutions were exposed to the fields for a 1 hour period.

At an AC field amplitude of .21 gauss RMS, a series of test runs at different AC frequencies revealed a narrow (1Hz wide) frequency resonance curve centered at 14.27 Hz, the cyclotron resonant frequency for $^{45}Ca^{2+}$ under the DC magnetic field conditions described. The peak scintillation count at 14.27 Hz represented an increased Ca^{2+} uptake three-fold greater than controls. Similar frequency tests for an AC amplitude of 1.5 gauss RMS revealed peak increased Ca^{2+} uptake 1 Hz on either side of the 14.27 Hz

frequency with no net effect at 14.27 Hz itself. Final test runs consisted of a series of different AC amplitudes at the 14.27 Hz resonant frequency. The resulting AC amplitude dependence curve showed no effect at zero AC amplitude, increasing to a maximum effect at .2 gauss RMS, and descending to null effects at .6 and 1.5 gauss RMS.

The authors conclude that the peak response of the lymphocytes exactly at cyclotron resonance conditions is further evidence for a cyclotron resonant mechanism for the field-cell interaction. They note the shift in cyclotron resonant frequency from previous experiments involving Ca^{2+} dependent systems apparently due to the increased mass of the $^{45}Ca^{2+}$ ion compared to a bare Ca^{2+} ion. The amplitude of the AC magnetic field applied has a curious effect on the system response. The effects observed reinforced the experimental evidence for the frequency and amplitude windows observed by other researchers.

Miscellaneous Systems

Dutta: Ca^{2+} Efflux from Human Neuroblastoma Cells

Another series of experiments [Dutta et al.,1984] revealed an effect of low-frequency modulated RF signals on Ca^{2+} efflux from human neuroblastoma cells (IMR-32), in vitro. Cells were grown as a monolayer in vitro, and then exposed to electromagnetic fields traveling in the TEM mode in a Crawford cell waveguide chamber similar to the experiments of Blackman et al. [1979]. The carrier frequency of the radiation was 915 MHz. The carrier was amplitude modulated to 80% by a 16 Hz

sinusoidal signal. After exposure to the fields for 30 minutes, the $^{45}Ca^{2+}$ efflux from the cells was measured via scintillation counting. Signal power levels were measured as Specific Absorption Rate (SAR), defined as the power absorbed by the sample divided by the sample mass. SAR levels of 0, .01, .05, .075, .1, .5, .75, 1.0, 1.5, 2, and 5 mW/g were tried.

Significant increases in the Ca^{2+} ion efflux was observed for SAR's of .05 and 1.0 mW/g only. At .05 mW/g, the effect required the 16 Hz modulation, while at 1.0 mW/g, the effect remained when the amplitude modulation was removed. The authors conclude that human neuroblastoma cells are sensitive to extremely weak microwave radiation, if the radiation is confined to narrow SAR ranges. The major contrast between this work and the work of Bawin and Blackman is that at one power level the signal was found to be effective without low frequency modulation. The modulation was found to be essential by both Bawin and Blackman.

Marron: Mitotic Delay in Slime Mold

One of the early experiments involving low frequency electromagnetic fields and living organisms was performed by Marron et al. [1975]. The slime mold Physarum Polycephalum undergoes synchronous mitosis naturally. An entire culture of 10^9 nuclei will undergo mitosis simultaneously at predictable intervals. This mitotic interval was used as the experimental variable for these experiments. Two rectangular wire coils were used to generate AC magnetic fields of 2 gauss at 60 and 75 Hz frequencies. An electric field of .7 V/m was generated perpendicular to the magnetic field by imposing a voltage across two stainless steel electrodes in contact with the growth medium. The applied

magnetic and electric fields were synchronized in phase to simulate radiative fields.

Both the 60 Hz and 75 Hz frequencies caused a significant delay in the mitotic cycle after approximately 100 days of exposure. After the cultures were removed from the fields, the samples showed continued delay for 30 to 60 days, during which time the mitotic cycle slowly converged back to normal.

Liboff: DNA Synthesis in Human Fibroblasts

These experiments [Liboff et al.,1984] showed an effect of weak low frequency magnetic fields on human embryonic fibroblast cells in vitro. DNA synthesis in the cells was indirectly measured by recording the incorporation of radioactive [^{3}H]Thymidine into the cells. Helmholtz coils of 25 cm radius and 25 cm separation were used to generate fields for two separate experimental runs. The first run involved magnetic fields of .16 gauss RMS, and 76 Hz. The exposure period was 24 to 96 hours. The second run employed fields of .16 to .4 gauss RMS, at 15 Hz to 4 kHz, for an exposure period of 18 to 24 hours.

The first test run resulted in increased thymidine uptake throughout the incubation period. The increase was as large as 80% over controls and was highly significant ($p<.0001$). The second test run also showed across-the-board increases in thymidine uptake for all field and exposure period combinations.

The authors interpreted the second set of experiments as indicating that the magnetic field effect on the cells was not likely to be due to Faraday induction. By Faraday's law, a sinusoidal magnetic field induces an electric field whose amplitude

varies with the product of the frequency and amplitude of the imposed magnetic field. The experiments showed a similar effect due to magnetic fields whose frequency-amplitude product varied over four orders of magnitude. If eddy currents due to Faraday induction were the cause of the observed phenomenon, some dependence of the results on this frequency-amplitude product should be evident. Since no such dependence is observed, the effect is either saturable, or completely independent of the induced electric field.

Goodman: Cellular Transcription

Pulsed electromagnetic fields were found [Goodman et al.,1983], to have an effect on the RNA transcription rates of salivary gland cells from the dipteran "Sciara coprophila". Two different pulsed waveforms comprised the applied fields in these experiments. The first waveform consisted of bursts of 4 pulses of 200 μsec duration repeated at a 15 Hz rate. The second waveform consisted of 380 μsec pulses repeated at a 72 Hz rate. The pulses generated a 1.5 mV/cm electric field. Magnetic field strength was not recorded.

Exposure of the cells for 15 and 45 minute periods resulted in marked RNA transcription increases. Exposure for a 30 minute period did not appear to produce a significant effect on the RNA transcription. This experiment is unique in that it appears to introduce exposure period "windows" as being important in the biological response.

In a later report by the same research group [Goodman and Henderson,1986], the experimental signals were expanded to include a sinusoidal 72 Hz signal. Similar transcriptional increases were obtained, indicating that the fundamental frequency, and

not the exact waveshape of the applied signal was the crucial parameter in inducing the effect.

Smith: Cyclotron Resonance and Diatom Motility

One of the most dramatic reports supporting a cyclotron resonance theory of cell-field interaction was given by Smith et al. [1987]. The experimental variable for these studies was the motility of marine diatoms (Amphora Coffaeformis) when placed on nutritional agar. A previous report [Cooksey and Cooksey,1980] had shown a well characterized response curve linking percentage of motile diatoms with concentration of Ca^{2+} in the agar. Motility was measured as the percentage of diatoms leaving tracks in the agar longer than about 10 μm. Magnetic fields for the experiment were generated by 3 pairs of Helmholtz coils. One pair was used to eliminate the vertical component of the geomagnetic field, one pair was used to set the north-south horizontal field to a desired value, and a third pair (collinear with the second) was used to generate a desired AC magnetic field. The field exposure period was 1 hour.

Before performing experiments to ascertain effects of fields on diatom motility, a calibration curve characterizing motility versus agar Ca^{2+} concentration was performed. A dose response saturating at about 45% motility for a 2.5 mM Ca^{2+} concentration was observed. Then a dose response curve was obtained at the same Ca^{2+} concentration levels but with Ca^{2+} cyclotron resonant magnetic fields applied. The fields consisted of a .209 gauss DC magnetic field, and a .209 gauss peak collinear AC magnetic field with a 16 Hz frequency. The resonant fields produced a shift in the Ca^{2+} dose response curve.

The curve shape was nearly identical to that obtained without fields, but shifted so that features appeared at significantly lower concentration levels. For example, motility saturation occurred at approximately .25 mM Ca^{2+} concentration instead of 2.5 mM for controls.

Next, the response of diatom motility to various harmonics of the fundamental cyclotron resonant frequency was obtained. The DC magnetic field was set to .209 gauss, the AC magnetic field to .209 gauss peak, and AC frequencies of 16, 32, 48, and 64 Hz were tested. The 16 Hz frequency represents the fundamental cyclotron resonant frequency for Ca^{2+} for a .209 gauss DC magnetic field. The other frequencies represent the second, third, and fourth harmonics of this fundamental. The most significant results appeared for low Ca^{2+} concentrations (.25 mM and .5 mM). At these concentrations, the first and third harmonics (16 and 48 Hz), proved to be highly significant in stimulating diatom motility ($p<.001$). Percent of motile diatoms increased by up to 7 fold when exposed to these fields. In contrast, the second and fourth harmonics were ineffective in stimulating motility.

To test the requirement for both DC and AC magnetic fields in the cyclotron resonance model, tests involving elimination of one or the other of the fields were performed at .25 mM Ca^{2+} concentration. Neither the DC or AC fields alone were found to significantly affect diatom motility.

To test the requirement for collinearity of the DC and AC magnetic fields in the cyclotron resonance model, the field resonance conditions were maintained except that the AC field was applied orthogonally to the DC field. No significant effects on diatom

motility were observed under these conditions.

To determine the effect of AC field amplitude on the motility results, resonant fields of .209 gauss DC, and 16 Hz AC were held constant, and a series of AC amplitudes from 0 to .627 gauss were applied. At .25 mM Ca^{2+} concentration, this AC amplitude series resulted in a peak of 40% motility at .209 gauss peak AC amplitude, falling off on either side of this value.

Addition of lanthanum chloride to the experimental agar at any concentration above 10^{-6} molar inhibited diatom motility as expected. When resonant fields were applied to 5 mM Ca^{2+} cultures with added lanthanum the inhibition was at least partially reversed for all $LaCl_3$ concentrations tested.

Lastly, a resonance curve showing diatom motility versus AC field frequency was obtained. For the resonance curve tests, the DC magnetic field was maintained at .209 gauss, and the AC amplitude at .209 gauss peak. Ca^{2+} concentration was .25 mM. The results showed a resonant peak of 38% motility at the expected frequency of 16 Hz, falling to 5% motility at 0 and 32 Hz. The "bandwidth" of the resonant curve (frequency width where the effect was at least .707 times the peak value), was approximately 4 Hz.

Several conclusions were drawn by the authors from these experiments. The results were taken to be supportive of the cyclotron resonant model of field-cell interaction as it had been articulated to that point [Liboff,1985; McLeod and Liboff,1987]. Many of the experimental features were strikingly supportive of the predictions of that model. Specifically, the effectiveness of odd harmonics of the fundamental frequency and ineffectiveness of even harmonics was supportive. Also, the

requirement for both DC and AC magnetic fields directed collinearly was predicted by the model. The observed resonance curve with its peak at precisely the frequency predicted by the cyclotron resonance model was another striking observation. The experiments with $LaCl_3$, chosen for its ability to competitively inhibit attachment of Ca^{2+} to sites on the cell membrane, pointed to Ca^{2+} ions at the cell membrane as responsible for the motility effects. The authors finally suggest that a possible reason for the inability of many experimenters to replicate others' work might be due to the lack of control of the local DC geomagnetic field in their experiments. This point of view is also supported by Blackman et al. [1985], who observed similar patterns of effective odd harmonics dependent on the local geomagnetic field value.

McLeod: Diatom Resonance Curves and Harmonics

These studies [McLeod et al.,1987] represent an extension of previous results relating diatom motility and ion cyclotron resonant fields. Effects of harmonics 1 through 17 of the fundamental cyclotron resonant frequency for both Ca^{2+} and K^+ ions were observed. For the Ca^{2+} harmonic series plates containing agar with .25 mM calcium concentration were used. At this concentration diatom motility had been strongly inhibited in the previous experiments. For the K^+ experiments, a calcium concentration of 5 mM was used, yielding maximum (45%) diatom motility with no fields applied. The exposure apparatus was identical to the previous experiment described above. For these experiments the vertical magnetic field was not eliminated since previous work had showed no effect of the vertical field on the results. The peak

magnitude of the AC magnetic field applied throughout the experiments was .15 gauss.

The first experimental runs were designed to test the hypothesis that the frequency which would enhance diatom motility could be determined solely by the cyclotron resonance condition for Ca^{2+}. Eight separate tuning frequencies ranging from 8 Hz to 64 Hz were employed. The DC magnetic field at each of these frequencies was adjusted according to the resonance condition:

$$f_c = \frac{qB}{2\pi m} \tag{2.3}$$

where q is the ion charge in coulombs, B is the DC magnetic field in Tesla, m is the ion mass in kg, and f_c is the frequency in Hz. The resulting combination of DC field and AC frequency corresponds to the first harmonic tuning condition. Resonance curves were obtained for each of the 8 conditions by varying the frequency around the peak resonant point and recording the resulting motility. Strikingly similar resonance curves were found for each of the 8 conditions. The peak frequency of each resonance curve corresponded closely with that calculated from the cyclotron resonance model.

A resonance curve for fields tuned to the K^+ ion at a DC magnetic field value of .41 gauss was also obtained. At .41 gauss, the cyclotron resonance frequency for the K^+ ion is 16 Hz. A resonance curve which was the exact inverse of the Ca^{2+} resonance curve was obtained. The shapes of the curves were identical, but the Ca^{2+} tuned fields enhanced motility from 4% to 40% in agar with .25 mM calcium concentration, while the K^+ tuned fields decreased motility from 40% to 4% in agar with 5 mM calcium concentration.

Further experiments were undertaken to determine the effect of harmonics of the fundamental cyclotron resonant frequency on the motility results. For the Ca^{2+} harmonic series, agar plates with a .25 mM calcium concentration were used, and the DC magnetic field was maintained at .1045 gauss. The resulting fundamental cyclotron resonant frequency was 8 Hz. Harmonics 1 through 17 of this fundamental frequency were tested. Significant enhancement of diatom motility was found only for harmonics 1,3,5,and 15. The ineffectiveness of the even harmonics was predicted by the cyclotron resonance theoretical model, but the ineffectiveness of odd harmonics 7 through 13 was unexpected.

Similar harmonic series tests were performed for K^+ tuned fields. Throughout the K^+ series the DC magnetic field was maintained at .2045 gauss, once again yielding a fundamental frequency of 8 Hz. Calcium concentration of the agar was held at 5 mM. The results of the K^+ series were once again the inverse of the Ca^{2+} results. Harmonics 1,3,5 and 15 were effective in decreasing the motility of diatoms.

The authors point out that the similar harmonic patterns observed for the Ca^{2+} and K^+ ions is one of the most remarkable of the results. Though the ions travel through different channels, the authors interpret this result as indicating similar structures for the channels. No definitive explanation is given for the absence of effects from harmonics 7 through 13, except the possibility of interference from resonance of other ions.

Ramirez: Drosophila Characteristics

Another group of researchers [Ramirez et al.,1983] has reported effects of low frequency magnetic fields on mortality rates and egg-laying characteristics of Drosophila melanogaster. Three different magnetic fields were used for these experiments. The first

was a pulsed waveform with pulses .5 msec in length at a repetition rate of 100 Hz. Peak field amplitude was 17.6 gauss. The second waveform was sinusoidal at a 50 Hz frequency with a 10 gauss RMS amplitude. These first two waveforms were generated by a wire solenoid 17 cm long and 6 cm in diameter. The third test field consisted of a 45 gauss permanent magnet.

For the egg-laying tests, two identical boxes connected by a plastic tube were placed 30 cm apart. Magnetic fields were applied to one of the boxes, with the other reserved as a control. Each day the eggs were removed and counted. When pulsed or sinusoidal fields were applied, the flies avoided laying eggs in the exposed side with a high degree of significance ($p<.01$ for pulsed fields, $p<.001$ for sinusoidal). The permanent magnet had no significant overall effect on egg-laying position.

Mortality studies of eggs laid in the exposed environment versus those laid in the control side were performed. For all three field regimes mortality was greater for the exposed eggs, ($p<.05$ for pulsed, $p<.005$ for sinusoidal, and $p<.05$ for static fields).

The authors mention a possible reason for the differences between the effects of time varying versus static magnetic fields on the drosophila. They state that a static magnetic field induces currents in flies only when they are in motion, while a variable magnetic field induces currents also in a stationary fly. This view might be slightly oversimplified, due to the fact that charged particles within an organism have mean thermal velocities which are generally far in excess of any velocity at which the entire organism is likely to move. Static fields can have an influence on ionic motion in a stationary organism due to the inherent thermal motion of the ions.

Phillips: Colon Cancer Cells

Effects of separate and combined low frequency electric and magnetic fields on human colon cancer cells in vitro have been reported [Phillips et al.,1986]. The cell lines involved were the Colo 205 and Colo 320 DM tumor lines. Three different field conditions were applied to the cultured cells during experiments. These consisted of an electric field at 60 Hz inducing a 300 mA/m^2 current density, a rotating 60 Hz magnetic field generated by 5 foot diameter orthogonal coils, and a combination of the electric and magnetic fields. The cell cultures were assayed for surface properties by measuring cell surface antibody binding properties. The clonogenic capacity of the cell cultures (colony forming rate when soft agar cloned), was also measured under experimental conditions.

Both the magnetic field alone and the magnetic and electric fields combined increased clonogenic capacity of exposed cell cultures versus controls ($p<.05$). The magnitude of the difference was quite variable with a maximum increase of four fold. The electric field alone produced a mixed response with no overall significant shift in clonogenic capacity versus controls.

Both the magnetic field alone and the combination of electric and magnetic fields were also effective in increasing the binding of the monoclonal antibodies to the cell surface ($p<.05$).

The authors interpret the results as supporting the hypothesis that the interaction site for low frequency electromagnetic fields with cells is the cell membrane surface. The alteration of antibody binding under exposed conditions is supportive of this hypothesis.

Delgado: Chick Embryos

This series of experiments [Delgado et al.,1982] documented effects of low frequency electromagnetic fields on chick embryo development. Fertilized chick eggs were placed in a wire solenoid which was driven by pulsed currents (.5 msec pulse width), to create continuous electromagnetic fields in the eggs. Pulse repetition frequencies of 10, 100, and 1000 Hz, and magnetic field strengths of .0012, .012, and .12 gauss were employed. After 48 hours of incubation the morphological and histological characteristics of five embryo organs were compared with control embryos kept in the same incubator. The five organs compared were the cephalic nervous system, truncal nervous system, heart, vessels, and somites.

Consistent abnormalities in gross morphological development occurred for 100 Hz-.012 gauss fields and 1000 Hz-.012 gauss fields. Mixed abnormalities occurred at other frequency-intensity combinations but lacked consistency. Histological studies revealed that embryos exposed to 100 Hz, .012 gauss fields exhibited little cellular differentiation and lack of cell organization. Less pronounced developmental delays were exhibited by embryos exposed to 100 Hz-.12 gauss fields, 1 kHz-.12 gauss fields, and 10 Hz-.12 gauss fields.

The authors report that all embryos showed some development, indicating that the effect of the fields was slow and cumulative. The only field combination that showed consistent adverse effects throughout the experiments was the 100 Hz-.12 gauss combination. These data therefore support the concept of effective frequency and amplitude "windows" for electromagnetic fields applied to biological organisms.

Animal Behavior

Several experiments have demonstrated that weak, low frequency electromagnetic fields can have an effect on the behavior of live animals. Some of these experiments are documented below.

Friedman: Human Reaction Time

Early experiments to determine if artificially generated magnetic fields could affect human performance were reported by Friedman et al. [1967]. A Helmholtz coil apparatus composed of 14.5 inch diameter coils in a wooden frame was fabricated. The entire coil apparatus was placed over a subject's head. Reaction time performance was measured as the time interval between appearance of a red light and the pressing and release of a telegraph key by the subject.

The first fields tested were 5 and 17 gauss static magnetic fields. No significant reaction time alterations were observed when the static fields were applied. A second field pattern consisted of a sinusoidal AC magnetic field of 5 to 11 gauss amplitude and .1 Hz or .2 Hz frequency. These frequencies were chosen to coincide with naturally occurring fluctuations of DC potential in the brain. The .2 Hz AC field produced significantly longer reaction times than both the control and .1 Hz field groups. This experiment constitutes one of the early indications that weak, low frequency electromagnetic fields could affect behavior patterns of a complex organism. It also provides early evidence for the concept of the crucial factor of the applied frequency in the biological results.

Sagan: Chick Behavior

These experiments [Sagan and Medici,1979] tested activity levels of white leghorn chicks exposed to RF electromagnetic fields modulated at frequencies within the normal range of observed electroencephalogram frequencies. The 8-12 day old chicks were conditioned on a fixed time schedule. A reinforcement of water was given at 30 second intervals. Activity of the chicks was quantified by observing the interruption of 3 light beams directed through the cage holding the chicks. In general, the activity level was low at the beginning and end of the 30 second interval, rising to a peak in the middle of the interval. After conditioning, chicks were exposed for 20 minutes to an RF signal delivered via waveguide and tapered horn to the cage. The signal consisted of a 450 MHz carrier modulated to 80-90% with a 3 Hz or 16 Hz sinusoidal signal. These frequencies were chosen as the result of the authors' investigation of EEG patterns of newly hatched chicks, during which they observed 3 Hz as being associated with periods of somnolance, an 16 Hz with periods of activity. Power densities of 1 mW/cm^2 and 5 mW/cm^2 were tried.

No significant alteration of chick activity levels was observed for any of the field combinations tried. The authors caution that this evidence does not necessarily imply that such behavioral effects don't exist. They suggest that the existence of amplitude and frequency windows for effective fields raises the possibility that their experiments may not have included effective combinations.

Gavalas-Medici: Monkey Schedule Control

The behavior of monkeys trained on a performance schedule when exposed to low

frequency electric fields was investigated in these experiments [Gavalas-Medici and Day-Magdaleno,1976]. The experiments involved five adult female monkeys, trained on a Skinner conditioning schedule. The animals had to wait 5 seconds between lever presses, and press the lever within a 2.5 second interval to obtain a reward. The experimental variable was the inter-response time (IRT), or the time between lever presses. Electric fields at 1, 10, and 56 V/m and 7, 45, 60, and 75 Hz were applied in the experimental monkey cages.

Field combinations that proved to be effective in altering the IRT were 10 V/m at 7 Hz ($p<.05$), and 56 V/m at 7 and 75 Hz ($p<.05$). The authors interpret the results as being consistent with a threshold phenomenon, with the 7 Hz frequency exhibiting a lower intensity threshold than the 75 Hz frequency. They propose that sensitivity to weak electric fields might be present in all organisms whose nervous system exhibits spontaneous slow electric waves. They suggest that the macromolecular system on cell surfaces might be able to transduce extracellular fields by altering surface ion binding.

Thomas: Operant Behavior in Rats

A series of experiments [Thomas et al.,1986] revealed an effect of cyclotron resonance tuned magnetic fields on the behavior of rats trained on a multiple reinforcement schedule. The multiple schedule was such that when a red light and tone were present, the rat was required to press a lever 30 times to produce a food pellet. When a green light was illuminated and no tone was present, a pellet would be produced only if the rat responded with a lever press during an interval between 18 secs and 24 secs after the light was turned on. The first schedule, called a fixed ratio (FR), schedule,

generally produces a rather high and constant responding rate. The second schedule, called differential reinforcement of low rate (DRL), generally produces a low and steady response rate, with the highest frequency of interresponse times centered around the differential time period (18-24 secs in this case).

After training, the rats were exposed to one of four magnetic field configurations, generated by orthogonal Helmholtz coils. The first configuration was a sham exposure, where no fields were actually generated. The second consisted of an AC magnetic field only, generated horizontally along the cage axis. The AC field had a 60 Hz frequency and a .5 gauss amplitude. The third field configuration consisted of a DC adjustment of the vertical component of the earth's magnetic field, so that the sum of the geomagnetic field and the coil DC field was .261 gauss. The value of .261 gauss was chosen since it was as close as the equipment employed could come to the value of .271 gauss, which is the DC field required to maintain cyclotron resonance conditions for the Li^{+1} ion at an AC frequency of 60 Hz. The fourth field configuration consisted of a sum of the DC and AC fields generated in the second and third cases, attempting to maintain cyclotron resonance conditions for Li^{+}. In experimental trials, the animals were exposed to the appropriate fields for 30 minutes prior to a one hour session with the reinforcement schedules mentioned above.

The FR schedule response pattern of the rats was not significantly altered by any of the field combinations. The DRL schedule response pattern was not altered by any of the first three field configurations (sham, DC alone, AC alone). However, when the cyclotron resonance conditions were applied, the distribution of response period, which

normally exhibited the largest number of responses in the 16-20 second range, was significantly flattened and shifted toward shorter response times. Accompanying this change in response pattern was a marked decline in food pellet frequency. These behavioral changes appeared to last at least one hour after the field exposure, but performance patterns returned to normal within 24 hours after the exposure period.

The authors postulate that the behavioral effects observed could possibly be due to the resonant efflux of lithium ions from cells in the rat brains. It should be noted that the resonance conditions in this experiment were obtained in a manner different from other cyclotron resonance experiments [Smith et al.,1987; McLeod et al.,1987; Liboff et al,1987]. In these previous experiments, the DC and AC magnetic fields were collinearly applied, so that the maximum value of the AC field occurred in the same direction as the DC field adjusted for cyclotron resonance conditions. In the present experiment, the AC field was applied along a horizontal direction, while the DC field adjustment was made along a vertical direction. The resulting total DC field had a magnitude of .261 gauss, as reported, but its direction was declined at an angle of 36.8° to the horizontal, as explained in a later report [Liboff et al.,1989]. The authors point out that the horizontally directed AC field does indeed have a component along this declined direction equal to approximately 80% of its maximum horizontal value. Thus the maximum value of the AC field is not directed collinearly with the controlled DC field. This is perhaps a minor point, since viewed from a vector component standpoint, cyclotron resonance conditions are still maintained in the declined direction, but it nonetheless constitutes a difference between this experiment and those previously

reported. The later report also extends the results to include a profile of the rat responses to the same resonant fields, but with varying AC amplitudes. The response exhibits a threshold effect, where the behavioral changes are observed for AC amplitudes above .27 gauss and are absent at AC amplitudes below this value. An additional report [Smith et al.,1988], deals with objections that lithium is virtually absent from the internal milieu of mammals and thus could not be responsible for the behavioral effects observed in these experiments. Smith argues that lithium is a normal constituent of mammal tissue, is metabolically active in many tissues, and has been demonstrated nutritionally critical in both of the two mammals tested: rats and goats. In humans, the salt LiCl has been found to be effective in relieving symptoms of manic-depressive psychosis. Though Smith does not conclude that cyclotron resonance of lithium is definitely the cause of the rat behavioral effects, he does conclude that the possibility cannot be eliminated on the basis that lithium is an unimportant ion in rat brain processes.

Summary of Experimental Results

The experimental evidence reviewed above reveals several features that must be addressed by any model or models proposing to explain the interaction of low frequency electromagnetic fields with living systems. Extremely weak fields have been demonstrated effective in altering processes in living tissue. Fields as low as 10^{-5} V/m [Bawin and Adey,1976] and 1 mgauss [Blackman et al.,1985] have reportedly proven effective. Extremely low frequencies (0-300 Hz) are crucial to the effects. These low frequencies may be applied directly or as a modulator of an RF signal [Blackman et

al.,1985]. Pulsed [Goodman et al.,1983] and sinusoidal [Goodman and Henderson,1986] waveforms have both proven to be effective. The exact waveshape does not appear to be crucial to the effect [Goodman and Henderson,1986]. Not all AC frequencies and amplitudes are effective. Rather, effective frequency and amplitude "windows" have been observed in numerous experiments [Bawin and Adey,1976; Smith et al.,1987]. There may be multiple effective windows [Blackman et al.,1988a]. Some effects have demonstrated a dose response relationship to exposure time, though a saturation point may be reached [Smith et al.,1987b]. Reportedly effective exposure times have ranged from less than one minute [Smith et al.,1987b] to many days [Marron et al.,1975]. The local DC magnetic field can determine which AC frequencies will prove effective [Blackman et al.,1985]. Furthermore, magnetic fields tuned to cyclotron resonance conditions for unhydrated ions have dramatically altered the biological processes of several systems [Smith et al.,1987a; Liboff et al.,1987; Deibert et al.,1991; Smith et al.,1991]. Even harmonics of the fundamental resonant frequency have generally proven ineffective in stimulating these results [Blackman et al.,1988a]. Odd harmonics of the fundamental frequency can be effective, and at least one system has demonstrated a curious pattern of effective odd harmonics (1,3,5 and 15) [McLeod et al.,1987]. The DC and AC portions of the cyclotron resonant magnetic fields are ineffective if applied individually or orthogonally [Smith et al.,1987a]. Virtually all of the experiments implicate ionic flux as being a factor in the observed effects [Bawin et al.,1975; Blackman et al.,1985; Liboff et al.,1987]. In addition, several experiments have implicated cell membrane surfaces as the likely interaction site between the fields and

cells [Bawin et al.,1978; Lin-Liu and Adey,1982].

Table 2 in Appendix A is a summary of the experiments reviewed in this chapter, providing a quick reference to the experimental literature that can serve as a basis for further study of the biological implications of low frequency electromagnetic fields.

Other Experiments

The foregoing review of experiments relating to biological effects of weak, low frequency electromagnetic fields is not exhaustive. Rather, an attempt was made to include experimental results from a broad range of biological systems. As documented in table 2, the experiments chosen for detailed review reveal quite a number of features that must be considered in proposing a theoretical model of cell-field interactions. Additional reports concerning similar effects are numerous. While each of these additional experiments cannot be reviewed in detail, the following paragraphs comprise a brief synopsis.

Blackman et al. [1988b], has reported a Ca^{2+} efflux shift in chicken brains that had been exposed as eggs to 60 Hz electric fields, when a 50 Hz field was applied after hatching. No effects were seen when a 60 Hz field was applied under the same conditions. Martin [1988] has reported that pulsed 100 Hz magnetic fields of 10 mgauss amplitude caused abnormalities in developing chick embryos if applied within the first 24 hours of incubation, but not if applied during the second 24 hours. Dutta et al. [1989], have extended their studies of calcium ion efflux from neuroblastoma cells exposed to a low frequency modulated RF signal to include a Chinese hamster-mouse

hybrid. Significant efflux enhancement at certain power densities confirmed that the calcium efflux effect is observable on cells from widely different animal species, including avians [Blackman,1979], felines [Bawin and Adey,1976], humans [Dutta et al.,1984], and rodents [Dutta et al.,1989], indicating the general nature of the phenomenon.

Several experiments have been reported relating to the cyclotron resonance model of interaction. An independent confirmation of part of the results concerning diatom motility in cyclotron resonant magnetic fields [Smith et al.,1987; McLeod et al.,1987] was given by Reese et al. [1991], who reported an increase in diatom motion at .25 mM agar Ca^{2+} concentration induced by calcium tuned fields (B_{DC}=.21g, B_{AC}=.21 g pk, f=16.0 Hz). The magnitude of the effect, however, was not consistent enough to determine frequency dependence, as reported by the previous researchers. Parkinson and Hanks [Parkinson and Hanks,1989] have reported a failure to observe changes in cytosolic calcium concentration in rat osteosarcoma cells exposed to Ca^{2+} cyclotron resonance magnetic fields (B_{DC}=.5 g, B_{AC}=.5 g pk, f=38.15 Hz), as measured by the fluorescent Ca^{2+} chelating agent fura2. In another search for ion cyclotron resonance effects, Liboff and Parkinson [1991] found no changes in transepithelial currents across cell membranes of turtle colonic tissue when resonant conditions were applied for several different ions. Lyle et al. have reported two experiments involving lymphocytes exposed to calcium ion cyclotron resonant magnetic fields. In the first report [Lyle et al.,1989] a significant increase in the proliferation rate (by 9-125%) of normal and leukemic lymphocytes was observed. In the second [Lyle et al.,1990], a blockage of the increased $^{45}Ca^{2+}$ uptake of

rat spleen lymphocytes induced by ouabain was observed when calcium ion cyclotron resonant magnetic fields (B_{DC}=.165 g, f=11.1 Hz) were applied. The blockage did not occur when the fields were applied to cells stimulated by concavanalin A, suggesting that the field might not be affecting calcium membrane channels directly, but by an indirect mechanism. Walleczek and Liburdy have observed a 60% increase in Ca^{2+} transport across membranes of mitogen activated rat thymic lymphocyte cells exposed to combined DC and AC magnetic field conditions (B_{DC}=.21 g, B_{AC}=.21 g RMS, f=14.3 Hz) for a period of one hour [Walleczek and Liburdy,1990]. No effects were observed when the AC field alone was applied, or when the lymphocytes were in a quiescent state, unstimulated by mitogens.

Conclusions

Considered as a whole, the experimental evidence for effects of weak, low frequency electromagnetic fields on biological systems is diverse and convincing. Positive effects have been obtained from systems ranging from synaptosomes (which are not even whole cells), to microscopic one-celled diatoms, to higher animals, including humans. Most of the research has indicated that the primary effect of the electromagnetic fields is to alter ionic flux across cell membranes. The mechanism coupling the applied electromagnetic fields to ionic flux is not yet understood, though several studies have indicated that the coupling is likely to occur at the cell membrane surface. The extremely weak nature of the effective fields, as well as their low frequencies compared to normal cellular events make the task of forming an appropriate

model for the interaction mechanism a difficult one indeed. Several speculative models have been proposed. These models will be reviewed and evaluated in Chapter 6.

CHAPTER 3

BONE GROWTH STIMULATOR

Introduction

The piezoelectric nature of bone tissue has spawned the hypothesis that small electrical currents induced by stress in bone material are an important factor in the healing process. This in turn led to some early experiments with implanted electrodes [Bassett,1971] which created similar small electrical currents at the site of non-union bone fractures. These tests seemed to indicate that small electric fields in the tissue could indeed stimulate bone growth. The next experimental step was to use externally applied electromagnetic fields to induce electrical currents in the tissue without the need for surgically implanted electrodes [Bassett et al.,1974]. Positive results from these tests eventually led to commercial products employing pulsed magnetic fields created by passing current pulses through wire coils placed near the fracture site.

In light of the early successes of these bone growth experiments, it is not surprising that one of the first attempts at testing the Ion Cyclotron Resonance theory involved bone growth stimulation. Early experiments with chick femur bones in vitro [Smith et al.,1991], and live rabbits with fibular osteotomies [Deibert et al.,1991] demonstrated that magnetic fields tuned for cyclotron resonance conditions for the Ca^{2+}

ion or one of its harmonics could stimulate bone growth. The encouraging results of these experiments led to a decision to develop a prototype device to employ the cyclotron resonance principle in a bone healing application. The design and development of this device formed part of the research work documented by this thesis. This chapter is a description of the device.

Device Design Goals

The main task of the bone healing device is to maintain the correct DC and AC magnetic fields at a bone fracture site in order to promote healing of the fracture. As the design for the device was begun, experimental results with rabbit fibular osteotomies [Deibert et al.,1991] revealed that a most effective combination of fields consisted of a DC field of .209 gauss, and an AC field of .209 gauss peak at a frequency of 76.6 Hz. This combination represents the fifth harmonic of the fundamental cyclotron resonance frequency for the calcium ion. It also corresponds to the third harmonic of the fundamental resonant frequency for the magnesium ion. In the rabbit fibular osteotomy experiments, calcium tuned and magnesium tuned cyclotron resonant fields were both found to enhance bone growth. Since higher harmonics of the fundamental frequency were also found to be effective, it seemed reasonable that a field combination in which harmonics for both the calcium and magnesium ions were involved might also be effective in bone stimulation. The same report reveals that indeed, this combination of fields was effective in enhancing bone growth when applied for just 1/2 hour out of each 24 hour period. Accordingly, the main design goal for the bone healing device was that

it should be able to create these DC and AC field conditions for a period of 1/2 hour per day at a fracture site.

The bone healing device was targeted for use in human non-union bone fractures. In addition to the device's ability to maintain the correct magnetic fields at a fracture site, convenience and ease of use were also major considerations in its design. In order to promote ease of use, the unit was to be small, lightweight and non-invasive. Since a patient would only be required to wear the device 1/2 hour per day, it was essential that the device be easy to put in place over the treatment area, as well as easy to remove after a treatment period. Battery powered operation was desired in order to eliminate dependence on AC electrical power outlets. A degree of programmability was to be built into the device so that a clinician could specify exact field conditions and treatment protocols for each unit. This programmability was required in order to give the device a measure of flexibility. Future research which might reveal other field conditions and treatment parameters could then be easily incorporated into the treatment scheme. The device was also required to have data storage capability. A daily record of actual treatment times was to be kept on board the unit. This information was required in order to monitor patient compliance with treatment procedures during clinical tests. In addition, the unit was to have the ability to detect certain error conditions, record the error condition as a data log entry, and take any appropriate actions as a result of the error. For example a complete shutdown of the device would be required if a hardware failure rendered the device unable to maintain the correct magnetic fields at the treatment site.

Design Description

The requirements of programmability and data storage capability for the unit dictated from the outset that a microprocessor would be at the heart of the unit design. Considering size, weight, and cost restrictions, the most practical processor for the task proved to be a highly integrated microncontroller. A microcontroller contains all the basic components of a microprocessor system in one integrated circuit. These basic components include a central processing unit (CPU), Random Access Memory (RAM) for temporary data storage, and non-volatile Read Only Memory (ROM). In addition, modern microcontrollers often have several other commonly used microprocessor system features built in. The microcontroller selected as the heart of the bone device design was the Motorola MC68HC811. This microcontroller has a number of useful features built in, including 256 bytes of RAM, 2 kbytes of Electrically Erasable Programmable Read Only Memory (EEPROM), three 8-bit parallel data ports, a serial data port, an Analog-to-Digital (A/D) converter, and a timer circuit. Such a high level of integration was a benefit to the design since it minimized the number of supporting integrated circuit chips required for the final working system. The basic idea behind the bone healing device was to use the microcontroller in conjunction with a Digital-to-Analog (D/A) converter to drive an electrical current through a pair of wire coils in near-Helmholtz configuration oriented around the fracture site. The current through the coils was to be continuously controlled so that the total DC magnetic field (the sum of the DC field from the coils and any ambient DC fields present) matched the desired DC field prescribed by the cyclotron resonance conditions. In this case the total DC field was to be .209 Gauss.

Superimposed on this DC field was to be an AC field also created by the microcontroller through the D/A converter. The AC field was to have a .209 Gauss peak amplitude and a frequency of 76.6 Hz. Note that the DC field magnitude and the frequency need not be absolutely fixed at these values to maintain cyclotron resonance conditions. However, the DC field and the frequency must exhibit the linear relationship defined in Equation (1.10).

The bone healing device's main design challenge proved to be the maintenance of correct cyclotron resonance conditions in the face of changing ambient DC magnetic fields. It is well known that the earth generates a weak DC magnetic field (called the geomagnetic field). The magnitude of the geomagnetic field is on the order of .5 gauss in most inhabited earth latitudes. The nature of the geomagnetic field is that of any vector field. Two quantities are required to define it at any given point in space (field magnitude and direction). One consequence of this is that at any given point in space, the magnitude of the measured geomagnetic field is not unique, but varies continuously with the direction of measurement. The goal of the bone healing device was to maintain the desired resonant conditions as measured along one direction relative to the fracture site. However, as a patient wearing the device moves the limb involved, the geomagnetic field component along this direction changes continuously. Referring to Equation (1.10), it becomes clear that in order to maintain cyclotron resonance conditions in the face of the slowly changing geomagnetic field due to patient motion, two options are available. The first is to continuously adjust the DC current in the generator coils so that the total DC field at the treatment site remains constant in spite of the varying

ambient field. The second is to continuously alter the frequency of the applied AC field to match the changes in the total DC field caused by patient motion. Either of these options requires a simple control system. Either option also requires an accurate, continuous measurement of the DC magnetic field at the treatment site as the feedback signal for this control loop. The first of these two options was selected for use in the bone device since the first option requires a magnetometer that is absolutely accurate at only one value of total DC field. By contrast, the second option would require a magnetometer that is accurate over the entire range of fields likely to be encountered.

A diagram of the appearance of the bone healing device is shown in Figure 1. A block diagram of the bone device electronics is shown in Figure 2. A schematic drawing of the electronics appears in Figure 3.

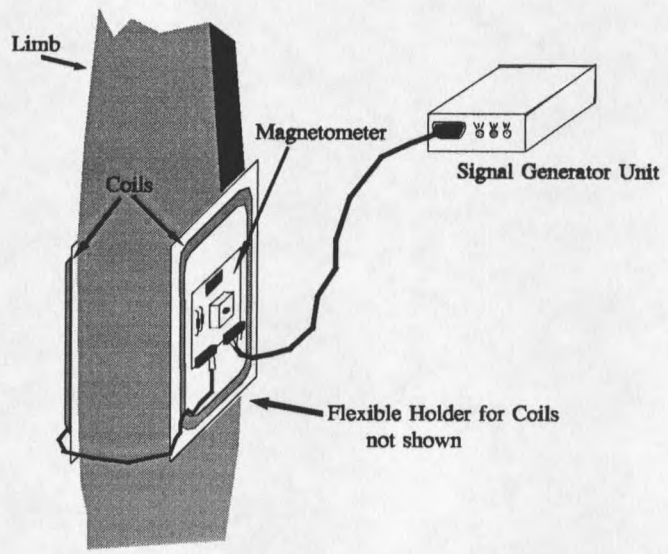

Figure 1. Bone device appearance.

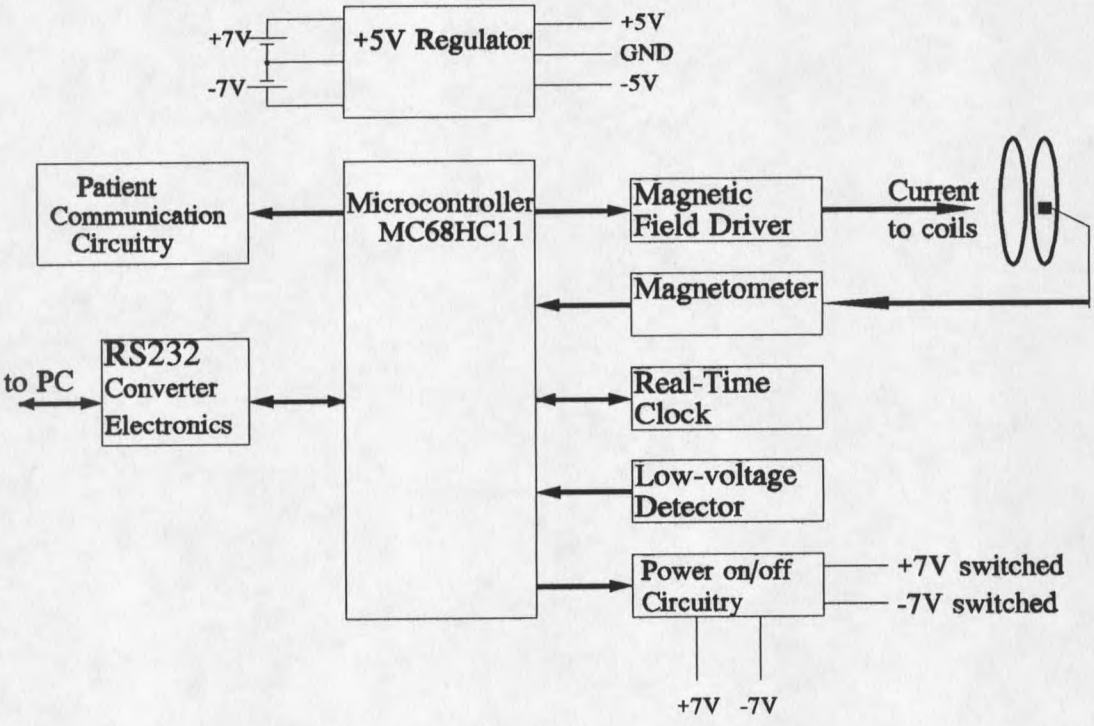

Figure 2. Block diagram of bone device.

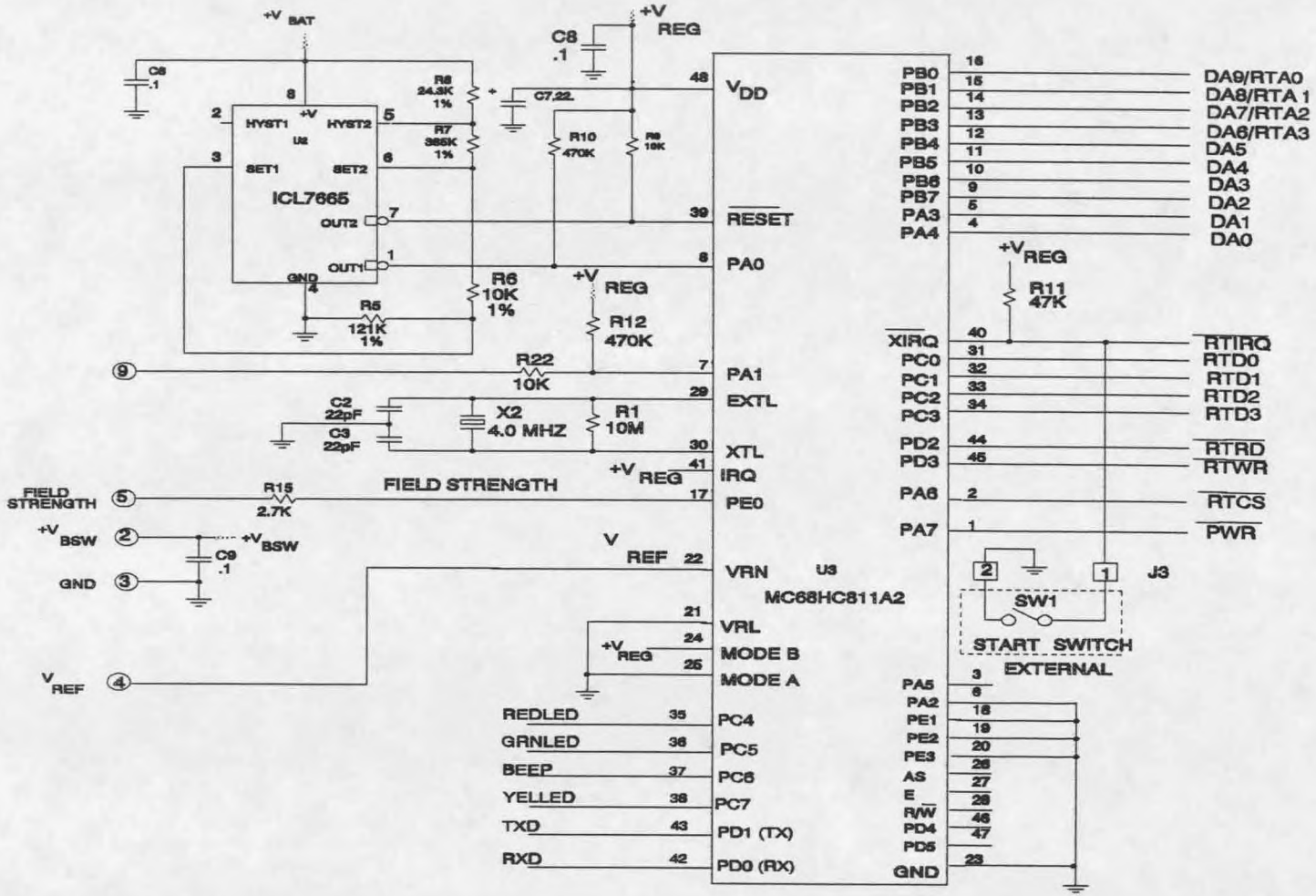

Figure 3. Bone Device Electronics

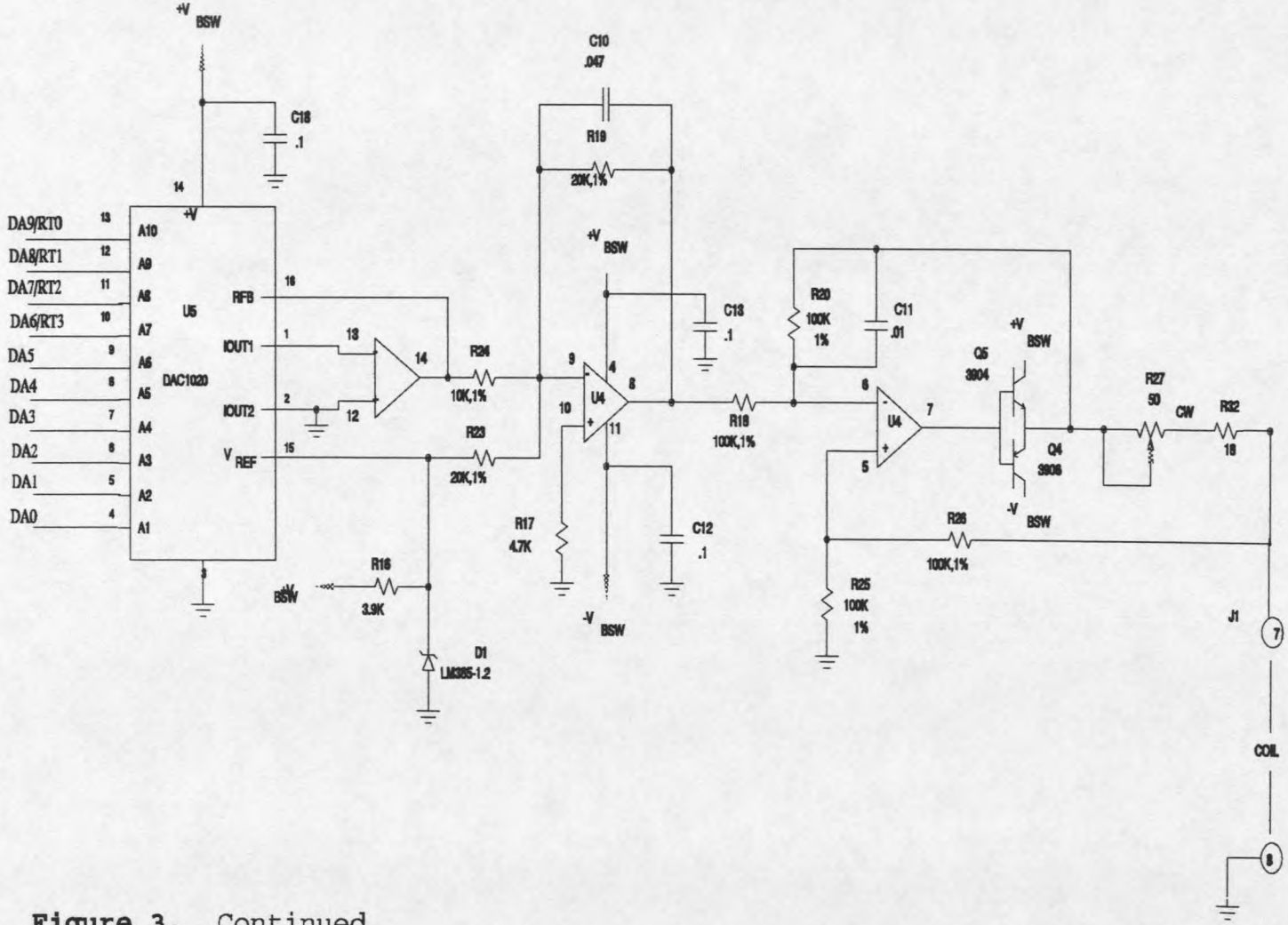

Figure 3. Continued

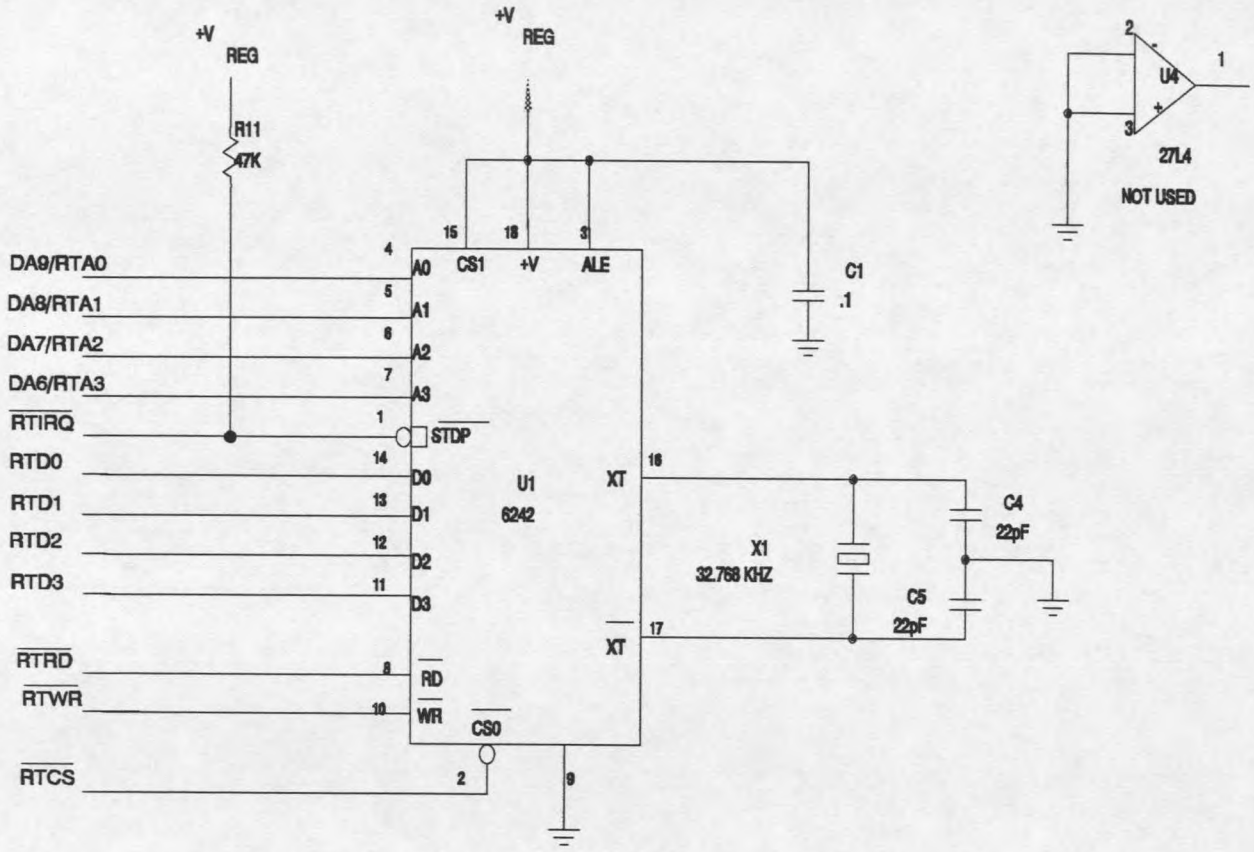

Figure 3. Continued

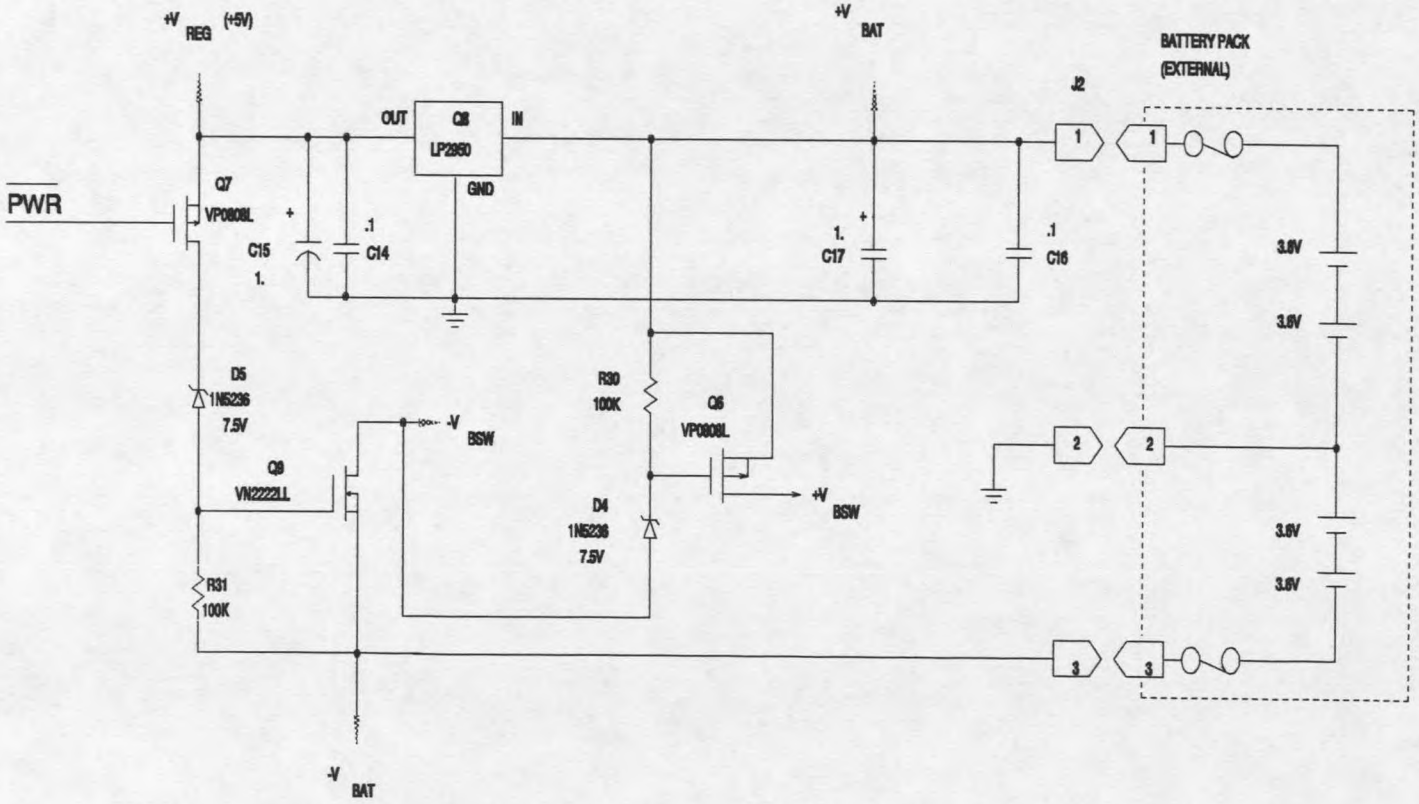

Figure 3. Continued

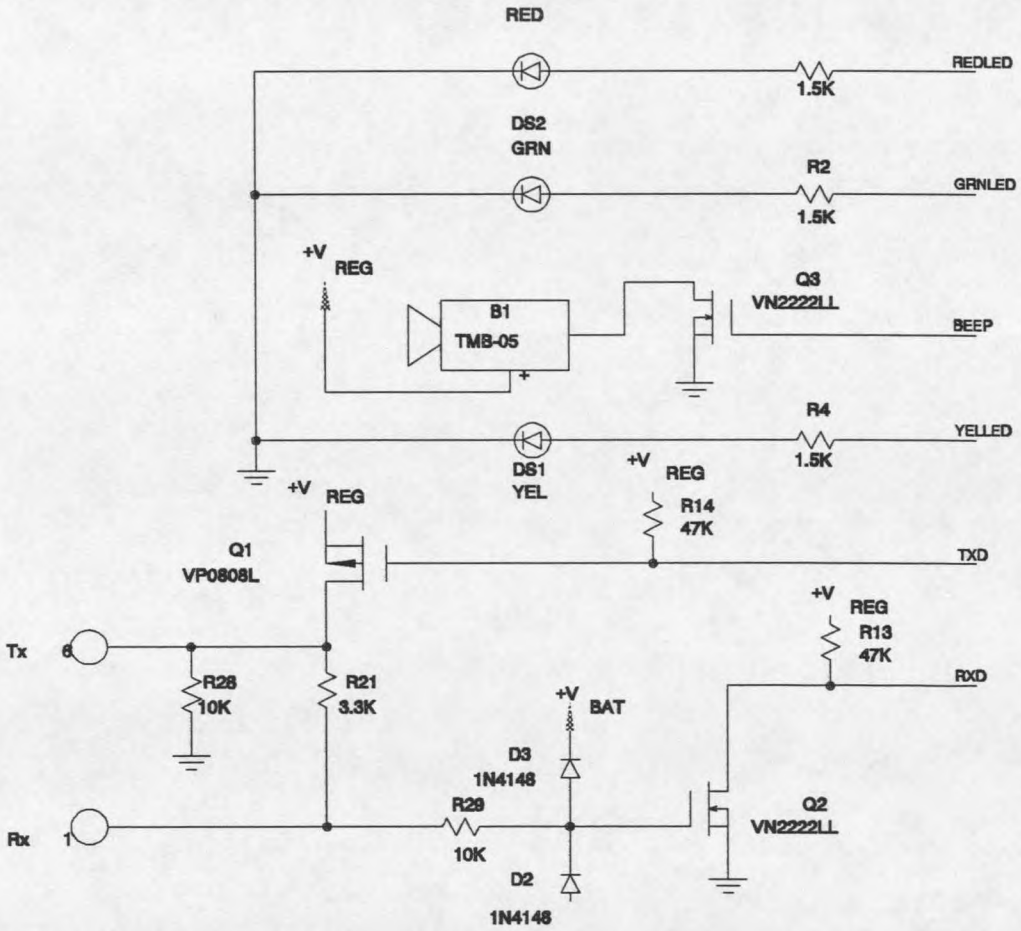

Figure 3. Continued

Description of Device Operation

Power Supply

Power for the bone device is obtained from a battery pack consisting of 10 AA sized alkaline batteries, with the batteries arranged in a series configuration. Each cell has a nominal output voltage of 1.5 volts DC, but this output voltage drifts downward during use. The power supplies for all analog circuitry are +7.5 and -7.5 volts. A 5 volt DC regulator is employed to provide the power supply for the microcontroller and digital circuitry. The positive power supply voltage is continuously monitored with an ICL7665 low voltage detector chip which provides two outputs. The first notifies the microcontroller when the power supply voltage has drifted below 5.5 volts. When this occurs, the microcontroller suspends further treatments since accurate magnetic fields cannot be maintained at the treatment site when the power supply goes below this value. The second output resets the microcontroller completely when the power supply falls below 5 volts. This is done to avoid unpredictable microcontroller operation at low voltages which could erase valuable log data in the microcontroller.

Microcontroller

The MC68HC811 microcontroller orchestrates operation of the entire device. The control strategy to maintain the correct DC magnetic field at the fracture site is part of the program residing in the microcontroller's EEPROM. During treatment, the microcontroller obtains field magnitude information from the magnetometer circuitry via its 8-bit A/D port. The field is sampled twice during each cycle of the AC waveform,

at the positive and negative peaks of the sine wave.

The microcontroller first averages the two most recent A/D values to eliminate the AC component. The resulting DC value becomes the input to a digital filter routine in the microcontroller software designed to set the control loop response characteristics. The z-domain transfer function of the digital filter is given by:

$$H(z) = \frac{G_1(1+2z^{-1}+z^{-2})}{1-z^{-1}} \tag{3.1}$$

where G_1 is a gain value which influences the loop dynamic performance, and z is the complex z-transform variable [Oppenheim and Schafer,1975]. In practice, the z^{-n} factors in the above equation translate into delays of n iterations. This transfer function was chosen partly because of its approximation to the analog LaPlace domain transfer function given by:

$$H(s) = \frac{G}{s(s+\omega_1)} \tag{3.2}$$

The value G is a gain value and ω_1 is the radian frequency of the transfer function pole. Equation (3.1) is obtained from Equation (3.2) by setting the pole equal to twice the value of the digital sampling frequency (ω_1=2/T), and applying the bilinear transformation [Oppenheim and Schafer,1975] given by:

$$s = \frac{2}{T}\frac{z-1}{z+1} \tag{3.3}$$

where T is the period of the digital sampling frequency.

Note that Equation (3.2) is in the form of the familiar Proportional-Integral (PI) control scheme in the analog domain. This scheme provides zero steady-state error and loop characteristics determined by the gain and the pole 2/T. In practice, with a sampling frequency (1/T) equal to 76.6 Hz, a gain G_1 of 1/8 resulted in a satisfactory step response settling time of a fraction of a second for the control loop. The reason for setting the arbitrary pole ω_1 equal to twice the sampling frequency (2/T), is that the resulting z-domain transfer function given by Equation (3.1) has coefficients of 1 or 2 only. This is important for ease of implementation in microcontroller software. Multiplication by 2 is accomplished easily by a simple logical left shift in fixed point hardware. Coefficients other than some power of 2 would require more complicated and time-consuming calculations.

The digital filter output is applied to the 10-bit parallel output port of the microcontroller which controls the Magnetic Field Driver circuitry.

Further tasks of the microcontroller include the following.

1) The microcontroller must control communication with the patient to enable the patient to start treatments, and notify the patient of the device status.

2) The microcontroller must maintain a data log containing information about daily treatment lengths, and possible operation errors.

3) The microcontroller must control power shutdown circuitry to allow electrical power to peripheral circuitry to be shut off when the device is not treating, and reinstated when treatment is to begin.

4) The microcontroller must provide communication with a host IBM compatible

personal computer via serial port, in order to allow programming of the device and collection of log data.

A complete listing of the assembly language code which directs the microcontroller to accomplish these tasks is included in Appendix B.

Magnetic Field Driver

The responsibility of the Magnetic Field Driver is to convert the 10-bit digital output of the microncontroller to a proportional magnetic field at the fracture site. The components of the Magnetic Field Driver are: 1) a D/A converter, 2) current source circuitry, and 3) wire coils. The task of the D/A converter is to convert the microcontroller digital output to a proportional analog voltage. The analog voltage can range from -1.2 volts to +1.2 volts. The sign of the voltage corresponds to the sign of the 2's-complement numerical value as output by the microcontroller. This analog voltage is applied to the current source input. The current source converts the voltage from the D/A converter to a proportional electrical current. This current is applied to the wire coils, creating a magnetic field in the volume between the coils. A current source is employed to drive the coils because the magnetic field generated by the coils is directly proportional to the current applied. The relationship between the applied current and the resulting field at the center point between the coils is given by [Zahn,1979]:

$$B = \frac{\mu n I r^2}{\left[\left(\frac{d}{2}\right)^2 + r^2\right]^{3/2}} \qquad (3.4)$$

where μ is the permeability of the material, I is the current in each coil, n is the number of turns in each coil, r is the coil radius and d is the distance separating the two coils. The positioning of the wire coils is critical for correct operation of the unit. The coils must be aligned so that their axes of symmetry are collinear in order for Equation (3.4) to apply. They must also be connected so that the current flows in the same direction through each coil. This is important to ensure that the magnetic field contributions from each coil will add at the central location, instead of canceling. The spacing between the coils is also crucial. This is true because the field resulting from a concentric coil configuration varies continuously with position. Equation (3.4) above is a valid expression for the field at the point exactly in the center between the coils. The field value at any other position differs from this value. The goal of the bone device was to create a constant magnetic field covering the total volume of an internal bone fracture site. Thus it was desirable to maximize the volume inside which the field was within a given tolerance of the central value. The tolerance was taken to be 10%, based on the diatom experiments of Smith et al. [1987], that showed a resonant response curve of diatom motility having approximately this width. The maximum volume within tolerance is obtained when the field function has a minimum variation with position at the central target site. This is obtained using the Helmholtz coil configuration [Zahn,1979], in which the spacing between coils is equal to the radius of each coil. The original design plan was to employ the Helmholtz coil configuration in the bone device, but this presented a difficulty which forced a design change. The difficulty arose from the requirement to continuously regulate the total DC field in the face of changes in the

ambient field caused by patient motion. In order to provide such control, an accurate measurement of the total field at the fracture site is essential, but since the fracture site is internal to the body, a direct measurement of the field at the site is impossible without an implanted device. To avoid the need for an implanted device, it was decided to place the magnetic field measurement device (magnetometer), in the plane of one of the coils, as shown in Figure 1.

If the coils are in the Helmholtz configuration, the field in the coil plane is smaller than the field at the central target site by approximately 6 percent. This 6 percent difference translates into an error in the controlled DC field that varies with the magnitude of the ambient field. For example, if the ambient geomagnetic field in the direction of the coil axis is -.5 gauss, and the device corrected the field in the coil plane to .209 gauss, the field at the central target point would be .251 gauss. This amounts to a 20 percent error in the target site field. The magnitude of this error is a function of the magnitude of the ambient geomagnetic field. Thus it is not possible to introduce a software correction factor to compensate for the difference unless this ambient field value is known. A magnetometer can only measure the total field at a given point. It cannot distinguish between the ambient and coil field contributions, and thus software correction was not a practical solution to this problem. The solution that was finally adopted involved a simple adjustment of the coil spacing. The spacing between the coils was increased until the central target field value due to the coils was equal to the field value in the coil plane. In this way the difference between the fields at the two sites was eliminated. As a result, controlling the field at the coil plane insured the field at the

target site would be accurate as well. Figures 4 and 5 illustrate the effect that the coil spacing increase has on the field along the coil axes.

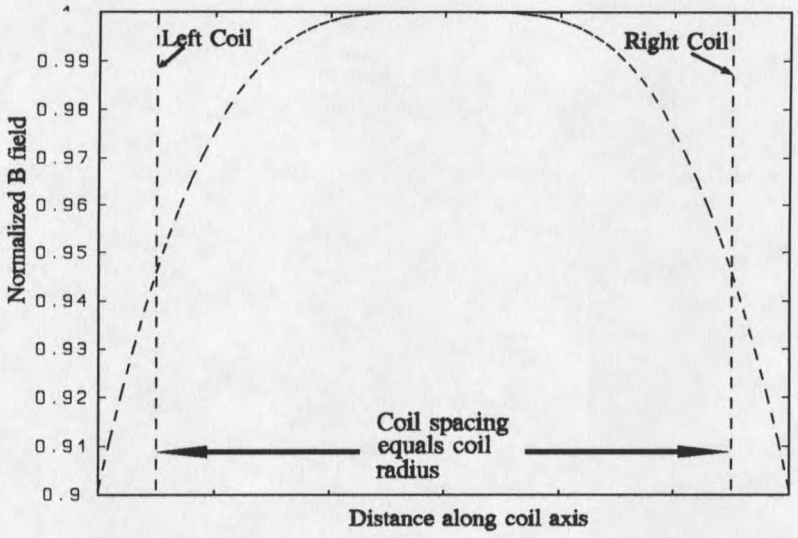

Figure 4. Central B field from Helmholtz coils.

The plots show the field profiles along the coil axes in the whole space between the coils. The data are normalized to the central value. Note that the 6 percent difference at the coil plane for Helmholtz spacing is eliminated when the spacing is increased to 1.2 times the coil radius. This was the spacing adopted for use in the device.

Magnetometer

An accurate measurement of total magnetic field is necessary to control the fields at the treatment site. This measurement is the task of the magnetometer. A schematic diagram of the magnetometer electronics appears in Figure 6.

The heart of the magnetometer is an SS94A1 Hall Effect device manufactured by

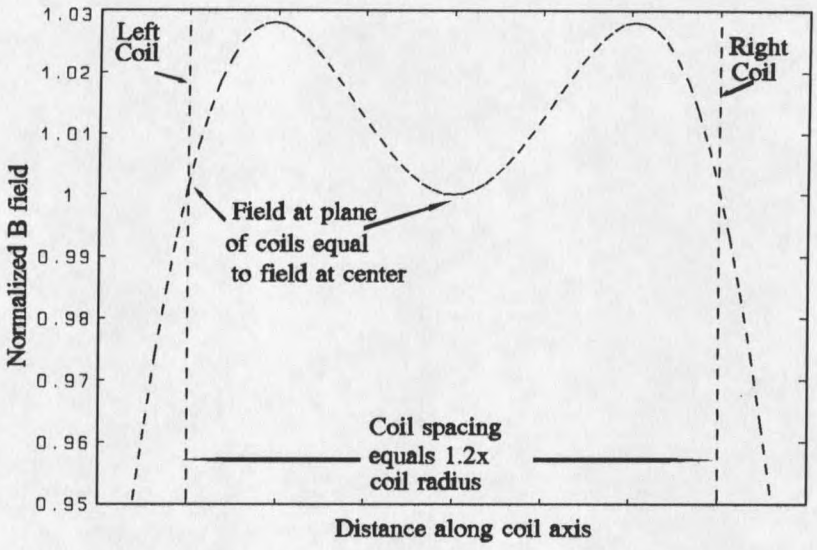

Figure 5. Central field from coils with increased spacing.

Honeywell. The device is in a small (.3" x .6" x .07"), package, and comes complete with a first-stage electronic amplifier. The sensitivity of the device is 5 mV/gauss. Since the desired magnetometer output was 2 V/gauss a voltage gain of 400 was required. This gain was supplied by a two-stage amplifier with low-pass filtering to limit high-frequency noise. The overall sensitivity was adjusted by potentiometer to be 2 V/gauss, while offset circuitry centered the output voltage to 2.5 Volts at 0 gauss. The magnetometer output was applied directly to the A/D converter on board the microcontroller. Since the A/D converter range was 0 to 5 Volts a magnetic field range of -1.25 gauss to +1.25 gauss was obtained.

The major problem encountered in the magnetometer design was temperature stability of the Hall Effect Device. Even though some temperature compensation is incorporated in the SS94A1 design, it was found that its output showed temperature drifts

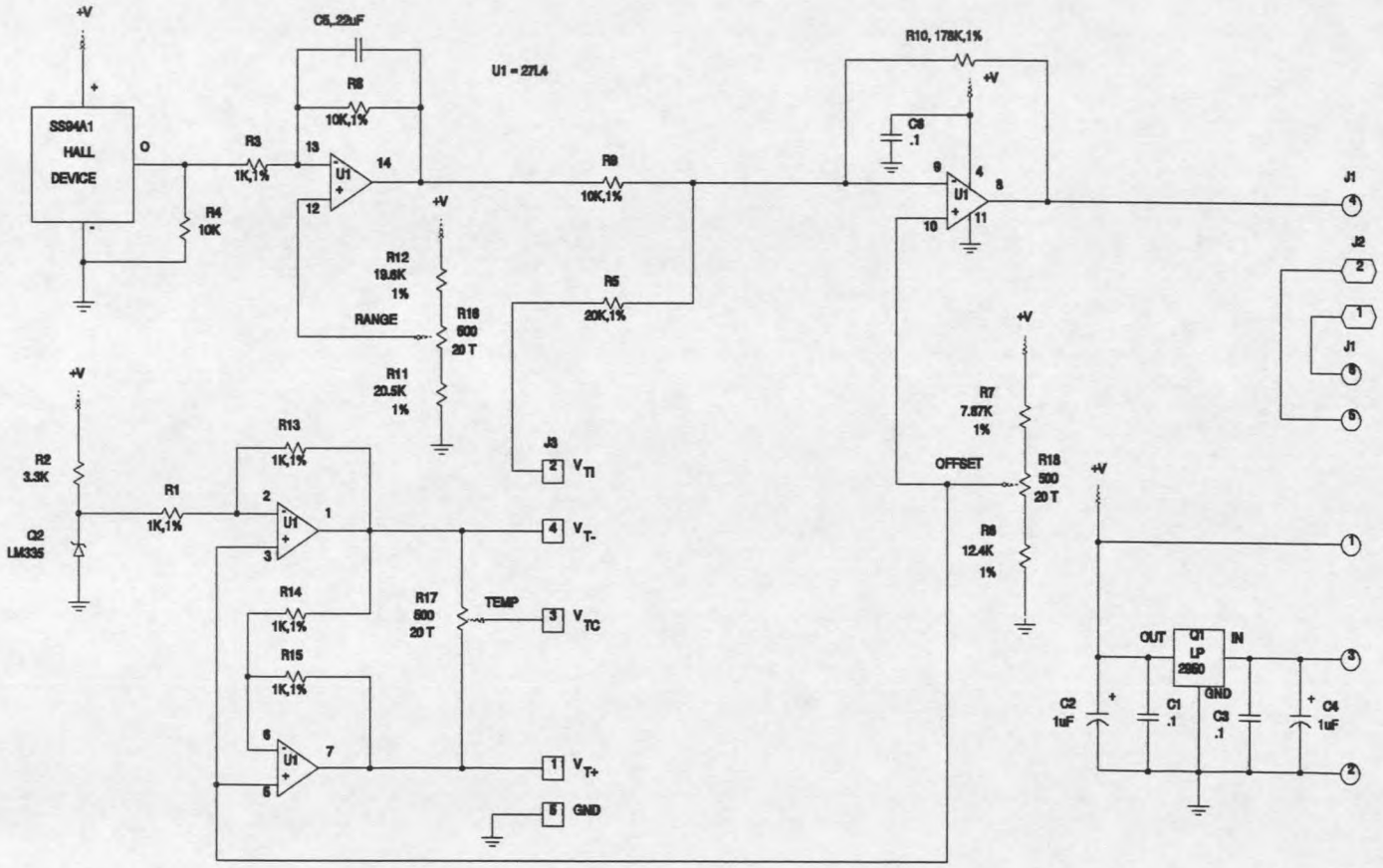

Figure 6. Magnetometer Electronics

of up to 5 mgauss/°C. Since specifications required that the DC field be held constant within plus or minus 10% of the .209 gauss target value, this temperature drift was clearly unacceptable. The final solution adopted was to incorporate a temperature sensitive device near the Hall Effect Device, and to use its output to provide a voltage compensation for the temperature drift. The temperature compensation allowed the magnetometer to operate over a 65°F to 95°F temperature range within the acceptable plus or minus 20 mgauss error limits. The main disadvantage of this temperature compensation was that each magnetometer had to be individually trimmed for correct temperature compensation. This is a time consuming procedure which is inefficient from a manufacturing standpoint. In addition, some of the magnetometers have exhibited long term output drifts. A burn-in period combined with periodic checks of the magnetometers are thus required. These inefficiencies have motivated a redesign of the magnetometer. Preliminary measurements have revealed that a fluxgate magnetometer design can yield accurate magnetic field measurements with far less temperature drift. However, it is beyond the scope of this thesis to document these additional magnetometer design efforts.

Patient Communication Circuitry

The patient communication circuitry consists of three small light-emitting diodes (LED's), a miniature beeper, and a pushbutton momentary switch. The three LED's are different colors (red, green and yellow). One or more of the LED's are flashed at three second intervals to indicate the status of the unit. Flashing yellow means the unit is ready to begin treatment for the day, and can be activated by pressing the switch.

Flashing green and yellow means that treatment is in progress. Flashing green means that treatment for the day is completed. When in this mode, the unit cannot be activated for treatment until the following day when the yellow light reappears. The beeper is used as an audible reinforcement of treatment start and finish. A flashing red LED means an error has been detected. Errors which can be detected by the unit include a disconnected drive cable to the coils, a low power supply voltage, or failure of the device to control the fields properly. The control failure can occur due to a hardware malfunction or an ambient field exceeding the correction range of the device. This failure is detected by the device as an overflow of its output drive capabilities while the control loop is in operation.

Real-Time Clock

The real-time clock (RTC) is an OKI Semiconductor integrated circuit designed to keep date and time accurately. The microcontroller programs the current date and time into the RTC during the device programming procedure. Thereafter the microcontroller has access to date and time via one of its parallel ports. Date and time information is used to apportion daily treatment periods, and to record date information in log entries.

Power On-Off Circuitry

In normal operation, the bone device was required to treat only 1/2 hour per day. During the remainder of the day, it was desired to shut off the power supply to the analog circuitry in order to prolong battery life. The power on-off circuitry accomplishes

this task using a single digital output from the microcontroller. Enhancement mode field effect transistors are employed to switch both positive and negative power supplies on and off under microcontroller control.

RS232 Communication Circuitry

The microcontroller must communicate with a host IBM compatible personal computer to allow device programming and retrieval of log data. The microcontroller has a built in serial port which supports asynchronous serial data transfers. The RS232 communication circuits are designed to convert the RS232 voltage levels of the IBM PC serial port to the CMOS logic voltage levels of the microcontroller serial port. In this way, direct communication between the serial ports is made possible.

Uses for the Device

The bone healing device is currently undergoing nationwide clinical tests for its effectiveness in stimulating repair of non-union bone fractures. The testing is being performed under the supervision of IatroMed Inc. in Phoenix, Arizona. Results of the testing cannot be released until the tests are complete. Meanwhile, the field-controlling and log-keeping capabilities of the device have enabled it to be adapted to several laboratory experiments with minor modifications. Specifically, the yeast metabolism and the plant growth studies described in Chapter 4 both employed a modified bone healing device in performing at least part of the experiments described.

CHAPTER 4

EXPERIMENTS AND RESULTS

Introduction

The experimental investigations briefly reviewed in Chapter 3 are a testimony to the ability of extremely low frequency electromagnetic fields to alter the behavior of systems of cells. Cyclotron resonant magnetic fields have been demonstrated to be effective in altering growth characteristics of bone tissue [Deibert et al.,1991; Smith et al.,1991], motility of marine diatoms [Smith et al.,1987,McLeod et al.,1987], and Ca^{2+} uptake in human lymphocytes [Liboff et al.,1987]. Some evidence also exists linking cyclotron resonant fields to effects on animal behavior [Thomas et al.,1986]. Based on the wide variety of cell systems that have demonstrated susceptibility to these fields, it appears likely that the processes of many other organisms might also be alterable. Part of the research work on which this thesis is based consisted of determining the effect of ion cyclotron resonant magnetic fields on two new biological systems. The two biological systems consisted of dry baker's yeast (Saccharomyces Carlsbergensis) in liquid culture medium, and legume plants grown from seed in vermiculite and distilled water. The experiments were undertaken in an attempt not only to verify the

effectiveness of cyclotron resonant fields in additional organisms, but to gain experimental data that would be helpful in formulating and evaluating models of field-cell interaction mechanisms. The procedures and results of the two series of experiments are described here in detail.

Yeast in Liquid Culture Medium

Yeasts have become a popular model system for investigating the biology of eukaryotic cells [Botstein and Fink,1988]. Yeast cells have also been reported to exhibit a resonant growth rate response upon exposure to weak microwave electromagnetic fields [Grundler et al.,1977]. These two factors, coupled with the known dependence of yeast cell system growth rates on ion concentrations in the culture medium [Morris,1958], prompted experiments to determine the effect of cyclotron resonant magnetic fields on yeast cells in liquid culture medium. Several minerals have been known to play an essential or at least stimulatory role in the growth and proliferation of the yeast cells in culture. These ions include phosphorous, chlorine, iodine, bromine, fluoride, potassium, calcium, and magnesium [Morris,1958]. In a series of experiments, resonant fields tuned to several of these ions were applied to yeast cells in various culture mediums at various temperatures, to ascertain their effect on yeast growth and metabolic rates.

Experimental Methods

Prior to each experiment, the liquid culture medium was prepared by dissolving 1.2 grams of L-glucose, 2.1 grams of peptone (bacto-peptone or phytone-peptone), and 3.3 grams of yeast extract in 500 ml of distilled, deionized water (18 MΩ-cm). For a

few experiments, one or more of these weights were altered. Such alterations are noted in the table of results to follow. This Yeast-Extract-Peptone (YEP), mixture was autoclave sterilized and allowed to equilibrate for a period of 12 hours to 7 days at 4°C. After equilibration, 100 ml of the YEP was removed from refrigeration, diluted with an equal amount of deionized water and warmed to the desired temperature. For most experiments, the initial YEP temperature was 25°C. After warming, .1 or .2 grams of dry baker's yeast (Saccharomyces Carlsbergensis) was added to the YEP and dissolved by swirling for at least 1 minute. The resulting mixture was divided equally between two 500 ml bottles and each bottle was capped. This yeast culture was allowed to remain in the bottles for a period of time varying from 2 minutes to 30 minutes before the beginning of the experiment. Unless otherwise noted, this equilibration time was approximately 30 minutes. At the end of the equilibration period, each of the bottles was placed into a receptacle in the exposure apparatus. The exposure apparatus consisted of 2 tightly wound wire solenoids (6 inches diameter, 11 inches long, 460 turns of #24 AWG wire). The solenoids' centers were separated by a distance of 7.5 inches. At the center of each solenoid was mounted a plastic and aluminum bracket designed to hold one experimental bottle so that the yeast culture in the bottle was positioned at the center of the solenoid. Both solenoids were mounted securely to a plastic platform which was in turn mounted to an oscillating shaker table. The function of the shaker table was to provide agitation for the yeast cultures in order to allow carbon dioxide gas trapped in the mixture to evolve. An illustration of the shaker table, solenoids and yeast culture bottles appears in Figure 7.

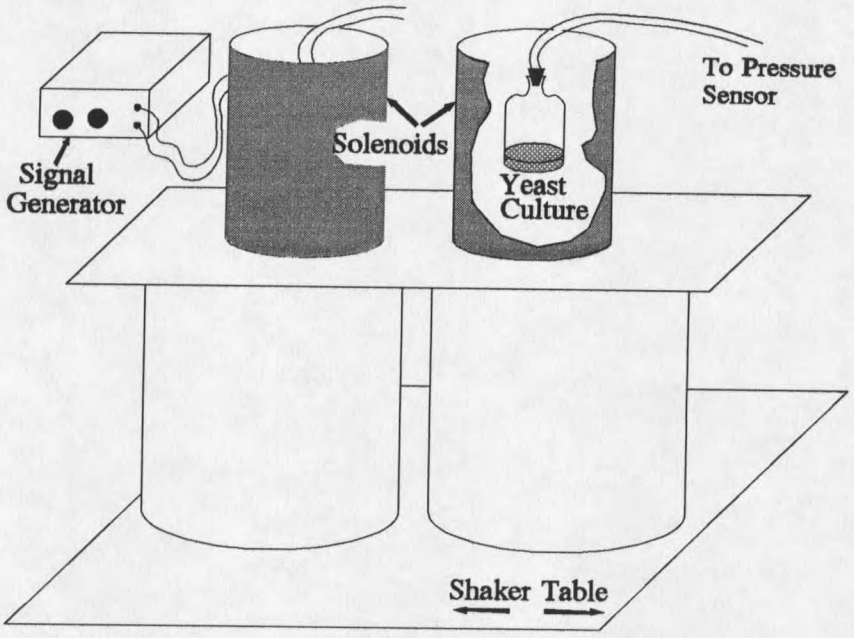

Figure 7. Setup for yeast experiments

During the course of each experiment, evolution of CO_2 gas was measured in the form of a pressure change in the sealed bottle. The amount of evolved CO_2 was meant to be an approximate measure of the proliferation and metabolic activity of the yeast cells in the culture. Two forms of pressure measurement were employed. The first method, used in experiments 1 through 46, measured the gas pressure in the bottle by noting the amount of the liquid culture forced up into a glass tube connected to the side of the bottle, as shown in Figure 8.

One clear disadvantage of this type of pressure measurement was that as the liquid was forced up the column, the volume of gas in the bottle changed, affecting the gas pressure. Also, as the liquid climbed the external column, significant amounts reached heights where the magnetic fields were no longer the same as at the center of

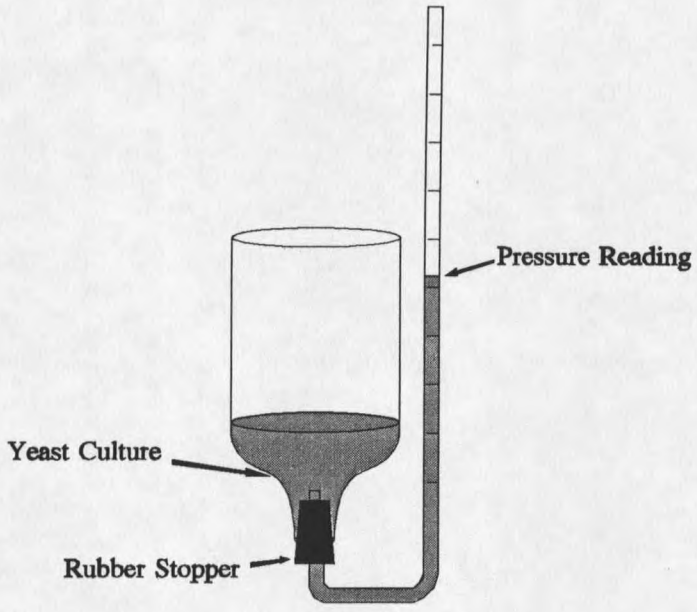

Figure 8. Pressure measurement by height of liquid column

the solenoid.

The second method of pressure measurement, used in experiments 47 through 101, employed electronic pressure sensors. The experimental bottles were sealed with rubber corks which had a small gas outlet in the middle. A plastic tube was connected from this gas outlet to a pressure sensor (Omega part number PX121-015DV). The pressure sensor was connected to some supporting electronics (constant current supply, output differential amplifier), and the resulting pressure dependent voltage output recorded at half hour intervals. A schematic diagram of the pressure sensor electronics appears in Figure 9.

Regardless of the pressure measurement method used, it proved essential to agitate the yeast cultures periodically to allow the CO_2 gas trapped in the liquid to

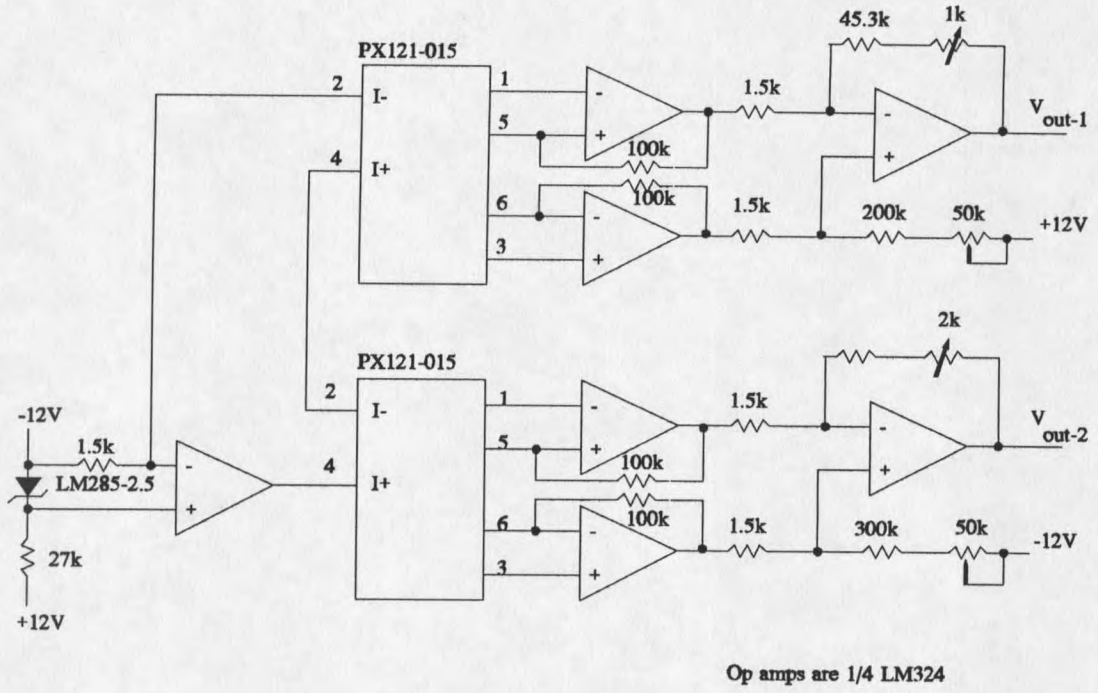

Figure 9. Pressure sensor electronics.

evolve. Under microprocessor control, the shaker table was turned on for a specified period every hour. The shaker oscillated at 100 rpm with a stroke of 1 inch. Pressure measurements were taken 1 minute after the completion of the automatic agitation. For experiments 49 through 101, the pressure measurements were made automatically via the A/D converter built in to an MC68HC11 microcontroller. The microcontroller was part of a device similar to the bone-healing device described in Chapter 3, but with several modifications to allow automatic control of these experiments.

Results

Table 3 in Appendix C summarizes the results of the many experiments

undertaken. When initial attempts to affect CO_2 evolution with exact ion cyclotron resonance fields failed to produce consistent results, several additional lines of investigation were followed. Experiments 79 through 87 and 95 through 98 represent a series of frequencies tested in an attempt to locate effects that may occur away from a known cyclotron resonant frequency. Experiments 35 through 40, 50 through 57 and 60 through 66 represent an attempt to "stress" the yeast by altering the pH with hydrochloric acid. Experiments 50,52 and 56 through 65 represent an attempt to add various concentrations of $CaCl_2$ to the medium before applying Ca^{2+} resonant fields. Although experiments 60 through 63 show that the addition of $CaCl_2$ to the culture at low pH did indeed affect the CO_2 evolution, the applied magnetic fields did not seem to alter this effect in any way. The pH was adjusted prior to the addition of $CaCl_2$, so the possibility remains that the $CaCl_2$ affected the CO_2 evolution rate by simply altering the pH. In experiments 71 through 78, the concentrations of one or more of the YEP ingredients were significantly altered in the hope that a deprivation of a particular ion would result, accentuating any effects that applied ion resonant magnetic fields might have. Experiments 88 through 94 represent another attempt to "stress" the culture by heat shocking the yeast culture mixture at 98°F to 104°F before the start of the experiment.

None of the experimental conditions attempted produced consistent magnetic field effects on CO_2 evolution by the yeast culture. A few large shifts appeared under certain conditions, but upon further investigation they were found to be due to an equipment calibration problem or another experimental artifact. The experimental system was

chosen for its relative ease of use and the short duration of experiments, in conjunction with its common use as a good model of eukaryotic cell systems. The ineffectiveness of the fields to affect the yeast metabolic rate may signify that the system is not sensitive to such fields, or that the proper conditions for observing such an effect were not discovered.

Plant Growth

After the extensive experimentation with yeast cultures failed to show a magnetic field effect on growth or metabolic rates, attention was shifted to the growth of plants as another process which might exhibit sensitivity to ion cyclotron resonance field conditions. As a first step, it was decided to test plant growth exposed to Ca^{2+} resonance conditions. The choice of the Ca^{2+} ion as a starting place is logical from several viewpoints. All of the previous systems that have shown susceptibility to cyclotron resonant fields have been particularly sensitive to Ca^{2+} tuned fields. Also, the requirement of plants for Ca^{2+} is well known. Concentrations in the range of .1-1 mM are normally required for plants to maintain normal structure and function. The growth of plant root systems is especially sensitive to Ca^{2+} deprivation [Campbell,1983]. It was therefore decided to test the growth of plants exposed to Ca^{2+} resonant fields from seed planting through a two week period of growth. Several different kinds of seeds were tested in pilot studies to estimate the effectiveness of the Ca^{2+} resonant fields on their growth characteristics. As a result of the pilot tests, Romano bush beans (Phaseolus Vulgaris) were chosen as the focus of further studies. The beans were obtained from the

Lilly Miller Co. of Portland, Oregon.

Experimental Methods

The pots used to contain the plants were 12" x 9" x 2.5" clear plastic containers with 20 small slots cut in the bottom to allow circulation of water into and out of the pot. At the start of each experiment, vermiculite was poured into each of two such containers to a depth of 1.75" and smoothed into a level surface. On top of this vermiculite layer the seeds were planted with their hilum facing down into the vermiculite. For most experiments, 24 seeds were planted in each container in 3 rows of 8 seeds each. The seeds were then covered with an additional .5" of vermiculite. Each of the plastic containers was then placed within a larger plastic container (14" x 10" x 3"), and the combination was placed in one of the experimental sites. Each experimental site consisted of a platform in the center of a 24" diameter Helmholtz coil pair. Directly over each platform at a distance of 24 inches was a 75 watt incandescent grow-light (Sylvania Spot-Gro). Each experiment requires two identical coil setups, one for control plants and one for those exposed to the magnetic fields. The two setups were placed 3 feet apart to minimize coupling of the magnetic field from the treated site to the control site. The entire experimental setup is illustrated in Figure 10.

As each experiment was begun, the magnetic field parameters at each site were recorded. These parameters include the DC and AC magnetic fields along the coil axis, and the magnitude of any extraneous AC fields present. In general, extraneous 60 Hz magnetic fields existed at approximately a level of 5 mgauss peak-to- peak. For most experiments, the AC magnetic field at the treatment site had an amplitude of .4 gauss

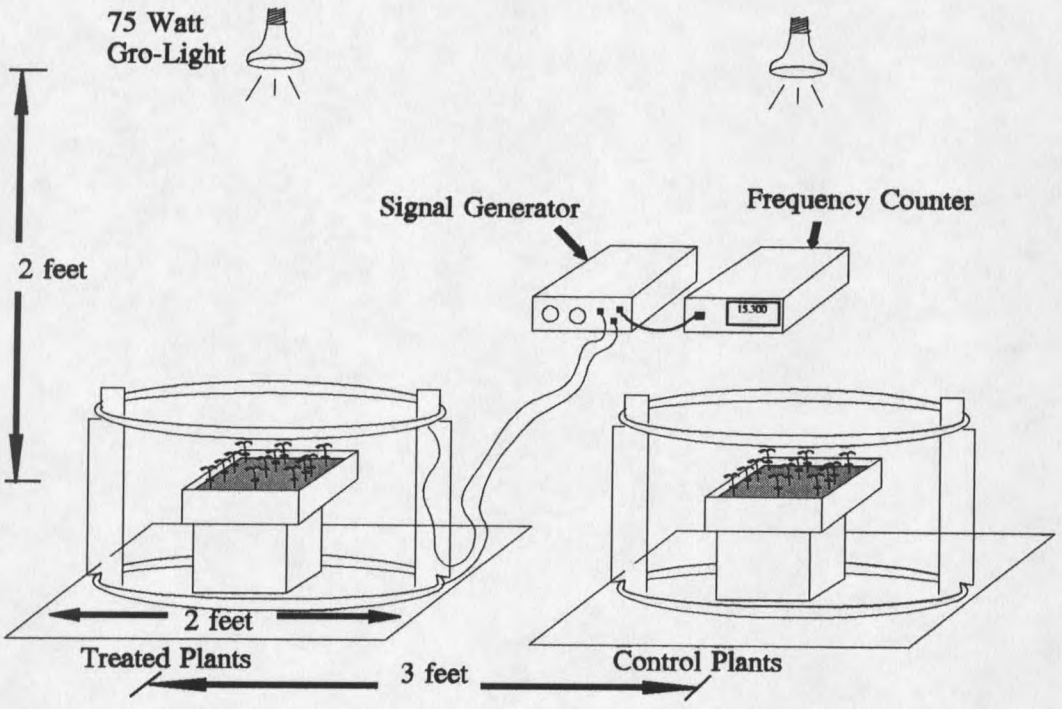

Figure 10. Setup for plant experiments

peak-to-peak at a frequency of approximately 15 Hz. Slight coupling of this AC magnetic field to the control site resulted in a corresponding AC field of approximately 5 mgauss peak-to-peak at the control site.

On the first day of each experiment, one liter of distilled, deionized water was added by pouring it into the outer plastic container and letting it soak into the inner one. On each day thereafter, 150 ml of deionized water was added in the same manner. Daily records of temperature and height of plant stems were kept on a standard data sheet. Examples of the standard protocol and data sheets are included in Appendix D. Termination of the experiment occurred when the plants reached an average stem height of approximately 12-20 cm. The experiment duration varied from 11 to 16 days,

depending on the ambient temperature of the laboratory during the experiment. At the termination of the experiment, the root and plant masses of each of the plants were recorded in the data sheet. Visual data plots and statistical analyses were performed for each of three experimental parameters: plant height, root mass, and plant mass.

Results

Figures 11 through 22 visually summarize the results of applying Ca^{2+} cyclotron resonant fields to the bean plants during their growth period. Each plot represents the data taken at the termination of one experiment, and each "*" character on the plot represents an individual measurement of root mass, plant mass, or plant height as labelled. Each of the data points is normalized to the mean of the control sample for the given parameter. Results of treated and control plants are juxtaposed for easy comparison. A dotted line joins the means of the control and treated samples for each parameter while horizontal lines mark one standard deviation on either side of the sample mean for all samples. The legend in the upper left corner of each plot shows the magnetic field, temperature conditions, and the day on which the plants were harvested.

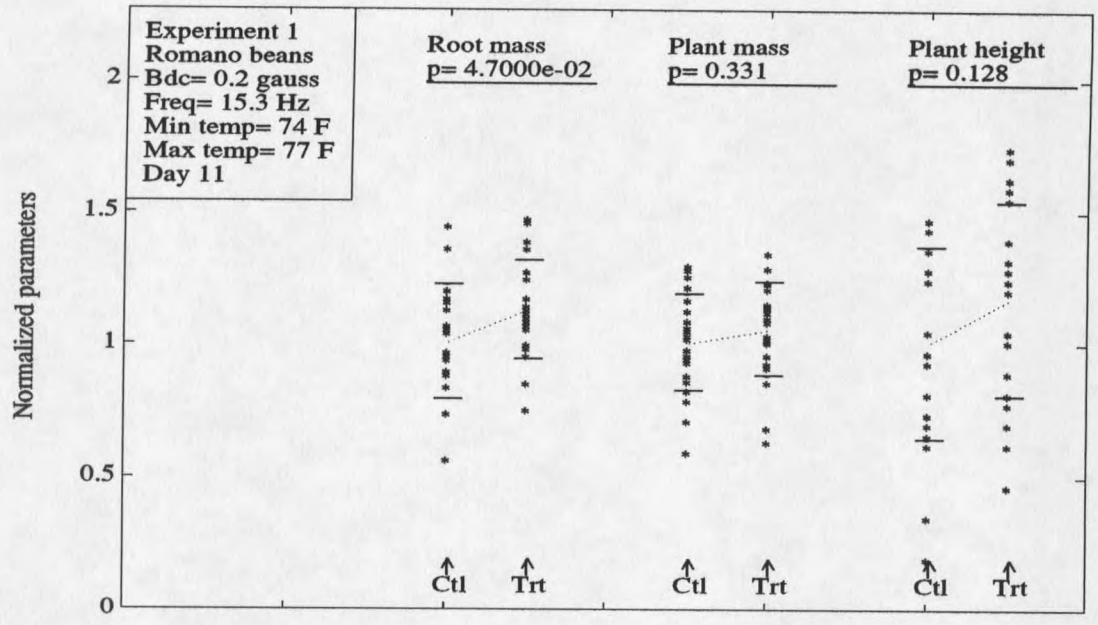

Figure 11. Results of plant experiment 1.

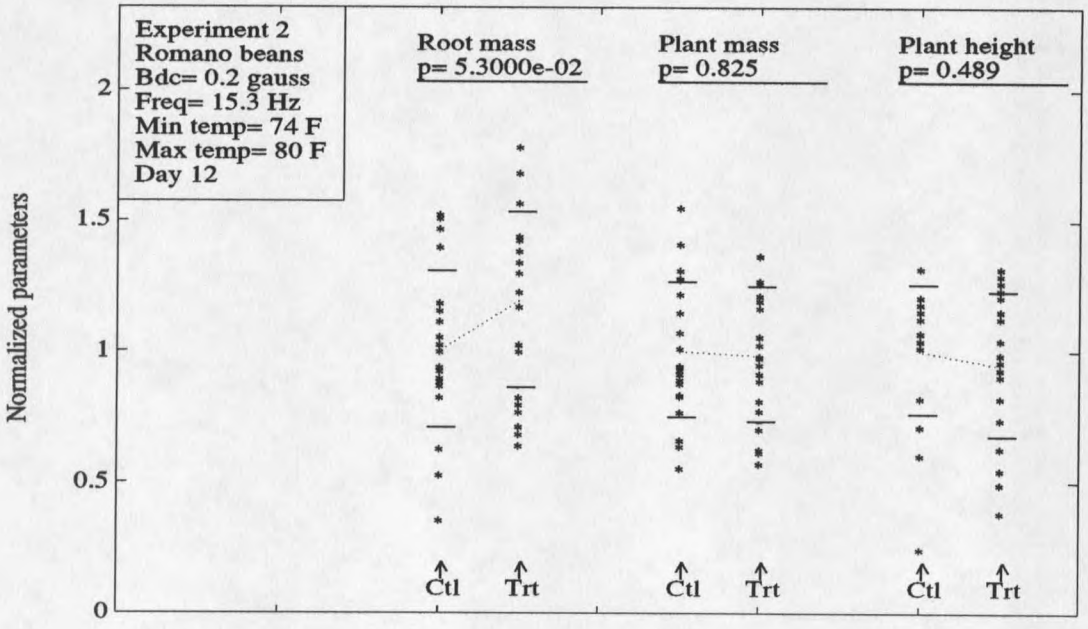

Figure 12. Results of plant experiment 2.

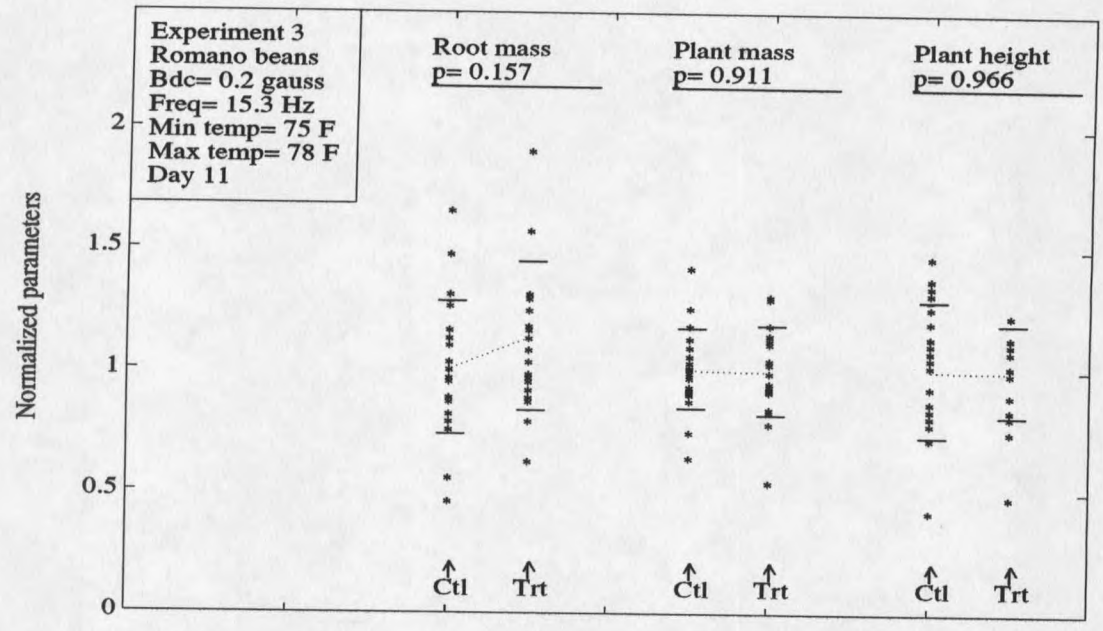

Figure 13. Results of plant experiment 3

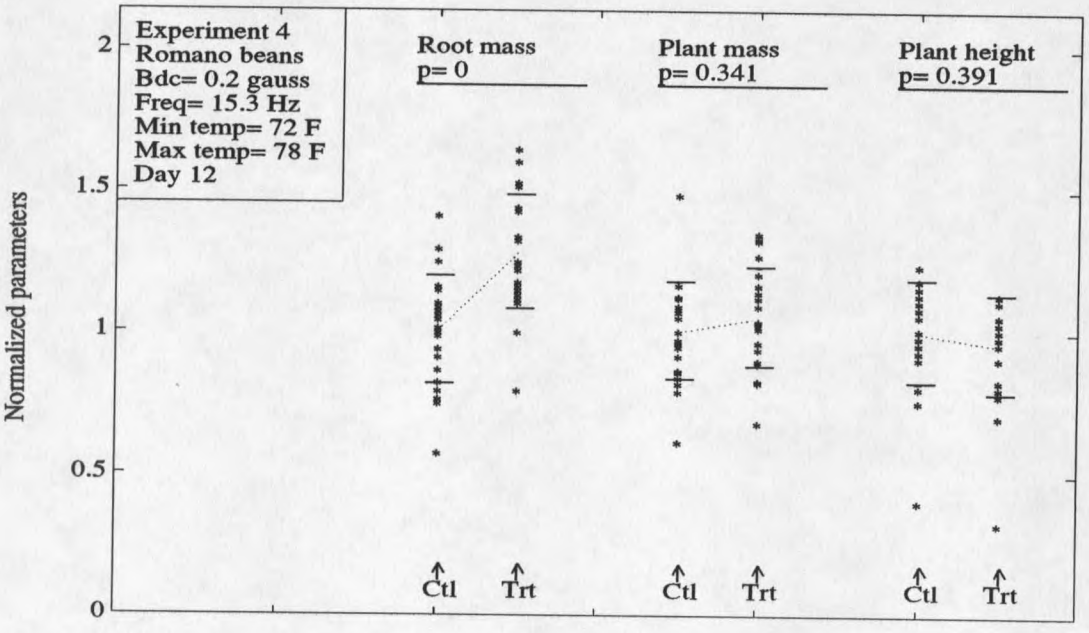

Figure 14. Results of plant experiment 4.

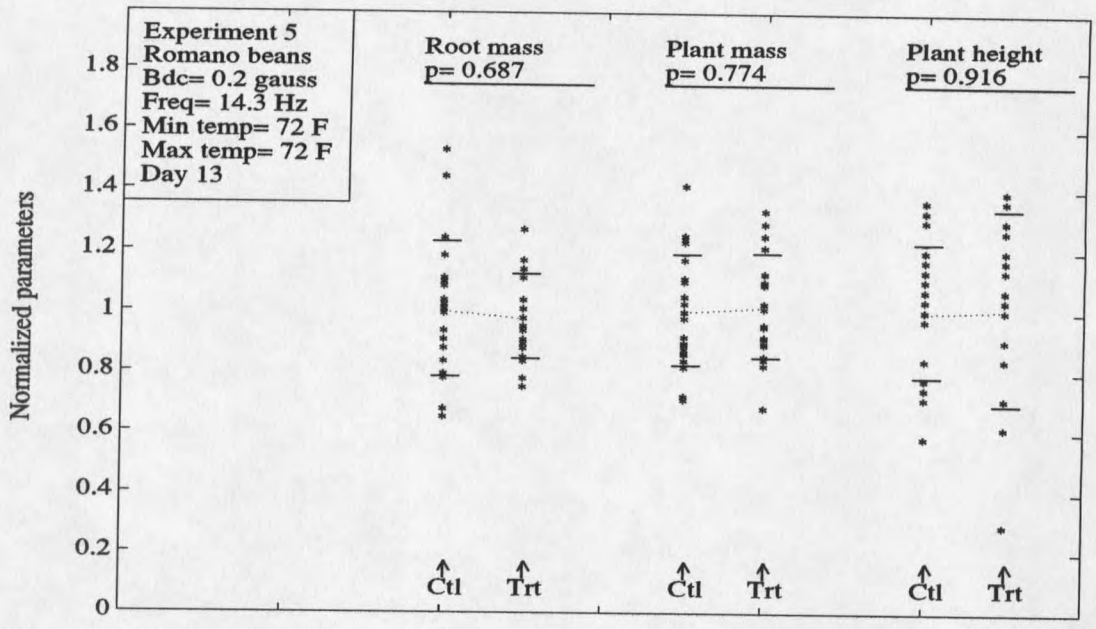

Figure 15. Results of plant experiment 5.

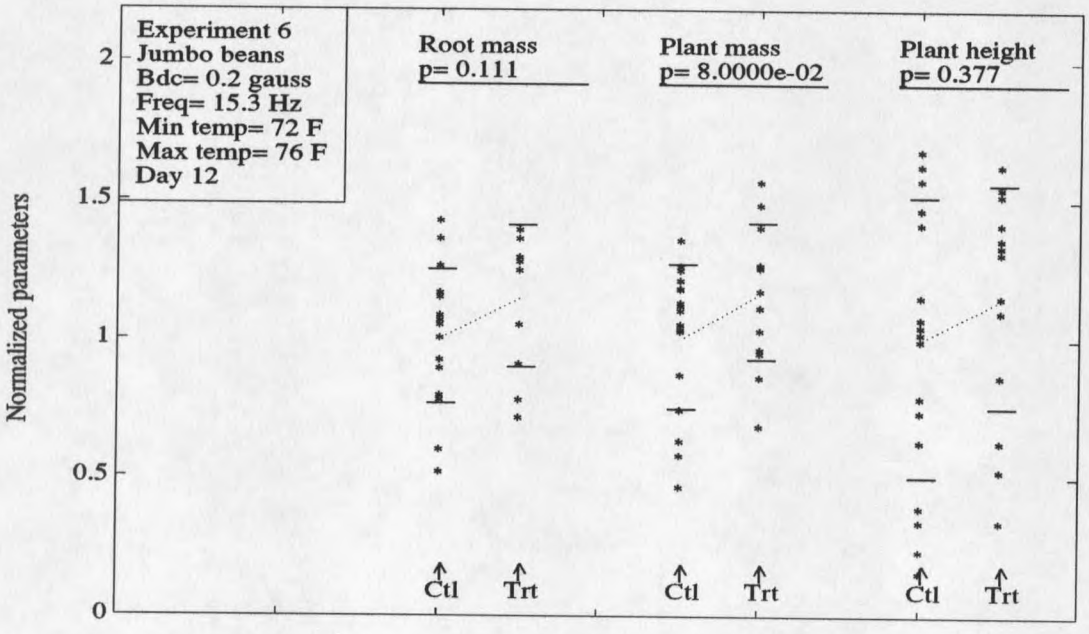

Figure 16. Results of plant experiment 6.

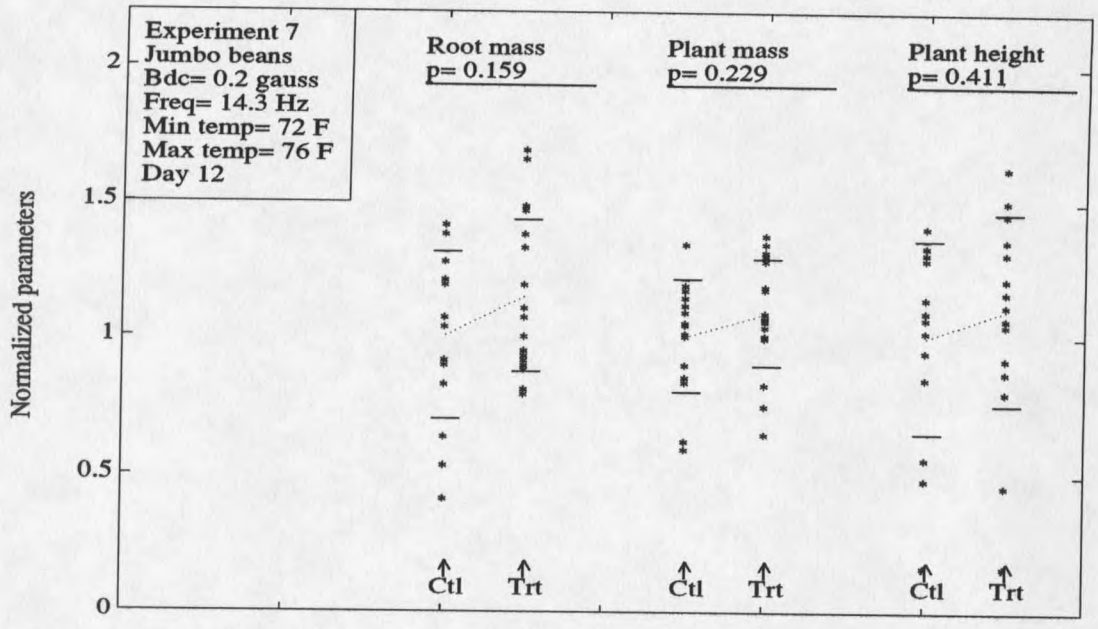

Figure 17. Results of plant experiment 7.

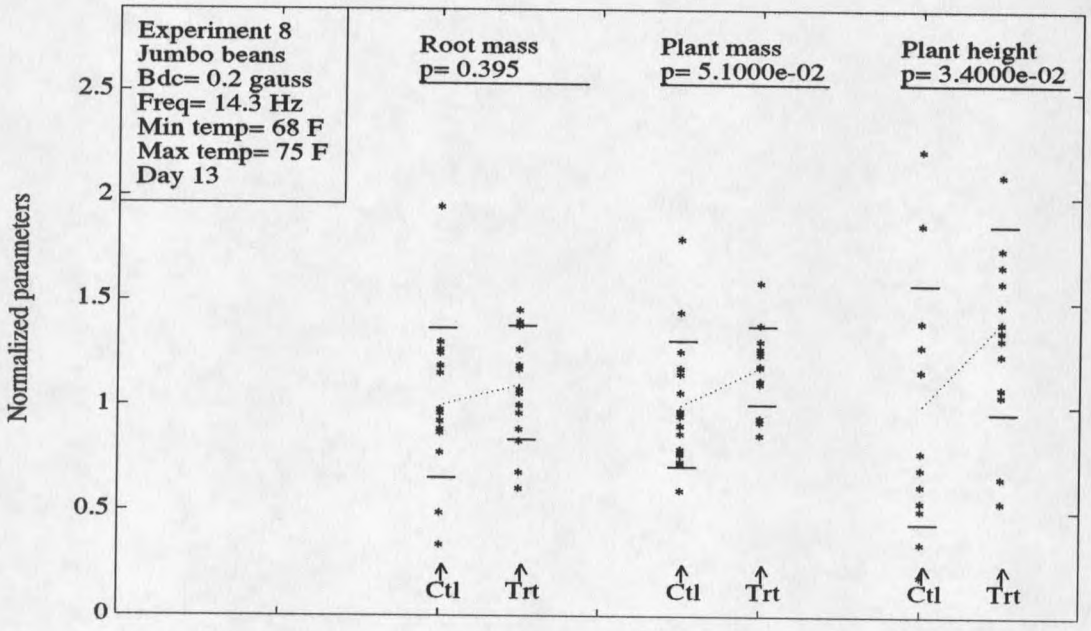

Figure 18. Results of plant experiment 8.

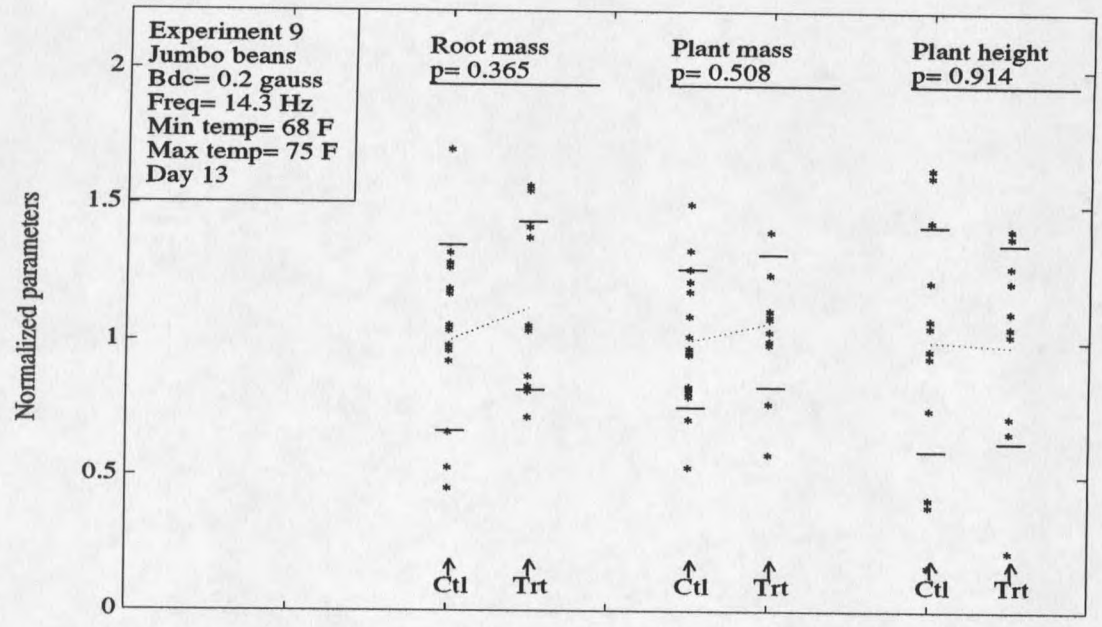

Figure 19. Results of plant experiment 9

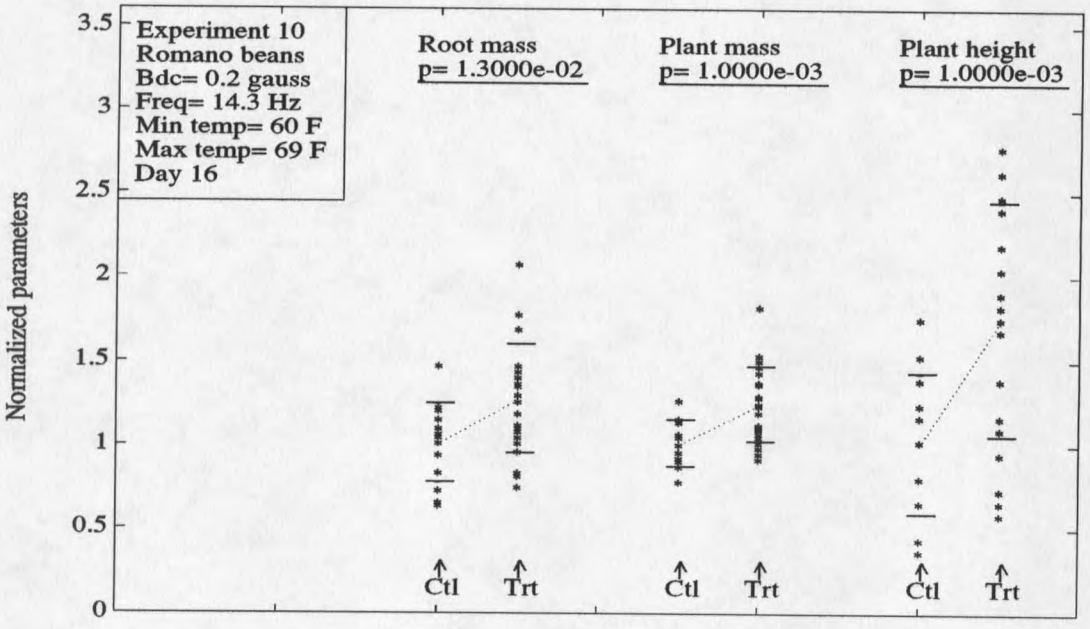

Figure 20. Results of plant experiment 10.

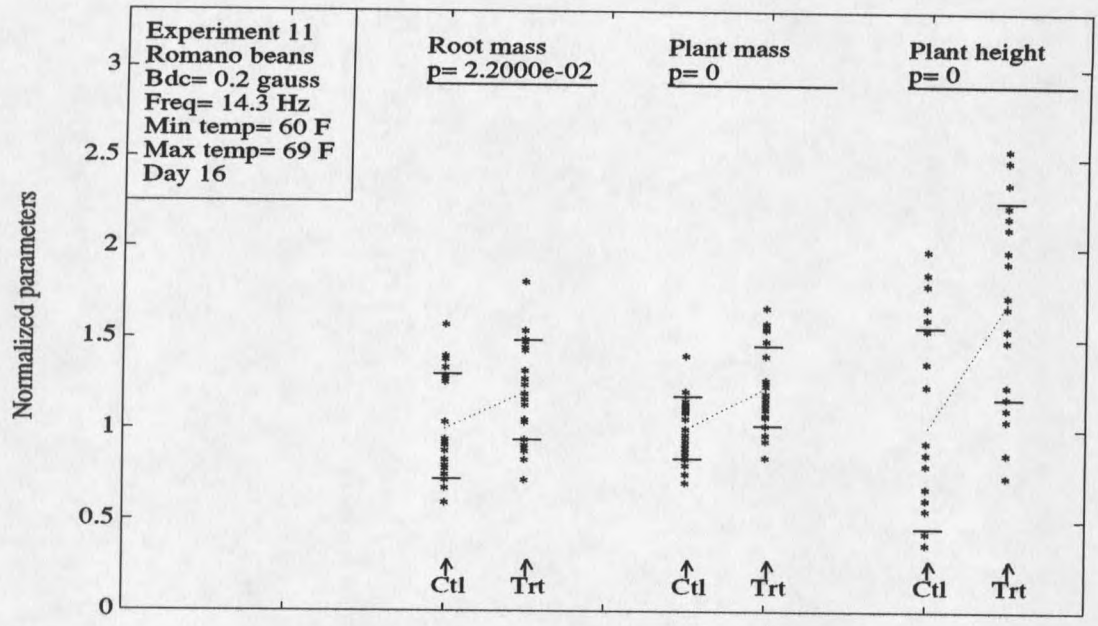

Figure 21. Results of plant experiment 11.

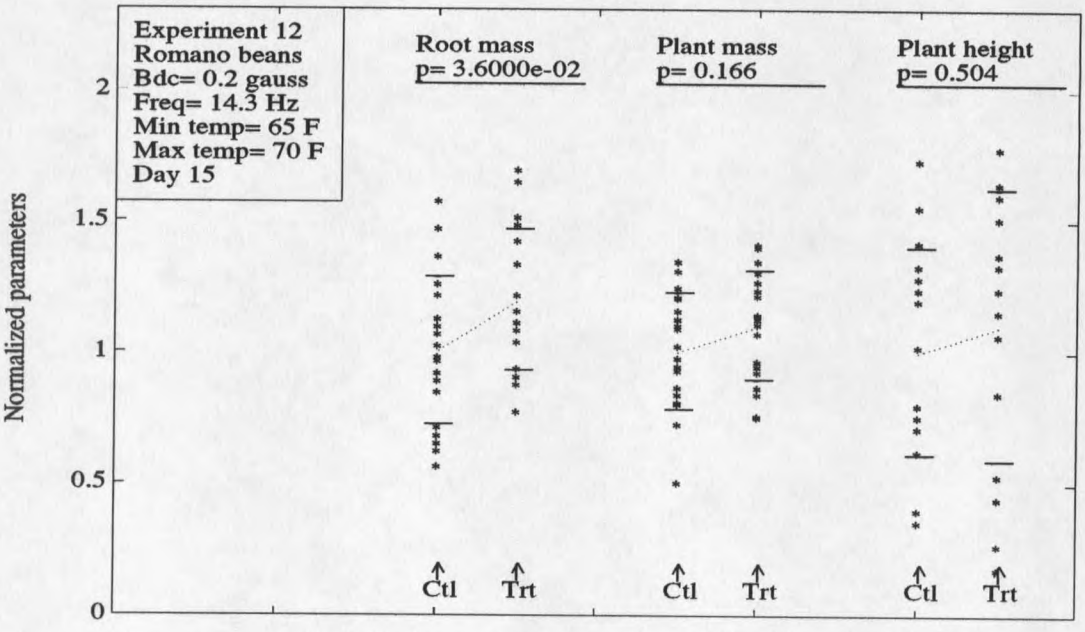

Figure 22. Results of plant experiment 12.

For all experiments, the DC magnetic field was maintained at .2 gauss and the AC magnetic field amplitude was also held at .2 gauss peak. For some experiments, the AC frequency was varied slightly around the Ca^{2+} cyclotron resonant value of 15.3 Hz in an attempt to determine if the results exhibited a resonant behavior around the center frequency.

Experiments 1 through 4 were performed with the AC frequency tuned to exact cyclotron resonance conditions for Ca^{2+} (15.3 Hz). The ambient temperature throughout the experiments was kept in the range of 74°F to 80°F. The experiments were performed at two different locations. Two experiments were performed in succession at each location. The sites of the control and treated plants were switched between successive experiments so that any site-dependent artifacts would be apparent. For each experiment, 24 plants per container were originally planted, but roughly 2 or 3 plants from each container failed to sprout, and these plants were excluded from the data pool.

A first glance at the visual plots of experiments 1 through 4 reveals a consistent but moderate (20-25%) increase in root mass of treated plants versus controls. By contrast, neither plant mass nor plant height exhibited consistent differences between control and treated samples. Statistical analysis of the data began with an analysis of variance to determine the validity of using a pooled estimate for the population variance. No significant variance differences were found, and consequently the statistical tests for mean differences were performed using a one-sided student's t test with a pooled variance estimate and degrees of freedom equal to the sum of the number of treated and control plants minus 2. The p values obtained for these t tests on the mean are shown

on the experiment data plots. A statistical examination of the apparent trend toward larger root masses in treated plants shows that a significant shift does in fact exist. Two of the four individual experiments (1 and 4), show significant increases in root mass of treated plants ($p<.05$). The root mass increase in experiment 4 was especially significant ($p<.0001$). A statistical analysis of the pooled data from experiments 1 through 4 revealed a highly significant ($p<.0001$) increase in root mass of approximately 19%. By contrast, the pooled data for plant mass and plant height showed almost identical mean values for treated and control plants.

Experiments 6 through 9 involved bean plants of a slightly different kind from the other experiments. The seeds were obtained from a different company (Nichols Garden Nursery, Portland Oregon), and were slightly larger than those obtained from Lilly Miller Co. Experiment 6 involved exact Ca^{2+} cyclotron resonance conditions and 72°F to 76°F temperatures. The results showed moderate increases in all three experimental parameters, but none were highly significant. Experiments 7 through 9 employed an AC frequency of 14.3 Hz, which is 1 Hz lower than the calculated resonant value for Ca^{2+}. The treated plants in all three experiments all showed moderate increases over controls for all three experimental parameters. Viewed individually, none of the experiments demonstrated highly significant differences. However, the pooled results yield significant increases in root mass and plant mass ($p<.05$), while the plant height difference was nearly significant at the .05 level ($p=.061$).

Experiments 10 through 12 were performed using the original Lilly Miller seeds. All three were performed at the lower 14.3 Hz AC frequency. During these experiments,

an attempt was made to keep the ambient temperature in the laboratory low. However, poor temperature regulation resulted in fairly wide temperature fluctuations throughout the course of the experiments. Experiments 10 and 11 were carried out under the lowest temperature conditions. Though the temperature varied widely during the experiment (60-69°F), it clearly had an adverse effect on plant growth. Growth was much slower than in previous experiments run at 75°F. In these two experiments, the treated plants showed significant increases of all three experimental parameters over control plants ($p<.022$). This level of significance was obtained without a need for pooling the results of the two experiments. When pooled, the experiments showed highly significant shifts in all three parameters ($p<.002$ for root mass, $p<.0001$ for plant mass and plant height). Experiment 12, which did not reach such cold temperatures as did experiments 10 and 11 (65-70°F), exhibited the same pattern of results seen in the earlier experiments involving higher temperatures (experiments 1 through 4). A significant ($p<.005$) increase in root mass was evident, but moderate increases in plant mass and plant height were not significant.

Conclusions and Interpretation

The results of the plant experiments described above provide evidence for an effect of magnetic fields at or near cyclotron resonance conditions on the growth of bean plants. The effect on root mass appears to be the most pronounced. At higher temperatures (70-80°F), the fields appear to have no significant effect on either plant mass or plant height. The greater sensitivity of root growth to the fields seems to be consistent with the known special sensitivity of plant roots to Ca^{2+} concentrations

[Campbell,1983].

The addition of an environmental "stress" factor in the form of low temperatures (60-65°F) appears to accentuate the effect that the fields have on plant growth. Several theoreticians [Adey,1990; Findl,1987; McLeod et al.,1991), have proposed that biological systems may be more susceptible to low frequency electromagnetic field effects if some additional factor stresses the system or moves it away from equilibrium conditions. The altered low temperature behavior in these experiments may point to temperature as a possible stress factor in the plant system.

The results outlined here are consistent with an effect of low frequency electromagnetic fields on the growth of bean plants. However, additional questions remain to be answered by future investigations. The effect of varying the AC frequency around the calculated cyclotron resonant value needs further quantification. Of particular interest is whether or not a resonance curve similar to that exhibited in diatom motility [Smith et al.,1987], and Ca^{2+} uptake in human lymphocytes [Liboff et al.,1987] results. The temperature effect can also be further quantified under conditions of better temperature control. Only then can the actual role played by temperature in the process be more clearly determined.

CHAPTER 5

IONS IN CELL LIFE

Introduction

A basic understanding of living cells and their processes is indispensable to an ability to propose and evaluate models of electromagnetic field interaction with cells. As described in Chapter 3, a large body of evidence has implicated ionic flux as being a prime mechanism for the interaction. All of the currently proposed models involve ion dynamics in some way. Thus, a working knowledge of the importance of ions in cell life, and the methods by which cells regulate ion movements are essential. The following pages are included as a review of cell structure and processes with a special emphasis on the role of ions.

Living Cells and Ions

Living cells vary widely in size and shape. However, for the purposes of this work, a cell can be reasonably approximated as a spherically shaped object of radius 10 μm [Weaver and Astumian,1990]. The boundary which separates the cell from its external environment is known as the cell membrane. The material inside the cell consists of the nucleus, housing the genetic code in the form of DNA, and the cytoplasm.

The cytoplasm consists of a semifluid medium called the cytosol, in which are suspended various specialized compartments called organelles. Surrounding each of the organelles is another membrane which defines its boundaries.

Cells undergo many complicated metabolic processes to stay alive. It has long been known that the movement of electrically charged particles (ions), is an integral part of many of these processes. A well known example is the rapid exchange of Na^+ and K^+ ions that creates a voltage spike known as an "action potential" in nerve cells. This voltage spike is transmitted from cell to cell and forms the basis for the electrical communication essential to the nervous system of animals [Campbell,1987]. Far from being an isolated example, this is but one of a great many roles that ions play in animal and plant physiology. Among those ions most prevalent in biological systems are the elemental metallic ions calcium (Ca^{2+}), potassium (K^+), sodium (Na^+), and magnesium (Mg^{2+}). Several others, both cations and anions, play lesser roles in cell physiology. Many of the experiments documented in Chapter 3 have demonstrated that weak, low frequency electromagnetic fields can alter calcium ion flux across the cell membrane [Bawin et al.,1975; Bawin and Adey,1976; Bawin et al.,1978; Blackman et al.,1979; Blackman et al.,1980a; Blackman et al.,1980b; Blackman et al.,1982; Blackman et al.,1985; Lin-Liu and Adey,1982]. This effect has wide implications, as evidenced by the wide range of cell processes in which the calcium ion plays a role.

The calcium ion has been experimentally shown to affect many cell processes. Cell motility, muscle contraction, cytoplasmic streaming, chromosome movement, neurotransmitter release, endocytosis, and exocytosis are examples of processes in which

Ca^{2+} plays a crucial role [Cheung,1980]. Calcium has been shown to be an important triggering mechanism in the activation of T-lymphocytes by an antigen [Lewis and Cahalan,1989], and to play a role in numerous processes in brain cells, including cell shape and mobility, energy metabolism, and body thermoregulation [Michaelson,1985]. The calcium ion plays an essential role in several events in the normal mitotic cell division cycle [Poenie et al.,1985], and its concentration in the extracellular medium has been shown to affect proliferation rates of cells [Shirakawa et al.,1986]. In nerve cells, the intracellular calcium concentration increases during each action potential, and eventually reaches concentration levels which activate cytoplasmic proteins that change the morphology of the cell [Smith et al.,1983; Silver et al.,1990]. Calcium ions in the extracellular medium are essential for normal DNA synthesis in many cells [Swierenga et al.,1978]. Calcium ions are used by ameboid cells to regulate contraction and relaxation which allow the ameboid cell to move [Taylor et al.,1980].

The functions of the calcium ion sketched above are representative of the roles of messenger and regulator that ions play in cell life. The demonstrated effect of electromagnetic fields on ionic flux have therefore led to the hypothesis that a majority of the physical effects of electromagnetic fields on organisms are the direct result of an effect on ionic flow into or out of the cells of the organism. All of the models for cell-field interaction to be reviewed in Chapter 6 involve some sort of field effect on ion dynamics. Ideas concerning interaction, therefore, must be based on a working knowledge of the mechanisms by which cells regulate their ionic concentrations.

Membranes as Regulators

The cell membrane does more than just define the boundary of a cell. The membrane is responsible for maintaining molecular and ionic concentrations in the cell to maintain the delicate balances required for life. The chemical makeup of the external milieu and the internal cytoplasm of a cell are widely different, and the membrane acts as the primary barrier preventing indiscriminate diffusion of biological materials from ruining the internal environment. The cell membrane is generally 50 to 75 angstroms thick [Stein,1986]. Structurally, it has the form of a bilayer of phospholipids with hydrophilic head groups (phosphate groups), and long hydrophobic tails (fatty acid chains) [Stein,1986]. This lipid bilayer forms a formidable barrier against the entry or exit of electrically charged particles, though small electrically neutral molecules such as water can pass freely. In the bulk solution outside the cell, ions are surrounded by several layers of water molecules, called hydration shells. The hydration shells reduce the free energy of the ion by orienting their dipoles to mitigate the electric field created by the ion. The ion can thus exist in a stable state in an environment with a high dielectric constant. The bilipid layer of the membrane is such an effective barrier to ions because of its low dielectric constant. To move from a medium with high dielectric constant (filled with water molecules), to a medium of low dielectric constant (the lipid region), requires a large increase in free energy of the ion, since the water bonds must be broken and the lipid region has few polarizable molecules to replace these bonds. The energy difference between the two states is proportional to the difference of the reciprocals of the two relative dielectric constants [Hille,1984]. Since the relative

dielectric constant of the extracellular fluid is approximately 80 and the membrane lipid relative dielectric constant is approximately 2 [Levitt,1978], the membrane presents a large energy barrier to ions. This large energy barrier effectively makes the bilipid layer impermeable to ions.

Ions are able to cross cell membranes, however, by means of membrane channels and ion carriers. Membrane channels are small pores formed by protein molecules spanning the membrane. One or more proteins cooperate to form a helical structure through the membrane [Unwin,1986]. Through the center of the helix a small pore is formed. Polar carbonyl groups in the protein molecules form part of the wall of the pore [Jordan,1984; Kwang,1985] , and thus the pore, or channel, presents an essentially hydrophilic environment [Stein,1986], reducing the energy barrier of the membrane as viewed by an ion [Parsegian,1969; Levitt,1978]. Calculations have indicated that the energy barrier can be reduced from approximately 40 kT to 2 kT [Parsegian,1969; Levitt,1978]. The reduced energy barrier allows ions with sufficient thermal kinetic energy to pass through the channel and thus the membrane. The effect of channel-forming proteins on membranes is to dramatically increase the permeability of the membrane to ions. Artificial membrane resistances are on the order of 10^8 ohm/cm^2. Addition of channel forming proteins to the membrane can reduce this resistance by a factor of 10^6 [Parsegian,1969].

The force responsible for driving ions through pores results from an electrochemical gradient. This gradient consists of contributions from concentration differences (chemical gradient), and electrostatic forces (electrical gradient). Across a

resting cell membrane a voltage, called the resting potential, is developed. Typical values for the resting potential range from 40 to 100 mV, with the cell interior at a lower potential than the exterior [Hille,1984]. Since the membrane is so thin (typically 50 angstroms), this voltage represents a very high electric field (10^6 V/m), which can exert strong forces on electrically charged particles.

The other method by which ions are transported across cell membranes is by active transport, which is accomplished by ion carriers. The process of active transport also takes place inside membrane spanning protein molecules. However, active transport differs from channel transport in that energy is required to drive the process, allowing ions to be transported against an electrochemical gradient.

Examples of Ionic Channels

Several ionic channels have been extensively studied in recent years. The best characterized channel is that formed by the gramicidin A molecule. When added to a phospholipid membrane, gramicidin dramatically increases the permeability of the membrane to cations [Stein,1986]. Another much studied channel is the acetylcholine receptor channel which binds the neurotransmitter acetylcholine, allowing communication between adjacent nerve cells. A channel permeable to light molecules (less than 800 daltons), has been found to span the gap between adjacent cells, allowing communication between the cells in the form of diffusion of molecules back and forth. This important channel is known as the gap junction [Unwin and Zampighi,1980]. A third channel whose DNA sequence has been reported is the cell membrane sodium channel. The

sodium channel is an example of a voltage dependent channel; its permeability to the sodium ion depends on the voltage across the membrane in which it is imbedded. Ionic channels are not limited to the plasma membrane of the cell. Similar channels are found in the membranes forming the boundaries between the cell cytosol and the various organelles in the cytoplasm. A channel highly permeable to potassium ions occurring in the membrane of the sarcoplasmic reticulum has been experimentally examined [Stein,1986].

The experimental method of single channel recording [Sakmann and Neher,1983], has allowed the identification of many ionic channels that are not yet well characterized in structure. Approximate conductances of many of these channels have been reported. Stein [1986], provides a list of these channels and some of their experimentally determined characteristics.

Channel Structure

The ionic channels that have been well characterized to this point reveal remarkable similarities in structure. The DNA sequence of the proteins that make up the various channels are similar in hydropathic characteristics [Unwin,1986]; they all have one or more amino acid chains approximately 20 residues long that are hydrophobic in nature. These regions are likely to be the membrane-spanning helically shaped regions [Unwin,1986]. The helical shape is maintained by hydrogen bonds between loops of the helix, with the bonds directed along the helix axis [Hille,1984]. Some of the proteins appear to span the membrane multiple times [Unwin,1986]. Usually, more than one such

protein is required to form a channel. The proteins will cluster in a remarkably symmetrical way to form the central pore of the channel, as barrel staves around the center of a barrel [Stein,1986]. The central pore diameter is a function of the number of clustered protein molecules that form its walls. A tetramer configuration (the sodium channel), yields a pore diameter of approximately 4 angstroms, a pentamer (the acetylcholine receptor), 7 angstroms, and a hexamer (the gap junction), 16 angstroms [Unwin and Zampighi,1980].

Electron microscopy and x-ray diffraction have been used to obtain views of the overall structure of some ionic channels. The images obtained have several characteristics in common. The most striking trait is the high degree of symmetry of the channel subunits around the central pore. When viewed end on, the subunits appear to be equivalently spaced, creating polygonal symmetry according to the number of subunits that form the channel walls [Brisson and Unwin,1985; Unwin and Zampighi,1980; Hucho et al.,1986; Toyoshima and Unwin,1988]. The channel mouth extends significantly into the extracellular fluid and has a relatively wide diameter. The mouth of the gap junction channel has a diameter of 20 angstroms [Unwin and Zampighi,1980]. The mouth diameter of the acetylcholine receptor channel has been reported at 30 angstroms [Brisson and Unwin,1985], and 25 angstroms [Toyoshima and Unwin,1988]. A pronounced constriction of the channel diameter at the cytoplasmic end also appears to be a common trait of the channels studied. Images of both the acetylcholine receptor [Toyoshima and Unwin,1988], and gap junction [Unwin and Zampighi,1980] channels show a narrowing of the channel diameter to a width unresolvable by the imaging

apparatus (less than 10 angstroms). The acetylcholine receptor widens again to a diameter of 20 angstroms as it enters the cytoplasm [Toyoshima and Unwin,1988]. A theoretical model of the structure of the K^+ channel in the sarcoplasmic reticulum, based on experimental evidence obtained from various channel blockers, bears a close resemblance to the actual images of the other channels described above [Stein,1986].

From the viewpoint of electrostatic environment, the gramicidin A channel has been most well defined. The gramicidin molecule is a chain of 15 amino acids [Stein,1986] that is not long enough to span the membrane completely by itself. Two gramicidin molecules join end to end to form a dimer which spans the membrane [Stein,1986; Jordan,1984]. The resulting channel is 26 angstroms long and approximately 6.8 angstroms in width, with a 4.2 angstrom diameter pore at its center [Jordan,1984; Koeppe et al.,1979]. The molecule has identical cation binding sites 2.5 angstroms from each end. Since the pore is too narrow to allow a completely hydrated ion to fit inside, the carbonyl groups in the walls of the channel must partially solvate an ion in the channel [Jordan,1984]. The turns of the helix formed by the gramicidin molecule are approximately 1.5 angstroms apart, and thus the energy profile of an ion passing through the pore consists of a large barrier (due to the necessary ion dehydration) at the channel end, followed by a periodic series of smaller barriers spaced by 1.5 angstroms inside the channel. Approximately 14 of these local potential fluctuations occur in the channel interior [Jordan,1984]. The carbonyl groups that cause this energy fluctuation are an illustration of the electrically polar nature of the channel interior. Channel interiors have been modeled as a series of small electric dipoles [Jordan,1984],

which not only provide a rationale for ion solvation in the channel, but may partially explain the sensitivity of channel permeability characteristics to externally applied electromagnetic fields.

Ions through Channels

Ionic channels are selective for particular ions [Hille,1984]. Besides being specific to cations or anions, channels also exhibit different degrees of permeability to different ions having the same charge. Some channels are very highly specific for one particular ion. The simplest explanation for channel selectivity is that the pore diameter accounts for the rejection of ions that have radii too large to fit inside [Stein,1986; Hille,1984]. This discrimination based on size is undoubtedly part of the reason channels exhibit ion selectivity, but other characteristics, such as ion binding sites and channel conformation also play a role.

Ionic channels are characterized by relatively high transport rates. Channel conductivities ranging from 1 pS to approximately 500 pS have been observed. In the future, it is possible that channels with conductances less than 1 pS will be discovered, but channels having conductances greater than 500 pS are unlikely [Hille,1984]. As a point of reference, a conductivity of 1 pS represents a transport rate of 1.6×10^5 ions per channel per second [Stein,1986]. The gramicidin A channel has a fairly typical transport rate of around 10^7 ions per channel per second [Stein,1986]. Most channels can only accommodate one ion at a time due to the large electrostatic repulsion that ions of like charge experience when they are in close proximity. Some longer channels may be able

to accommodate a maximum of two ions at a time [Hille,1984; Levitt,1978]. Obviously, if only one ion is allowed in the channel at a time and overall transport rates are on the order of 10^7 ions per second, ion transit times are very short (100 psec). With such high transport rates, relatively few channels are required to produce rapid transmembrane ionic flux, so that the channel density in the membrane is low. Experiments have placed the density of membrane sodium channels at 50-500 channels per μm^2, potassium channels at .03-100 channels per μm^2, and calcium channels at approximately 10 per μm^2 [Hille,1984]. Channel proteins rarely make up more than a trace component of membrane material [Hille,1984].

Channel Gating

Cells modulate the total ionic flux across their membranes by turning ionic channels "on" and "off". In the fully "on" state the channel is conducting ions at a maximum rate. In the "off" state the channel is rendered impermeable to ionic flow. Many channels exhibit more than one "on" state, each state representing a different discrete conductance value [Fox,1987; Krouse et al.,1986]. The channel oscillates between these different states. Channel opening and closing rates can be affected in a number of different ways, depending on the nature of the channel. The gating of voltage dependent channels is characterized by a dependence on the transmembrane voltage. Thus, a large ionic flux caused by some other means can shift the transmembrane potential and trigger opening of voltage dependent channels, as in the case of Na^+ and K^+ currents in the action potential of a nerve cell [Campbell,1987]. Other channels can

be chemically stimulated, as is the acetylcholine receptor, which is activated upon binding the neurotransmitter acetylcholine. A third type of channel is activated by the presence of controlling ions in the cytoplasm. An example is the gap junction channel which is turned completely off when the intracellular Ca^{2+} concentration rises from 10^{-7} M to 10^{-5} M [Stein,1986]. In this way, a leaky damaged cell can be isolated from the surrounding cells, protecting them from the adverse effects of unbalanced ion concentrations.

Though the means of triggering channel gating differs between different types of channels, the mechanism by which gating occurs appears to be similar. Changes in channel conductance levels seem to be associated with conformational changes in the proteins that form the channel [Stein,1986]. These conformational changes can be stimulated by a change in electrostatic environment caused by the binding of an ion or transmitter molecule, or an altered transmembrane potential. Koeppe et al. [1979] has described a major conformational change that occurs in the gramicidin A channel molecule upon binding cesium or potassium ions at one of two binding sites. The channel shortens from 32 to 26 angstroms, and widens from 5 to 6.8 angstroms. The conformational change is likely to facilitate carbonyl-ion coordination, compensating for the free energy gained in dehydrating the ion.

Several recent reports [Barinaga,1990; Hoshi et al.,1990; Zagotta et al.,1990], have presented evidence for an alternative model for channel activation characteristics in Drosophila shaker potassium channels. By examining the effects of channel protein mutations on gating characteristics, this research group found evidence suggesting the

channel employs a "ball and chain" mechanism for gating purposes. The "ball" consists of a chain of 19 amino acids at the amino terminus of the protein extending into the cytoplasm. Amino acid deletions in this "ball" tend to inhibit channel inactivation. The "chain" is a much longer amino acid sequence linked to the "ball". Deletions from the chain tend to speed up channel inactivation. The results are consistent with a model of inactivation where the positively charged "ball" has a mating negatively charged binding site at the mouth of the channel. Inactivation occurs when the channel is obstructed by the binding of the ball to its mating site. The speed of inactivation depends on the length of the protein "chain" from which the ball swings.

Molecular Dynamics Studies

Several simulations using numerical solutions to equations of motion have shed light on the character of ion dynamics inside a channel. To date, the simulations have all been performed for various models of a gramicidin A channel. The first molecular dynamics studies [Fischer et al.,1981; Fischer and Brickmann,1983], modeled the channel as a regular series of dipoles lining the helical structure of the channel protein. The studies showed individual ions oscillating many times at binding sites along the channel, before obtaining enough thermal energy to jump to the next binding site. The binding sites correspond to potential wells caused by attractions between the electric dipoles in the channel wall and the ion.

Subsequent molecular dynamics studies using fast array processors have included the entire proposed structure of the gramicidin molecule in the dynamic simulations.

Results indicate that the ion is accompanied in the channel by a linear array of 8 or 9 water molecules that partially solvate the ion by pointing their dipoles in the ion's direction [Mackay et al.,1984; Jordan,1984; Kwang et al.;1985; Polymeropoulos and Brickmann,1985]. Mackay calculates that solvation due to such a linear water array can be as much as 85% as effective as solvation in a bulk water solution [Mackay et al.,1984]. Further solvation is provided by the carbonyl groups of the gramicidin helix, which can distort to allow better carbonyl-ion coordination. The ion travels in short jumps (approximately 1 angstrom), from binding site to binding site in the channel. Once again, the binding sites are due to potential wells created by the attraction between the carbonyl groups and the ion [Kwang et al.,1985]. Motion of the ion is strongly correlated to the motion of the water molecules [Skerra and Brickmann,1987; Mackay et al.,1984]. Simulations involving different ions reveal different paths of motion through the channel. The lithium ion with its small ionic radius forms relatively strong bonds with the carbonyl sites and can execute many thermal oscillations at the site before hopping to the next. Three binding sites per turn of the helix are evident for the lithium ion [Skerra and Brickmann,1987]. The sodium ion, with greater mobility and a much larger ionic radius, exhibits no obvious binding sites in its path along the channel, although its path follows a distinctly helical arc in traversing the channel [Skerra and Brickmann,1987].

Active Transport

Modifying the motion of ions through membrane channels is not the only way

that ion flux through cell membranes can be affected. Active transport is another means by which ions are moved across membranes. Active transport differs from channel transport in that energy is required to drive the process. The energy is usually obtained by the hydrolysis of ATP to form ADP and the accompanying phosphorylation of the ion carrier protein molecule. The molecule responsible for active transport must therefore possess the properties of both an ATPase enzyme (to accomplish the ATP splitting), and an ion carrier [Stein,1986]. The ability to tap external energy sources enables the active transport mechanism to move ions against an electrochemical gradient. In this way, the cell maintains the large differences in ion concentration between the intracellular and extracellular environments that is essential to the life of the cell. Calcium concentration in a typical animal cell, for example, is on the order of 10^{-7} M, while the extracellular concentration is on the order of 10^{-4} M or greater [Campbell,1983; Sheppard et al.,1979]. This large concentration gradient is sustained in part by the constant extrusion of ions from the cell by active transport. The exact mechanism by which active transport is accomplished is still unknown [Hille,1984]. However, it is clear that the carrier molecule must bind both ATP and the ion to be transported, after which phosphorylation triggers a conformational change in the protein which in turn moves the ion across the membrane [Stein,1986]. Active transport of ions across membranes is much slower than channel transport. As an example the Ca-ATPase pump can extrude only about 200 ions per channel per second from a cell [Hille,1984]. Compared to the normal channel rate of 10^7 ions per channel per second, this rate is slow indeed.

Another prime example of active transport is the Na-K-ATPase pump that

transports 3 Na^+ ions out of a cell and 2 K^+ ions into a cell for every ATP molecule. This mechanism is ubiquitous in the animal world [Stein,1986], and maintains Na^+ concentrations at approximately 140 mM extracellular and 15 mM intracellular levels, and K^+ concentrations at 5 mM extracellular and 160 mM intracellular levels [Blank,1987]. These high concentration gradients are required to drive the rapid ion diffusion through channels required to produce action potentials in nerve cells.

Perhaps the best studied active transport process is that of the Ca^{2+} pump in red blood cells. The pump extrudes Ca^{2+} ions against a large concentration gradient, using ATP for energy. The process requires free Mg^{2+} ions [Stein,1986; Schatzmann,1983]. The carrier molecule has two ATP binding sites along with binding sites for Mg^{2+} and of course Ca^{2+} on the internal membrane surface [Schatzmann,1983]. The pump is activated by a calcium-calmodulin complex, although the Ca^{2+} that binds to the calmodulin is not the Ca^{2+} that is transported [Schatzman,1983]. Complete removal of calmodulin does not entirely deactivate the calcium pump, but drastically reduces its effectiveness [Schatzmann,1983]. The maximum transport rate of the calcium pump is 30 ions per second [Stein,1986]. Each red blood cell has on the order of 1000 calcium pumps in its membrane [Stein,1986].

A similar calcium pump is found in the membrane of the organelle called the sarcoplasmic reticulum. The sarcoplasmic reticulum acts as a calcium storage pool, and releases calcium into the cytosol of muscle cells to initiate contraction, and gathers the calcium once again as the cell relaxes [Stein,1986]. The carrier molecule has two stable conformations, and the conformation change responsible for the ion transport is the step

that limits the rate of transport of the pump to approximately 10 ions per second [Stein,1986]. K^+ ions are known to inhibit the action of the ATPase which drives the calcium transport process [Hasselbach et al.,1975].

Ion Binding

It is clear from the foregoing discussions of both channel and active transport processes that the binding of ions and cofactors to the involved proteins is essential to the transport. Thus, it is reasonable to expect that if electromagnetic fields could affect such binding processes in some way, ionic flux would also be affected. For example, the calcium pump described above requires the binding of calcium ions to calmodulin, the binding of the calcium-calmodulin complex, Mg^{2+} and more Ca^{2+} ions to the carrier protein, and also the binding of ATP to the carrier before the ion transport can take place. Presumably, an effect on any of these binding processes could also have an effect on the transport processes and thus the total ionic flux across the cell membrane. Several of the models attempting to rationalize the effect of electromagnetic fields on cells use this argument as the basis for their theoretical conclusions. Others rely on the proposed ability of the fields to alter the course of ions through a channel or in the extracellular space.

The Thermal Noise Problem

Several theoretical models attempting to explain the experimental observations coupling weak, low frequency electromagnetic fields with living cells have been

proposed. From the outset, the task of rationalizing the observed effects is a difficult one. A primary reason for this difficulty is the rather high level of electrical noise inherent in all biological systems due to random thermal motion of their constituent particles. As an illustration, consider an ion in a biological milieu at a temperature of 37°C. The mean thermal kinetic energy of the ion in joules is given by [Halliday and Resnick,1962]:

$$W = \frac{3}{2}kT \tag{5.1}$$

where k is Boltzmann's constant (1.3805×10^{-23} J/°K), and T is the temperature in °K. At 310°K, this thermal kinetic energy has a value of .04 eV. The thermal kinetic energy expresses itself as straight line motion in paths whose length and direction are determined by random collisions with other particles in the plasma. Chemical bonds constrain particles by overcoming the thermal kinetic energy with electrical forces which are energetically more powerful. Table 1 in Chapter 1 lists the approximate energy levels of familiar chemical bonds.

By contrast, the weak electromagnetic fields which are the subject of this thesis are too small to impart sufficient energy to an ion to overcome thermal fluctuations or break chemical bonds. For example, it is a revealing fact that a magnetic field alone cannot impart <u>any</u> kinetic energy to an ion, since the force from a magnetic field always acts perpendicularly to the velocity of the particle. Several experimental reports have documented biological effects due to weak magnetic fields [Blackman et al.,1985; Smith et al.,1987; Liboff et al.,1987]. It is therefore too simplistic to assume that such fields

have their effect on ions by simply imparting enough kinetic energy to overpower thermal noise in the cell system.

A Model for Thermal Noise Analysis

Two reports [Weaver and Astumian,1990; Barnes and Seyed-Madani,1987], have attempted to examine the problem of thermal noise in biological systems. Assuming that the interaction site for electromagnetic fields and cells is the cell membrane, they employ the common technique of modeling the membrane as an electrical network containing a parallel resistance and capacitance combination. Based on this construction, it is possible to express the thermal noise level as a noise voltage, and thus estimate the minimum electric field required to exceed the noise threshold. It is instructive to compare the calculated minimum fields with those found to be successful in producing biological effects in experiments.

The Baseline Noise Threshold

In a parallel R-C circuit, the RMS noise voltage is based on thermal fluctuations in the resistor. This noise voltage is given by:

$$V_{RMS} = \sqrt{4kTBR} \tag{5.2}$$

where V_{RMS} is the RMS thermal noise voltage, k is Boltzmann's constant (1.38×10^{-23} J/°K), T is temperature (°K), B is bandwidth (Hz), and R is the membrane resistance (ohms). For a first order evaluation, the bandwidth used is the noise bandwidth of the low-pass filter created by the parallel R-C combination. This filter noise bandwidth is

1/4RC [Ott,1988]. The value of R is calculated from typical resistivity values for living tissue. Weaver lists the resistivity range as between 10^5 and 10^7 ohm-m. The resistance R is calculated from the resistivity by multiplying by the membrane surface area (1257 μm^2 for a spherical cell of 10 μm), and dividing by the membrane thickness (typically 50 angstroms). The resulting resistance value is 4.0 megohm. The value of C is calculated from the dielectric constant and dimensions of the membrane according to:

$$C = \frac{\epsilon 4\pi r^2}{d} \tag{5.3}$$

where ε is the dielectric constant ($2.5\varepsilon_o$ or 2.21×10^{-11} F/m for membrane tissue, r is the cell radius (nominally 10 μm), and d is the membrane thickness (typically 50 angstroms). The resulting value of C for the membrane model is 5.6 pF. From the calculated values of R and C for the membrane, the equivalent noise bandwidth of the membrane is calculated to be 11.2 kHz. Using this bandwidth in Equation (5.2) gives a baseline thermal noise voltage of 2.8×10^{-5} V across the membrane. It should be noted that this noise level is calculated using the bandwidth inherent in the overall characteristics of the membrane itself. If by some mechanism the bandwidth can be narrowed the thermal noise floor will undergo a corresponding drop, allowing weaker signals to be detected.

Using the calculated value for the RMS noise voltage floor, an estimate can be obtained for the minimum detectable electrical signal for the membrane. This minimum signal is taken to be that external field which induces a transmembrane voltage of the same amplitude as the RMS noise voltage, giving a signal-to-noise ratio of 1:1. The voltage induced at a point on a non-conducting spherical cell membrane of negligible

thickness when exposed to an external electric field is [Foster and Schwan,1986]:

$$V_{ind} = 1.5Er\cos\theta \tag{5.4}$$

where E is the external electric field (V/m), r is the cell radius (typically 10 μm), and θ is the angle between a radial vector from the cell center to the desired point on the membrane and the direction of the applied field. For the present calculations, the maximum value of this voltage will be used, where the maximum value is obtained for a θ value of zero. Using Equation (5.4) with an induced voltage equal to the RMS noise value (2.8×10^{-5} V), a value of 1.9 V/m is obtained for the minimum detectable electric signal. When this value is compared to reports of biological effects from fields as low as 10^{-5} V/m [Bawin and Adey,1976], it appears that the biosystem must employ some means of lowering the noise threshold by as much as five orders of magnitude.

Lowering the Noise Threshold

As noted, if the frequency bandwidth of the system can be narrowed by some mechanism the minimum detectable signal can be correspondingly reduced. The bandwidth of the response curve for several experimental systems [Bawin and Adey,1976; Liboff et al.,1987; Smith et al.,1987], has been on the order of 10 Hz or slightly less. Using 10 Hz as a noise bandwidth in Equation (5.2), the RMS noise voltage drops to 8.3×10^{-7} V, and the minimum detectable external electric field drops to .055 V/m.

Experimental effects of electric fields have been documented for fields as low as 10^{-5} V/m [Bawin and Adey,1976]. Thus it would appear that the narrow bandwidth,

though important in allowing a weak AC field to affect a biosystem, cannot in itself account for the extremely weak fields which have been found effective. Barnes and Seyed-Madani have suggested that another means of improving signal-to-noise ratio in biological systems is some sort of accumulation of the signal effects over time [Barnes and Seyed-Madani,1987]:

> "With repetitive signals, the bandwidth may become very narrow, and it is possible for long-term, low-level signals to affect biological systems in ways that are not apparent with only short exposures. This is observed in the extraction of periodic signals from noise in electronic systems and would not be surprising if it were observed in biological systems."

Weaver and Astumian suggest a quantitative estimate for the signal-to-noise ratio improvement realized from such signal averaging over time [Weaver and Astumian,1990]. They cite that time averaging over N cycles of the applied signal can cause an improvement in the signal-to-noise ratio of $N^{1/2}$. In Bawin's experiments, fields at approximately 10 Hz frequency were applied for 20 minute exposure periods. The exposure period corresponds to 1.2×10^4 cycles of the 10 Hz applied signal. Thus, if a mechanism for signal averaging were active, the minimum detectable signal would be expected to drop to approximately 5×10^{-4} V/m. This level is within an order of magnitude of the actual applied field strength in Bawin's experiments. Another phenomenon which might also be expected to reduce the minimum detectable signal of a system would be some form of cooperativity. A weak field could have a very small effect on numerous system subcomponents. Individually, the effects would be far too small to be physiologically relevant, but if the effects showed a sufficient degree of

cooperativity, the collective effect could be large enough to cause a biological response. Several experimenters and theoreticians have suggested that such cooperativity is likely to play a role in the actual mechanism by which low frequency electromagnetic fields affect cells [Adey,1990; Sheppard et al.,1979; Halle,1988].

Relating the Noise Level

to a Magnetic Field

In several experiments [Smith et al.,1987; Liboff et al.,1987; Blackman et al.,1985], no direct electric fields were applied to the experimental systems. Instead, only a combination of a DC and low frequency AC magnetic fields was employed. To date, attempts to estimate the minimum detectable signal at a cell membrane have considered only electric fields. Either one of two criteria can be used to evaluate the magnetic field magnitudes in these experiments with respect to the thermal noise calculations outlined above. The first criterion assumes that the effect of the magnetic fields on the biosystem is due primarily to the magnetic fields themselves. The second criterion assumes the effect, though requiring the presence of the DC magnetic field, depends on the electric field induced by the AC magnetic field.

In the first case, a reasonable method of relating the magnetic field strength to the thermal noise voltage would be to calculate a minimum magnetic field strength which would create a force on an ion equal to the force an ion experiences when subjected to the minimum detectable electric fields calculated above. The maximum Lorentz force on an ion occurs when the ion velocity is perpendicular to the applied magnetic field. In this case the magnitude of the force is given by the product of the ion charge, the

velocity magnitude and the magnetic field magnitude. Setting this force equal to that experienced by the same ion in a minimum detectable electric field:

$$qE_{min} = qvB_{min} \tag{5.5}$$

where q is the ion charge (coulombs), E_{min} is the minimum detectable electric field (V/m), v is the ion velocity magnitude (m/sec), and B_{min} is the minimum detectable magnetic field for this calculation. The logical choice for a value for the velocity variable in Equation (5.5) is the mean thermal velocity of the ion at physiological temperatures. The mean kinetic energy of a particle at a given temperature is given by [Halliday and Resnick,1962]:

$$W = \frac{3}{2}kT \tag{5.6}$$

where W is the kinetic energy (Joules), k is Boltzmann's constant ($1.3805.10^{-23}$ J/°K), and T is the temperature (°K). The mean velocity of a particle having this kinetic energy can be easily calculated from [Halliday and Resnick,1952]:

$$W = \frac{1}{2}mv^2 \tag{5.7}$$

where W is the kinetic energy (J), m is the particle mass (kg), and v is the magnitude of the velocity of the particle (m/sec). Combining Equations (5.6) and (5.7), using a temperature of 310°K and a mass of $6.65x10^{-26}$ kg (for a Ca^{2+} ion), results in a mean thermal velocity of 440 m/sec for the Ca^{2+} ion. This result can now be used in Equation

(5.5), along with the minimum detectable electric field without frequency band limiting (1.9 V/m), to yield a minimum detectable magnetic field strength of 43 gauss. The same frequency band limiting improvement might be realized for the magnetic field case as for the electric field. For a 10 Hz bandwidth, the minimum detectable magnetic field would drop to 1.3 gauss. The experiments cited employed magnetic fields of approximately .2 gauss. Thus a slight further reduction in minimum detectable signal due to signal averaging or cooperative effects could result in a signal-to-noise ratio sufficient to produce biological effects.

A time-changing magnetic field always induces a corresponding electric field, and it has been postulated [Durney,1988] that this induced electric field may be crucial to magnetic field effects. This induced electric field can be calculated from Faraday's Law:

$$\oint \overline{E} \cdot \overline{dl} = -\frac{d}{dt} \int \overline{B} \cdot \overline{dS} \tag{5.8}$$

If the system exhibits cylindrical symmetry the induced E field is directed along a circular path surrounding the magnetic field axis of symmetry. Figure 23 illustrates this concept for the case of Helmholtz coils in free space.

Due to the cylindrical symmetry, the line integral in Equation (5.8) reduces to a simple product. The surface integral also reduces to a simple product if the magnetic field vector is constant over the surface element and is parallel to the surface element vector. With these simplifications, Equation (5.8) reduces to:

$$E_{\phi} 2\pi r = -\frac{d}{dt}(B\pi r^2) \tag{5.9}$$

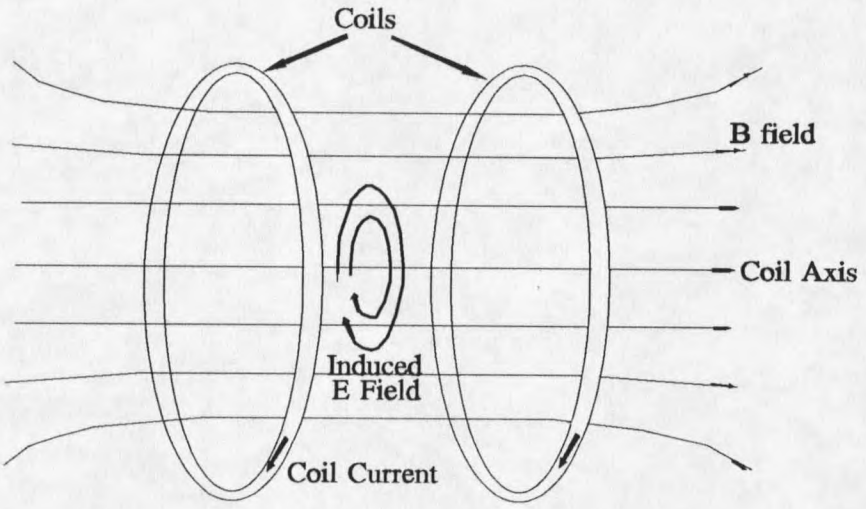

Figure 23. E field induced by Helmholtz coils.

where E_ϕ is the ϕ-directed electric field, r is the radial distance of the field point from the axis of symmetry, and B is the magnetic field. Assuming that r is not a function of time allows Equation (5.9) to be reduced to:

$$E_\phi = -\frac{r}{2}\frac{dB}{dt} \qquad \textbf{(5.10)}$$

The magnetic fields applied in the experiments of Smith and Liboff consisted of a sinusoidal magnetic field (nominally .2 gauss peak and 16 Hz), superimposed on a constant DC magnetic field. The sinusoidal field is the only contributor to the induced electric field in Equation (5.10). Assuming the magnetic field has the sinusoidal form $B = B_o \cos\omega t$ yields:

$$E_\phi = \frac{rB_o\omega}{2}\sin\omega t \tag{5.11}$$

The magnitude of this induced sinusoidal electric field is easily calculated. Using the values of .2 gauss and 16 Hz for the magnetic field amplitude and frequency results in an induced electric field amplitude of:

$$|E_\phi| = .001r \tag{5.12}$$

Thus the magnitude of the induced electric field is directly proportional to the distance from the symmetrical center of the system. For the experiments of Smith and Liboff, this radius is on the order of the dimensions of the generating coils. Using 1 cm as a nominal value gives an induced electric field of 10^{-5} V/m. This value is equal to that demonstrated [Bawin and Adey,1976] to be effective in enhancing Ca^{2+} efflux from chick brain tissue, and appears to approach the noise threshold defined by Weaver and Astumian only if some or all of the advantages of frequency band limiting, time averaging, and cooperativity are active.

CHAPTER 6

THEORETICAL MODELS

Introduction

Theoretical models attempting to explain the interaction of weak electromagnetic fields and cells have been proposed by several research groups. Though the basic mechanisms of the models vary widely, several common characteristics are evident.

Ion Dynamics: a Common Thread

In each proposed model, the primary action of the fields is to affect ion dynamics, either by altering ionic transport across cell membranes or ionic binding to membrane surface sites. The primary reason for this common thread is the large body of evidence showing direct effects of fields on ion efflux from cells or uptake into cells [Bawin and Adey,1976; Blackman et al.,1985; Liboff et al.,1987]. In addition, studies aimed at pinpointing the site of interaction using various chemical additives have unanimously pointed to the cell membrane surface as the likely candidate [Bawin et al.,1978; Lin-Liu and Adey,1982; Dixey and Rein,1982; Phillips et al.,1986]. Experimental evidence aside, it is also quite natural to suspect ion dynamics as a logical interaction mechanism. From a physical viewpoint, electrically charged particles are naturally suspect in any effects

due to electric or magnetic fields since the fields exert forces on ions, and not on electrically neutral particles. From a physiological viewpoint, ions are known to be crucial in the regulation of a large number of cell processes. It is quite natural, therefore, to suspect some aspect of ion dynamics to be a contributing factor in ELF field effects on biosystems.

How many Ions must be Affected?

It is illuminating to gain some idea of the minimum number of ions which must be affected in order to constitute a physiologically relevant signal. The resulting number can be used as a tool for evaluating the proposed models. To obtain an estimate of this number, it is helpful to examine the individual case of Ca^{2+} ion flux through a cell membrane. The concentration gradient of Ca^{2+} is large. Typical cells exhibit intracellular Ca^{2+} concentrations on the order of .1 μM and extracellular concentrations of 1 mM [Campbell,1983; Sheppard et al.,1979]. The low intracellular concentration of Ca^{2+} makes it a likely candidate for inciting a cellular response, since a small Ca^{2+} flux can result in significant intracellular concentration changes. Cellular responses have been observed with an overall cytosolic Ca^{2+} concentration change of 10 nM [Silver et al.,1990]. Though micromolar changes in cytosolic Ca^{2+} concentration are required to activate proteins controlling cell function, Ca^{2+} flux can be concentrated at "hotspots" yielding local micromolar concentrations without raising the total cytosolic Ca^{2+} concentration more than 10 nM [Silver et al.,1990]. The simple calculation detailed in Equation (6.1) is employed to obtain an estimate of the number of Ca^{2+} ions this 10 nM concentration change represents.

$$N = CN_o V \tag{6.1}$$

where N is the number of ions, C is the Ca^{2+} concentration (10 nM), N_o is Avogadro's Number (6.023×10^{23} ions/Mole), and V is the volume of a typical cell (4.19×10^{-12} liters for a spherical cell of radius 10 μM). The resulting number N is 2.5×10^4. Therefore a best estimate for the minimum number of ions which must be affected (in this case transported across the cell membrane), is about 10^4.

In terms of normal cell ionic flux, 10^4 ions is a small number. For instance, a single channel conducting 10^7 ions per second would need to be operating only 1 msec to conduct this number of ions. This raises the possibility that low frequency electromagnetic fields might affect biological systems indirectly by altering the gating characteristics of membrane ion channels. Several of the theoretical models to be reviewed below employ this argument in some form.

Description and Evaluation of Models

Blank: Effects of Electric Fields on Membranes

Blank [1987], has proposed a model attempting to explain shifts in ion concentration by means of an AC electric field applied across a cell membrane. The theory is based on a model of the cell membrane which the author names the "Surface Compartment Model" (SCM). In the SCM, the membrane environment is modeled as five compartments (outside the membrane, outside membrane surface, membrane, inside membrane surface, and inside the membrane). In the model, the concentration gradient

of ions at the membrane surface is approximated by the Helmholtz model of an electrical double layer, in which the ion concentration drops linearly from its surface value through the thickness of the double layer to its final value which matches the concentration in the bulk solution. A set of simultaneous, nonlinear, first-order differential equations results from the estimates of membrane capacitance, membrane conductances, ion mobility, and channel gating characteristics which constitute the SCM. To simulate ionic flux, the differential equations are solved numerically. The particular membrane diffusion process that has been modeled in this way using the SCM is the Na^+ and K^+ transfer in squid axon membrane. The model predicts a shift in steady-state values of ionic concentrations as a result of an applied AC electric field. At first thought, it would seem that such an AC electric field would have no net effect on ion flux, since the field reverses polarity each half-cycle and thus would tend to cancel its own effect on ion motion over time. The SCM does predict changes in concentration that are not self-canceling, however. It appears that the reason for this effect is the current rectification property of the membrane [Findl,1987]. The ionic concentration shift is reached within a few cycles of the applied electric field, and though cumulative, the effects do not increase indefinitely.

The model can perhaps be challenged from several viewpoints. Although the concentration shift is shown to be frequency dependent, the effective frequency bandwidth appears to be extremely wide (several hundred Hz), when compared with the bandwidths (less than 10 Hz) observed in several experiments [Blackman et al.,1976; Smith et al.,1987; Liboff et al.,1987]. The magnitude of the electric field required to have an effect in this model is also open to question. Though the author states that even

small electric fields can lead to significant changes over time due to additive effects, the electric field reported in the simulation was $2x10^6$ V/m (10 mV across the membrane). This value stands in stark contrast to the effects seen from fields as small as 10^{-5} V/m [Bawin and Adey,1976], and raises the question of the minimum field required to overcome the thermal noise threshold in this model. When viewed from the perspective of Weaver and Astumian [1990], the bandwidth of the modeled effect does not reduce the noise threshold by an amount sufficient to account for the effects at weak field levels. The improvement in bandwidth over the theoretical value inherent to the membrane is only about a factor of 20, far less than the factor of 10^5 which is a best estimate for the required noise threshold reduction. It appears, then, that the additive effects of the signal must account for the bulk of the noise threshold reduction in this model. Using the estimate of Weaver and Astumian that signal averaging lowers the threshold by a factor equal to the square root of the number of averaged cycles, a 16 Hz signal would have to be coherently averaged for almost 2000 hours to achieve a noise threshold improvement of 10^4. Thus it would appear that models incorporating a narrower frequency bandwidth and perhaps some form of cooperativity might be more successful at rationalizing the experimental results.

Additional experimental facts that are beyond the scope of this model are the observed effects of magnetic fields on biological systems [Blackman et al.,1976; Smith et al.,1987; Liboff et al.,1987]. Since the model is couched purely in terms of an electric field, the AC magnetic field effects and their dependence on the value of the DC magnetic field are outside its scope.

Chiabrera: Charged Ligand Motion

at a Binding Site

Chiabrera and Bianco [1987] have introduced a model that is aimed at explaining the experiments [Smith et al.,1987; Liboff et al.,1987; Deibert et al.,1991] that have shown a biological effect when magnetic fields are tuned to cyclotron resonance conditions for unhydrated ions of physiological importance. The model concerns the motion of a charged ligand (in this case an ion), in the vicinity of a binding site. An attempt is made to demonstrate that the velocity of the ion is affected in a coherent manner by the application of the appropriate magnetic fields. An effect on the ion velocity is assumed to affect association and/or dissociation rate constants and hence a bioelectrochemical process. The first difficulty which the proposed model addresses is the objection that an ion in the extracellular bulk solution has a tightly bound hydration shell and therefore a fundamentally different charge-to-mass ratio than a bare ion. The magnetic fields required to maintain cyclotron resonance conditions for such solvated ions are quantitatively different from those which have proven experimentally successful. In the model, it is stated that the molecular arrangement of the binding site can produce local electric fields that create hydrophobic environments in which the ion can exist in an unhydrated form, experiencing very few collisions with water molecules.

As a mathematical starting point, the equation of motion of an ion experiencing forces due to magnetic and electric fields, as well as viscous drag due to thermal collisions, is employed:

$$\frac{d\bar{v}}{dt} + \frac{\beta}{m}\bar{v} + \frac{q}{m}\bar{B}\times\bar{v} = \bar{n}_r + \frac{q}{m}\bar{E} \qquad (6.2)$$

where $\bar{v}$ is the ligand velocity, β is the coefficient of viscosity, m is the ligand mass, q is the ligand charge, $\bar{B}$ is the magnetic field vector, $\bar{n}_r$ is a random noise with zero average, and $\bar{E}$ is the local electric field. This equation is simply the well known Lorentz force equation with viscous drag and noise terms added. The next step in the analysis is to rewrite Equation (6.2) assuming that the exogenous electric field is zero to obtain an equation of motion for the ion under magnetic field, drag, and noise forces alone. The authors do point out that this step has no strict physical meaning since a time-changing magnetic field cannot exist without a corresponding induced electric field. However, the step is made to allow solution of the equations. Subtracting the two equations results in an equation in which the dependent variable becomes the difference in velocity caused by the exogenous electric field, relative to the total velocity due to all force contributions. Neglecting the noise term, and assuming a low value of β (few collisions), the mathematical solution of the resulting equation is obtained. The exogenous electric field is taken to be that field induced by the time-changing magnetic field in a Helmholtz coil configuration, or the field existing in a TEM wave inside a waveguide setup. Both configurations have produced experimental results [Smith et al.,1987; Blackman et al.,1979]. In both cases, the frequency of the AC electric field is equal to the AC magnetic field frequency.

Solution of the equation relating ligand velocity shift to the field values shows rather sharp resonance features with peaks at field conditions corresponding to the cyclotron resonance conditions for the ion:

$$f = \frac{qB_0}{2\pi m} \tag{6.3}$$

where f is the AC field frequency, q is the ligand charge, m the ligand mass, and B_0 the DC magnetic field. Integer multiples of the fundamental cyclotron resonance frequency cause the same resonant peak in the ligand velocity shift caused by the fundamental frequency. In addition, a velocity shift is predicted when a DC field is applied in the absence of any AC fields, a prediction that has not been substantiated by experimental results [Smith et al.,1987]. Further experiments [Smith et al.,1987; McLeod et al.,1987; Blackman et al.,1985] also contradict the prediction of the model that the same resonant response should be observed for all harmonics of the fundamental cyclotron resonant frequency. These experiments have generally indicated that only odd harmonics are effective. The model also predicts resonant responses as a result of varying the amplitude of the AC magnetic field. This result matches with the experimental finding that the fields are effective only within certain amplitude "windows" [Blackman et al.,1979; Smith et al.,1987].

Adey: Cooperative Surface Effects Transmitted to Cell Interior

Adey [1990], has proposed a model of cell-field interaction that attempts to describe a process by which weak, low frequency fields can induce cell changes which are energetically many times larger than the stimulus. The model is couched in conceptual rather than mathematical terms. The action of the model is divided into three parts: 1) sensing of the field by cell surface glycoproteins, 2) signalling of the surface event to the interior of cell through the transmembrane portion of an intramembranous protein, and 3) coupling of the signal to interior enzyme systems which affect cell

processes.

Physical and experimental reasons are given for suggesting that the initial trigger effect occurs at the cell membrane surface. Several experiments [Bawin et al.,1978; Luben et al.,1982; Lin-Liu and Adey,1982; Smith et al.,1987], have specifically implicated membrane surfaces as the interaction site by showing that applied fields can modify the effect of certain agents which are known to act at the cell membrane. In addition, the extracellular space is a preferred pathway for electrical currents, having resistances several orders of magnitude less than the lipid bilayer making up the cell membrane.

The mechanism by which the membrane surface is said to detect the electromagnetic fields is a cooperative modification of the binding of calcium ions to amino terminals of glycoproteins along the surface. The authors point out that in order for weak fields to induce macroscopic biological effects, the interaction process must include some method for amplification of the initially small signal. The hypothesis of the model is that the amplification is accomplished by coherent cooperation of many individual molecular groups. It is suggested that patterns of molecular organization develop in the system which can undergo sudden transitions to new configurations which are relatively stable over time. Some examples of known molecular conformational changes caused by the application of electric fields exhibit thresholds of $2x10^6$ V/m. Clearly, some extensive form of cooperation is necessary to reduce this threshold to the weak (10^{-5} V/m) signals which have proven experimentally effective. The concept of cooperativity is analogous to a "domino" effect in which a small amount of energy which

initially alters only a small part of the total system can spread via cooperation of the individual components to induce far-reaching effects. Adey estimates that to overcome thermal noise at physiological temperatures a 10^{-5} V/m signal would require cooperation over a distance of 300 m, and therefore suggests that cooperativity does not completely account for the experimental effects. Other factors, such as frequency band limiting may also be required to achieve the sensitivity demanded by experimental data. The model hypothesizes that after the initial detection and amplification stages, the signal must be transmitted across the cell membrane to the interior where its effects are produced. Adey cites studies [Luben et al.,1982], which have shown an ultimate effect of applied fields on the action of enzymes internal to the cell. He suggests that the signal could be transmitted through intramembranous proteins via longitudinal motion of the membrane spanning portion, or by soliton waves. The signal is then coupled through tubes and filaments in the cytoskeleton to organelles where the effects take place. The result is a disruption of the stream of signals into or out of a cell via electrical or chemical pathways. It is perhaps unclear why the transmembrane signalling step needs to be included in this model. The changes in membrane electrical forces caused by coherent transitions of significant numbers of surface molecules would seem likely to be able to affect membrane ion channel gating. The end result would be a change in the flow of electrical signals (ions), into and out of the cell without the requirement for an intermediate transmembrane signalling step proposed by the model. In this regard, it is interesting to note, as Adey does, that each of the internal enzymes that have exhibited sensitivity to experimentally applied fields are dependent on Ca^{2+} ions.

McLeod: Ion in a Model Channel

An alternative model has been proposed by McLeod et al. [1991] which deals with the motion of an ion in a simplified channel. The model was conceived primarily as a way of explaining the experimental results obtained by applying ion cyclotron resonance tuned magnetic fields to several biological systems [Smith et al.,1987; Liboff et al.,1987; Deibert et al.,1991]. Therefore the model attempts to account for the particular features observed in those experiments. Included in these experimental features are the relationship between the DC magnetic field and the AC frequency as predicted by the charge-to-mass ratio of the ion involved, the ineffectiveness of even harmonics of the fundamental frequency, the curious pattern of effective odd harmonics (1,3,5 and 15), and the sensitivity of the effect to the AC amplitude.

The model focuses on the motion of a single ion in a simplified channel. Several reasons for choosing the channel as the interaction site are given. The channel is expected to provide an environment where thermal collisions do not dominate the ion motion. It is also suggested that the spatial periodicity of the channel walls might in some way interact with the motion of an ion under the influence of periodic forces due to the applied AC magnetic fields. The attempt to locate the ion-field interaction in a membrane channel runs into a difficulty at the outset. Since the longest measured transit times for ions crossing channels are on the order of microseconds [Stein,1986], it appears impossible for an applied magnetic field of extremely low frequency (for example 16 Hz), to have a coherent effect on the path of an ion through the channel, since the period

of the applied signal is many orders of magnitude longer than the ion transit time. This difficulty is addressed in the model by postulating that a different kind of channel might exist in the membrane, possibly only under conditions of stress to the cell, which ions traverse at a much slower rate. To explain the highly frequency dependent effects seen in experiments, it is suggested that these "slow" channels must have transit times on the order of the period of the applied AC signals. Model simulations assume an ion transit time of 50 msec, which is almost 10^5 times greater than the slowest channel observed to date using single channel recording methods. It is suggested that these special slow channels may not be present in sufficient numbers to affect cellular processes in a normal cell at equilibrium, but may be formed in cells under some condition of stress. The stress could be caused by changes in the exogenous environment (heat, pH), or by endogenous changes (embryonic growth, cell transformation, wound-healing demands). The idea that slow channels exist only in cells whose equilibrium has been disturbed might serve as an explanation for the ineffectiveness of the applied fields on some biological systems.

At the outset, the plausibility of the "slow channel" assumption can be evaluated by examining the magnitude of the ionic flux it can create. The question arises whether a sufficient ionic flux can be generated by such slow channels to create a physiologically relevant signal in a reasonable time period. In answering the question it is necessary to make an assumption regarding the density of these slow channels in the cell membrane. Since the existence of these slow channels are only hypothesized at this point, their density is also a matter of hypothesis. However, a result may be obtained assuming a

channel density similar to known channels. Accordingly a representative density of 100 channels/μm^2 will be used. This number is chosen to approximate the channel densities of some known ion channels (50-500 sodium channels per μm^2 and .03-100 potassium channels per μm^2) [Hille,1984]. The simple calculation yielding the time required to produce a minimum ionic flux is given by:

$$t = \frac{N}{RDA} \tag{6.4}$$

where t is the minimum time value sought, N is the minimum number of ions which must be transported to make a physiologically relevant signal ($2.5x10^4$, see Chapter 5), R is the transport rate of ions in the channel (assumed to be 10 ions/channel-sec), D is the channel density (100 channels/μm^2), and A is the surface area affected by the fields. Assuming that the total surface area of a typical cell of 10μm radius is affected, the surface area becomes 314 μm^2. The result of the calculation for t is .08 seconds. The smallest time period in which an experimental effect of low frequency electromagnetic fields has been reported is 15 seconds [Smith,1987b]. Thus the hypothesis of a "slow" channel does not appear to require an inordinate amount of time to accumulate a significant ionic flux. The model cannot therefore be rejected on that basis.

The description of the model begins with an assumption for the shape of the channel lumen. In the model, the lumen exhibits cylindrical symmetry and has a length of 50 angstroms. At its mouth the channel diameter is 10 angstroms. The channel narrows to approximately 2 angstroms at a point 62% of the distance from the extracellular to the intracellular face. Another constriction appears right at the

intracellular face. This channel shape is fairly similar to profile images of acetylcholine channels [Brisson and Unwin,1985], and a shape proposed for sarcoplasmic reticulum K^+ channels [Stein,1986]. The basic scenario developed in the model concerns the motion of an ion starting from rest at the mouth of the channel, subjected to Lorentz forces from the applied magnetic fields and an inward force due to the transmembrane potential. Mathematical closed form solutions for the envelope of the ion trajectory are obtained under certain assumptions. It is shown that the envelope "fits" the channel under certain combinations of applied fields. Other combinations cause the ion trajectory to collide with the channel lumen at one or the other of the channel constrictions described above. It is suggested that the fit of the ion trajectory to the channel constitutes a form of electromagnetic "gating" which facilitates ion motion through the channel under certain field conditions. This channel gating is found to be sensitive to the fundamental frequency and amplitude of the applied AC magnetic field, in accord with experimental data. A harmonic pattern of effective frequencies similar to that observed in diatom mobility experiments also appears to emerge from the analysis.

It is important to follow the mathematical analysis on which the model is based in order to understand the assumptions and simplifications made along the way. In the analysis the following definitions will be used:

E = electric field intensity vector
$= E_r \hat{r} + E_\phi \hat{\phi} + E_z \hat{z}$

F = reaction force vector inside the channel
$= F_r \hat{r} + F_\phi \hat{\phi} + F_z \hat{z}$

B = applied magnetic field

$= B_z \hat{z}$

$B_z = B_0 + B_{ac} \sin(\omega t)$

U = velocity vector
$= U_r \hat{r} + U_\phi \hat{\phi} + U_z \hat{z}$

where $\hat{r}$, $\hat{\phi}$, $\hat{z}$ are unit vectors in the r, ϕ, and z directions

B_0 = magnitude of the DC magnetic field (Tesla)

B_{ac} = peak amplitude of the AC magnetic field (Tesla)

q/m = charge to mass ratio of the ion (coulomb/kilogram)

$\omega = 2\pi f$ = applied radian frequency (rad/sec)

$\omega_B = qB_z/m$ (cyclotron resonance condition)

τ = damping term, (seconds)

a = ion radius (meters)

r_o = channel radius (meters)

The starting point for the analysis is the Lorentz force equation describing the forces on the ion due to applied electromagnetic fields. In this instance the equations of motion are written in cylindrical component form:

$$\frac{\partial U_r}{\partial t} - \frac{\partial \phi}{\partial t} U_\phi = \left(\frac{q}{m}\right) E_r + \left(\frac{q}{m} B_z\right)(U_\phi) - \frac{U_r}{\tau} - \frac{F_r}{m} \qquad (6.5)$$

$$\frac{\partial U_\phi}{\partial t} + \frac{2}{r}\frac{\partial U_r}{\partial t} U_\phi - \frac{U_r}{r} U_\phi = \left(\frac{q}{m}\right) E_\phi - \left(\frac{q}{m} B_z\right) U_r - \frac{U_\phi}{\tau} - \frac{F_\phi}{m} \qquad (6.6)$$

$$\frac{\partial U_z}{\partial t} = \left(\frac{q}{m}\right) E_z - \frac{U_z}{\tau} - \frac{F_z}{m} \tag{6.7}$$

The next step is to assume that E_r does not vary with time, and also to assign the following definition to the radial component of the reaction force F_r:

$$F_r = -mU_\phi \frac{\partial \phi}{\partial t} \tag{6.8}$$

To analyze this assumption it is worth noting that the angular velocity U_ϕ can be written as:

$$U_\phi = r\frac{\partial \phi}{\partial t} \tag{6.9}$$

Substituting this expression into (6.8) gives another form for the assumed restoring force:

$$F_r = -mr\left(\frac{\partial \phi}{\partial t}\right)^2 \tag{6.10}$$

This choice of definition for the restoring force is made with a view to canceling the second term on the left-hand side of (6.5). In physical terms, the electrostatic forces applied to the ion by the channel walls must supply this restoring force. The definition of (6.10) states that these forces are functions of the ion mass, radial position, and angular velocity. The assumption that the restoring force varies with the ion mass and radial position both appear to be reasonable. The assumption that the restoring force

varies as the square of the angular velocity might be called into question. However, the angular periodicity of channel structures [Unwin and Zampighi,1980; Brisson and Unwin,1985; Toyoshima and Unwin,1988], would seem to indicate that the restoring force ought to at least be a function of angular position, if not velocity.

Proceeding under the assumption for the restoring force described above, and taking the partial derivative of Equation (6.5) with respect to time with the substitutions from Equations (6.6) and (6.8) results in:

$$f(r,t)=\omega_B[(\frac{q}{m})E_\phi-\frac{U_\phi}{\tau}-\frac{F_\phi}{m}]+(\frac{q}{m})U_\phi\frac{\partial B_z}{\partial t}-GU_\phi\omega_B \tag{6.11}$$

where

$$f(r,t)=\frac{\partial^2 U_r}{\partial t^2}+\frac{1}{\tau}\frac{\partial U_r}{\partial t}+\omega_B^2 U_r \tag{6.12}$$

and

$$G=\frac{2}{r}\frac{\partial U_r}{\partial t}-\frac{1}{r}U_r \tag{6.13}$$

Now an assumption is made for the angular restoring force F_ϕ:

$$\frac{\omega_B}{rm}F_\phi=[\frac{\omega_B}{\tau}+G\omega_B]\frac{\partial\phi}{\partial t} \tag{6.14}$$

which can be rewritten:

$$F_{\phi}=\frac{m}{\tau}U_{\phi}+m\frac{\partial\phi}{\partial t}[2\frac{\partial U_r}{\partial t}-U_r] \tag{6.15}$$

This assumption is also made for the purpose of eliminating several terms from Equation (6.11). The authors suggest that the second two terms in (6.15) are small compared to the first, or equivalently, that the velocities in the r and ϕ direction are small. If that assumption is granted, then (6.15) is equivalent to stating that the angular restoring force must balance the equivalent force term due to collisions of the ion in the channel.

Granting the assumption, a substitution of (6.15) into (6.11), and division by r results in:

$$\frac{f(r,t)}{r}=g(\phi,r,t) \tag{6.16}$$

where

$$g(\phi,r,t)=\frac{\partial\phi}{\partial t}[(\frac{q}{m})\frac{\partial B_z}{\partial t}]+(\frac{q}{m})\frac{\omega_B E_{\phi}}{r} \tag{6.17}$$

and with f(r,t) being defined in (6.12). To eliminate E_{ϕ} from the right-hand side, E_{ϕ} is replaced by the induced E field created by the sinusoidal magnetic field. The induced E field can be calculated from Faraday's Law:

$$\oint E\cdot dl=-\frac{\partial}{\partial t}\int(B\cdot dS) \tag{6.18}$$

Assuming cylindrical symmetry and a z-directed magnetic field results in a ϕ-directed electric field (E_ϕ). Also assuming that the applied magnetic field (B) is constant over the surface of integration results in the following solution for E_ϕ:

$$E_\phi = -(\frac{r}{2})\frac{\partial B}{\partial t} - B\frac{\partial r}{\partial t} \tag{6.19}$$

Substituting this result in Equation (6.17) results in an equation whose left side is a function of r and t only while its right side is a function of ϕ and t only. Therefore, the two sides can be set equal to an arbitrary constant α:

$$\frac{f(r,t)}{r} + (\frac{\omega_B^2}{r})U_r = \alpha = -\frac{q}{2m}\omega_B\frac{\partial B}{\partial t} + \frac{q}{m}\frac{\partial B}{\partial t}\frac{\partial \phi}{\partial t} \tag{6.20}$$

This equation is solved in its simplest form by setting α to zero:

$$\frac{\partial^2 U_r}{\partial t^2} + (\frac{1}{\tau})\frac{\partial U_r}{\partial t} + 2(\omega_B^2)U_r = 0 \tag{6.21}$$

and

$$\frac{\partial \phi}{\partial t} = \frac{\omega_B}{2} \tag{6.22}$$

The solution to (6.22) is

$$\phi = [\frac{\omega_{B0}}{2}]t + [\frac{\omega_{Bac}}{2\omega}]\cos(\omega t) - \frac{\omega_{Bac}}{2\omega} \tag{6.23}$$

(using $\phi = 0$ at $t = 0$ as an initial condition). Noting that the second and third terms of

(6.23) are small compared to the first, since they contain an inverse ω term, it follows that ϕ varies nearly linearly with time. Thus if the ion exhibits a constant velocity in the z direction, the ϕ solution will describe a helical motion for the ion.

A difficulty in solving (6.21) arises in that ω_B is time varying due to the sinusoidal applied magnetic field. To facilitate the equation solution it was assumed that ω_B is actually a constant and the error of this assumption determined. The result is an ordinary linear differential equation with constant coefficients. The equation is solved with the following boundary conditions: 1) initial and final velocities are set equal to zero, and 2) the ion starts at rest from the center of the channel and its radial displacement cannot exceed the channel radius. The problem is thus viewed as a boundary value problem with both spatial and time boundary constraints applied. The resulting solution for the radial position of the ion is:

$$r \approx \frac{(a-r_0)}{A} e^{-\frac{t}{\tau}} [\sinh(\frac{At}{2\tau}) + A\cosh(\frac{At}{2\tau})] + (r_0 - a) \tag{6.24}$$

where

$$A = \sqrt{1 - 8\omega_B^2 \tau^2} \tag{6.25}$$

It is stated that a requirement for (6.24) to be a reasonable solution of (6.21) the factor (A) must be kept in the range:

$$0.9 \leq A \leq 1 \tag{6.26}$$

The physical meaning behind this assumption can also be ascertained. Defining f_B as $\omega_B/2\pi$, (6.26) can be rewritten as:

$$0 \leq 40 f_B \leq \frac{1}{\tau} \tag{6.27}$$

Recognizing $1/\tau$ as the collision frequency and f_B as the applied field frequency, the assumption in reality states that the mean time between collisions must be a factor of 40 less than the period of the applied magnetic field. This appears to contradict the idea [Chiabrera and Bianco,1987] that the collision frequency must be less than the field frequency in order for the field to have a coherent resonant effect on the ion motion. If the collision frequency is too high, then the ion motion will be dominated by the collisions, and there will not be sufficient time between collisions to create any resonant effect due to the field forces.

The solution for the z position comes from (6.7) after assuming that E_z and F_z are not functions of time and that the ion starts from rest at z=0 (the mouth of the channel):

$$z \approx \frac{\tau q}{m}\left(E_z - \frac{F_z}{q}\right)t \tag{6.28}$$

This equation estimates the linear velocity of the ion in the z (transmembrane) direction as:

$$U_z = \frac{\tau q}{m}\left(E_z - \frac{F_z}{q}\right) \tag{6.29}$$

It is informative to evaluate this velocity expression for typical parameters associated with ion motion through a membrane channel. Using a value of 10^7 V/m for E_z (the transmembrane electric field created by a typical resting potential), a value of 4.8×10^6

coul/kg for the charge-to-mass ratio (equal to that of a calcium ion), and a value of 1 msec for τ yields a velocity of 4.8×10^{10} m/sec for the ion if F_z was equal to zero. Since this velocity would mean that an ion would cross the membrane in approximately 10^{-19} seconds, it is clear that in this formulation the restoring force F_z must almost completely balance the transmembrane driving force due to E_z in order to achieve the "slow" channel velocities required for coupling of the magnetic fields to ion motion during its channel transit. The source of this reactionary F_z force is not specified in the analysis. However, an idea of its magnitude can be obtained from the model by using the estimate that the channel transit time must be approximately equal to 1 period of a 16 Hz applied field (6.25 msec). To achieve this long transit time the ion velocity would need to be approximately 10^{-7} m/sec. From Equation (6.29), this velocity can only be achieved if the difference between E_z and F_z/q is on the order of 10^{-10}. Thus the reactionary F_z force must essentially cancel the force due to the transmembrane resting potential almost completely.

The final results of the model are obtained when the solution for the radial position (6.24), for times from 0 to 6.25 msec, is superimposed on a template of the model channel with its two constricted areas. The fluctuating radial envelope of the ion motion as defined by (6.24) causes the ion path to either just fit through the channel constrictions or collide with the channel lumen at the constricted points, depending on the nature of the DC and AC magnetic fields applied. The underlying assumption is that if the ion path can be made to "fit" through the constrictions without colliding, the channel permeability to the ion can be increased. Under this assumption, simulations for

various applied magnetic fields are shown. The shape of the channel walls was chosen so that magnetic field combinations which had been proven experimentally effective would create ion paths that would fit through the channel constrictions, whereas experimentally ineffective fields would create ion paths that would collide with the constrictions. Results show that the experimental features of resonance, AC amplitude sensitivity, and the 1,3,5, and 15 pattern of harmonics can be supported by the model.

The major strong points of the model appear to be its ability to match the experimental results obtained from experiments with cyclotron resonance tuned magnetic fields, and its reliance on fundamental electromagnetic forces to explain an effect on ion motion that could account for alteration of ion transport rates across cell membranes. The requirement for an ultra-slow channel in which ion transit times are several orders of magnitude longer than any channel yet discovered will need verification before any final acceptance of this model. In this regard, it is interesting to consider the possibility of a similar electromagnetic effect on active transport systems rather than ion channels. Active transport systems are also involved in ion flux across cell membranes, but ion transit times in active transport are much longer than their channel counterparts. As an example, the transit time for a Ca^{2+} ion in the calcium pump of the sarcoplasmic reticulum is approximately 100 msec [Stein,1986], comparable to cycle periods of low frequency fields. This raises the possibility that the "slow" channels proposed in this model might in fact be active transport systems. The method by which ions are transported in an active system is fundamentally different from channel transport in that it requires energy input (from ATP hydrolysis), and that it most likely involves a protein

conformational change to accomplish its task [Stein,1986]. However, these differences do not appear to completely rule out a possible effect of electromagnetic fields on ion motion within the active transport molecule similar to that described in this model for ion channels.

One characteristic of the model as it stands is that the ion motion is analyzed as if the only forces on it were due to the applied electromagnetic fields. In this way, smooth ion paths are obtained which do not include the random thermal motion which is inherent in all particle motion at physiological temperatures. It remains to be demonstrated that a form of ion motion resonance can occur in the face of thermal collisions. This point will be addressed further in Chapter 7 where some new ideas concerning the problem will be presented.

A further evaluation of the model can be made by considering its relation to the thermal noise level analysis. It appears that the only major feature contributing to the lowering of the thermal noise level in this model is that of the frequency band limiting inherently caused by the fit of the ion path to the channel shape. The model specifically involves motion of a single ion in a single channel, and thus employs no form of cooperativity to amplify the small effects of individual subunits. Also, the proposed time period over which the effect is observed is only one cycle of the applied magnetic field, so that the signal-to-noise improvement caused by an accretion of energy over a large number of cycles is not provided for.

The model is not purported to be the final, definitive answer to the question of electromagnetic field interaction with living cells. However, it does provide several

concepts that may well serve as a foundation for future contributions to the development of the theory. Specifically, the concepts of the "slow" ion channel as a locus for the field interaction, the direct effect of the magnetic field on the motion of the ion through the channel, the resulting effect on the permeability of the channel to the ion, and the crucial role that the shape of the ion channel plays in the process are basic precepts of the model which deserve further scrutiny.

Durney: Resonant Ion Motion

in Electromagnetic Fields

As a first step in modelling the possible interaction of electromagnetic fields with ions, Durney et al. [1988], have calculated the trajectories of ions exposed to various field combinations. The model is not presented as a comprehensive explanation of field-biosystem effects. Rather, it is intended to show how the coupling of applied fields to ions can result in resonant effects on ion motion. The model is limited to the calculation of motion for single ions in a homogeneous, viscous medium subject to applied electromagnetic fields. As such, the model is a very highly simplified representation of an actual physiological system. Thermal collisions are modeled in a crude way by applying a constant viscous damping force. However, random thermal motion of particles, forces from neighboring molecular structures, chemical gradient forces, and hydration effects are examples of some of the realistic biological parameters ignored by the model. Notwithstanding the extensive simplifications, the model is valuable as a first attempt at explaining resonant coupling between applied fields and ions at a fundamental level.

An assumption basic to the model is that the applied fields have their effect on a biological system by directly influencing the trajectories of free ions. The authors point out that the specific field-ion interaction site is not known, and hence a model completely including all biological parameters is impossible.

In order to solve for the motion of an ion subject to an applied magnetic field it is necessary to first calculate the electric field induced by the time-changing portion of the magnetic field, since this induced electric field also exerts a force on the ion. The beginning point for the calculation of the induced electric field is Faraday's Law:

$$\oint \overline{E} \cdot \overline{dl} = -\frac{\partial}{\partial t} \int \overline{B} \cdot \overline{dS} \tag{6.30}$$

If the system exhibits cylindrical symmetry, the electric field resulting from a time-changing magnetic field in the z direction has only a ϕ component. Assuming that the magnetic field does not vary over the region of interest, Faraday's Law can be simplified:

$$E_{\phi} = -\frac{r}{2}\frac{\partial B}{\partial t} \tag{6.31}$$

where r is the radial distance from the center of symmetry. Transforming to rectangular coordinates, and assuming B is sinusoidal of the form $B_{ac}\cos(\omega t)$, the induced electric field becomes:

$$E = (y\hat{x} - x\hat{y})\frac{\omega B_{ac}}{2}\sin(\omega t) \tag{6.32}$$

where $\hat{x}$ and $\hat{y}$ are unit vectors in the x and y directions respectively. Using this expression for the induced electric field, the total response of an ion to an applied magnetic field can be determined. The starting point for the calculation of the ion motion is taken to be the Lorentz equation describing the motion of any charged particle subjected to viscous damping and applied electromagnetic fields:

$$m\frac{d^2\bar{v}}{dt^2} = q(\bar{E} + \bar{v}\times\bar{B}) - \frac{m\bar{v}}{\tau} \tag{6.33}$$

where m is the ion mass, $\bar{v}$ its velocity, q its charge, $\bar{E}$ the applied electric field, $\bar{B}$ the applied magnetic field, and τ the mean time between collisions in the viscous medium.

The Lorentz equation above is a vector differential equation which can be written in component form as three scalar differential equations:

$$\begin{aligned}
\ddot{x} &= \frac{q}{m}E_x + \frac{qB_{ac}}{m}\left(\frac{y}{2}\dot{h} + h\dot{y}\right) + \frac{qB_{dc}}{m}\dot{y} - \frac{q}{m}\dot{x} \\
\ddot{y} &= \frac{q}{m}E_y - \frac{qB_{ac}}{m}\left(\frac{x}{2}\dot{h} + h\dot{x}\right) - \frac{qB_{ac}}{m}\dot{x} - \frac{q}{m}\dot{y} \\
\ddot{z} &= \frac{q}{m}E_z - \frac{q}{m}\dot{z}
\end{aligned} \tag{6.34}$$

where the magnetic field is assumed to be in the z direction only and has the form $B_{dc}+B_{ac}h(t)$, q is the particle charge, and m is the particle mass. It should be noted that

the above equations implicitly include the induced electric field separately from the E_x, E_y, and E_z terms, which are intended to represent any externally applied electric fields apart from that induced by the magnetic field. If these external electric fields are ignored, the particle motion can be viewed as a two-dimensional problem described by the following simultaneous differential equations:

$$\ddot{x} = \left(\frac{qB_{ac}\dot{h}}{2m}\right)y + \left(\frac{qB_{ac}h}{m} + \frac{qB_{dc}}{m}\right)\dot{y} - \left(\frac{q}{m}\right)\dot{x}$$
$$\ddot{y} = -\left(\frac{qB_{ac}\dot{h}}{2m}\right)x - \left(\frac{qB_{ac}h}{m} + \frac{qB_{dc}}{m}\right)\dot{x} - \left(\frac{q}{m}\right)\dot{y} \qquad (6.35)$$

Noting that the above simultaneous differential equations involve time-varying coefficients and will not yield a closed form solution, the authors resort to standard numerical methods in solving the equations. In order to accomplish this, the system of two second-order differential equations is rewritten as a system of four first-order equations by defining the state variables:

$$x_1(t) = \dot{x}(t)$$
$$x_2(t) = x(t)$$
$$x_3(t) = \dot{y}(t) \qquad (6.36)$$
$$x_4(t) = y(t)$$

The resulting first-order system can be written in matrix form:

$$\dot{x}(t) = A(t)x(t) \tag{6.37}$$

where x(t) is the vector:

$$x(t) = \begin{bmatrix} x_1(t) \\ x_2(t) \\ x_3(t) \\ x_4(t) \end{bmatrix} \tag{6.38}$$

and A(t) is the matrix:

$$A(t) = \begin{bmatrix} -\frac{1}{\tau} & 0 & (\omega_{ac}h + \omega_{dc}) & \frac{\omega_{ac}\dot{h}}{2} \\ 1 & 0 & 0 & 0 \\ -(\omega_{ac}h + \omega_{dc}) & -\frac{\omega_{ac}\dot{h}}{2} & -\frac{1}{\tau} & 0 \\ 0 & 0 & 1 & 0 \end{bmatrix} \tag{6.39}$$

In the above matrix, ω_{ac} represents qB_{ac}/m and ω_{dc} represents qB_{dc}/m. These quantities can be viewed as "cyclotron resonant" radian frequencies for the AC and DC applied magnetic fields.

Solutions of the first-order system are easily obtained once the nature of the time-varying signal (h(t)), is specified. The model focuses on solutions where h(t) is sinusoidal, in accordance with the magnetic fields employed in several experimental reports [Blackman et al.,1976; Liboff et al.,1987; Smith et al.,1987a]. Plots of resulting particle trajectories reveal several characteristics of motion under the influence of a magnetic field and its induced electric field. The DC portion of the applied magnetic field tends to bend the path of the particle around its axis, causing curved motion in the xy plane. The AC portion of the magnetic field modifies this curvature at periodic intervals, disrupting the normal circular path which would be observed in response to a DC magnetic field alone. Neither the DC or AC components of the magnetic field can alter the kinetic energy of the particle, since the force resulting from any applied magnetic field is always perpendicular to the velocity of the particle. To add energy to the particle, a force must be applied along the direction of particle motion. This force, crucial to the results of the model, arises from the electric field induced by the AC magnetic field. If "proper" field conditions exist, the electric field force reinforces the natural motion caused by the magnetic fields, and a resonant response ensues. The result of this type of resonance is a rapid increase in the distance of the particle from its starting point. Under resonance conditions, this distance will grow in an unbounded fashion, while unfavorable field conditions result in a kind of oscillation of the particle inside a bound area.

Considerable effort is devoted in the development of the model to determining what field combinations represent favorable conditions for resonance. An efficient

method for determining resonance conditions using the resolvent matrix $\Phi(t,s)$, associated with Equation (6.37) is outlined. By theorem, if the matrix A of the system described by Equation (6.37) is periodic with period T, then the system is uniformly stable if and only if all eigenvalues of $\Phi(T,0)$ are less than or equal to 1. Numerical methods are employed to solve for $\Phi(T,0)$ and its eigenvalues for given field combinations, looking for conditions which cause instabilities (unbounded displacement growth) corresponding to resonance. The results point to a pattern of resonant conditions that exhibit "windows" of instability that vary with the frequency and amplitude of the AC magnetic field. The areas of instability roughly coincide with the cyclotron resonance condition for the particular particle or one of its harmonics. Both even and odd harmonics of the fundamental cyclotron resonant frequency are equally effective at creating motion instabilities in the model. No specific harmonic pattern emerges from the model which would agree with experimentally effective harmonic patterns [Blackman et al.,1985; McLeod et al.,1987].

The model does provide a rational basis for the frequency and amplitude "windows" observed by several experimenters [Blackman et al.,1979; Smith et al.,1987; Liboff et al.,1987]. Within the simplified parameters defined by the model, the applied fields cause a net transport of charge by displacing an ion from its original position. Since this ion displacement reaches a maximum near cyclotron resonance conditions, the model suggests a physical rationale for the experimental finding that such fields can cause net ion transport (e.g. across cell membranes). Thus the model is interesting as a first step in describing the possible interaction of fields with ions.

Besides the aforementioned simplifications of biological realities that are included in the model, another assumption which may be called into question is the nature of the electric field induced by the time-changing magnetic field. The method described by Equations (6.30) through (6.32), which is based an a fundamental equation described by Maxwell, is valid for calculating the total electric field around a closed loop. The assumption made in the model is that cylindrical symmetry exists about some center so that the closed-loop integral of Equation (6.30) can be rewritten as a simple product with the electric field in the ϕ direction only. This assumption does not take into account the effect of the geometry of the field generating coils, nor the complexities caused by the material of any biological organism. In a typical experimental setup, circular Helmholtz generating coils are used to create the magnetic fields applied to the experimental sample. If the material in the region of the fields is homogeneous (free space, for example), the resulting electric field induced by a time-changing magnetic field will exhibit symmetry about the center of the coil axis, and increase in magnitude with the radial distance from this center, as in Equation (6.31). Thus, in the region of an ion associated with a typical cell in the experimental sample, the electric field may appear more linearly than circularly directed, as illustrated in Figure 24.

Of course, the actual electric field experienced by the ion in a biological sample is the critical parameter in the analysis. If by some mechanism the ion motion is constrained to a specific path, then the electric field of interest is that developed around the path. If, however, the ion is not so restricted, then the geometries of the field sources play a critical role in the forces on the ion. The electric field in any biological

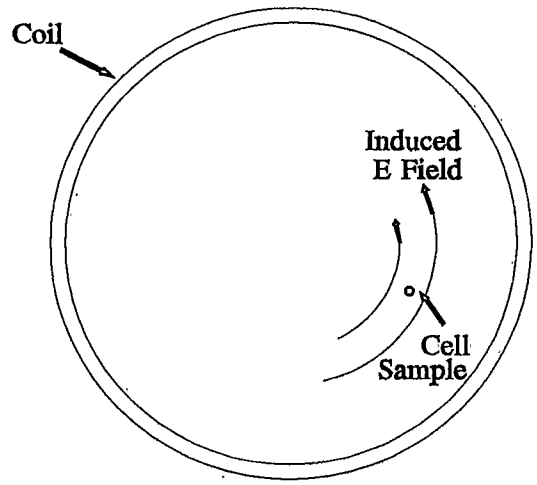

Figure 24. Induced E field from a coil setup

system is further complicated by electrical characteristics and charge distributions within the material. Thus, it would appear that the assumption of a uniform, circularly directed, induced electric field may not accurately represent the actual induced electric fields in a biological sample. However, the concept of a synchronized magnetic and electric field causing resonant ion displacement remains a reasonable foundation for possible field-biosystem interactions.

The idea that the induced electric field might cause biological effects by imparting kinetic energy to an ion deserves closer scrutiny. An initial method of evaluating the feasibility of this hypothesis is to calculate the magnitude of the induced electric field to see if it might be large enough to reasonably have an effect on a biological system. Using typical experimental values [Smith et al.,1987; Liboff et al.,1987] of .2 gauss peak

for the AC magnetic field amplitude and 16 Hz for the AC frequency in Equation (6.31) results in a circular electric field which varies with the radial distance from the center of symmetry:

$$E_\phi = .001r \tag{6.40}$$

Since the electric field magnitude varies linearly with this radial distance, the value chosen for r has a profound influence on the result obtained. If, for example, an ion was constrained to follow a circular path with radial dimension on the order of 10 angstroms (a typical membrane channel dimension), the induced field of interest would be 10^{-12} V/m. If typical cell dimensions are used (r = 10 μm), the electric field is 10^{-8} V/m. If typical source coil dimensions are used (r = 10 cm), an electric field of 10^{-4} V/m results. Comparing these values to the lowest reported effective electric field of 10^{-5} V/m [Bawin and Adey,1976], it appears that the induced electric field may possibly be a significant factor in magnetic field effects unless the ion path is extremely restricted, as may be the case for an ion crossing a membrane channel. However, extensive signal-to-noise improvements from frequency band limiting, signal averaging, cooperativity, or a combination of the three would be necessary in any case for such small signals to be detected in the presence of thermal noise.

One further limitation of the model is that the thermal velocity of the target ion is neglected. In the numerical simulations of the model, the ion motion is determined solely by the forces exerted by the applied electromagnetic fields. As a result, ion displacements, even under resonance conditions, are on the order of tens of nanometers per period (10 msec), of the applied fields. The simulated ion velocity is therefore about

10^{-6} m/sec. This stands in contrast to typical thermal velocities for ions in biological systems. For example, the mean thermal velocity for a Ca^{2+} ion in a plasma at 37°C has been calculated to be about 440 m/sec (see Equations 5.6 and 5.7). For classical cyclotron resonance, the radius of the ion orbit is a function of the velocity and applied field frequency:

$$R = \frac{v}{\omega} \tag{6.41}$$

where R is the orbit radius, v the velocity, and ω the applied frequency in radians per second. For ion velocities of 440 m/sec, and an applied frequency of 100 Hz, the orbit radius becomes .7 meters. Although the type of resonance observed in the Durney model differs slightly from classical cyclotron resonance due to the inclusion of the induced electric field in the equation, this calculation provides a good estimate of the required ion displacements necessary for the applied fields to have a resonant effect on ion motion for ions travelling at thermal velocities. Since ion motion in cellular processes involves displacements many orders of magnitude less than .7 meters, it appears that further consideration must be given to a mechanism by which low frequency fields can have a resonant effect on ions in spite of their high mean velocities.

Lednev: Alteration of Ion Binding Energy States

Lednev has proposed a model suggesting that electromagnetic fields may have their effect on biological systems by modifying the binding characteristics of ions to

certain receptor proteins [Lednev,1990; Lednev,1991]. The idea stands in contrast to the basic assumption that the fields have a direct effect on ion motion at some location in the biological system.

In the model, an ion in a biological atmosphere is viewed as a charged spatial oscillator which has a characteristic set of vibrational frequencies. The ion may form weak bonds with oxygen atoms in water molecules or in protein ligand groups. The energy state of the ion varies with its bonding relationships to nearby molecules. The model considers the simplest case, in which an ion has only an unbound (ground) state, and one excited state (ω), corresponding to the formation of a bond with some ligand. According to the authors, the excited energy level ω is split into two energy levels, ω_1 and ω_2, when a magnetic field B_o is applied. The distance between the two energy levels in radian units is qB_o/m, which is exactly equal to the cyclotron resonance frequency for the ion in a vacuum. If a sinusoidal magnetic field at the cyclotron resonance frequency is applied collinearly with the DC magnetic field, a frequency modulation of the energy levels ω_1 and ω_2 results. This modulation leads to a change in the probability that the ion will make a transition to its ground state, but only if the frequency is equal to the cyclotron resonance frequency or one of its subharmonics, according to:

$$n\omega = \frac{qB_{dc}}{m} \tag{6.42}$$

where n is an integer, ω is the radian frequency of the applied AC magnetic field, B_{dc} is the DC magnetic field, and q/m is the charge-to-mass ratio of the ion. The probability of a ground state transition under these conditions is said to increase according to:

$$\Delta p = 2A_1A_2J_n\left(\frac{B_{ac}}{nB_{dc}}\right) \tag{6.43}$$

where Δp is the change in probability, A_1 and A_2 are the amplitudes of electromagnetic radiation corresponding to ion transitions from each of the excited energy levels to the ground state, and J_n is a Bessel function of integral order. For the condition n=1, and a fixed value of B_{dc}, this altered probability varies with the AC magnetic field amplitude according to the first order Bessel function. For reference, a graph of $J_1(B_{ac}/B_{dc})$ is shown below:

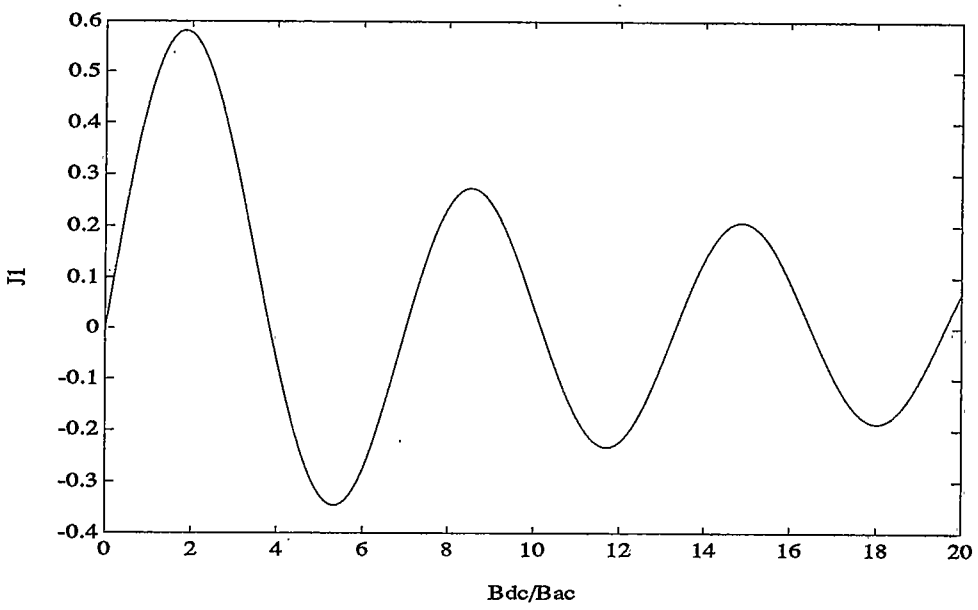

Figure 25. First order Bessel function

For a fixed value of B_{dc}, the Bessel function can be viewed as a profile of the predicted variation of the response with changing AC field amplitude. Assuming that the altered binding characteristics correspond to a macroscopic experimental effect, the pattern of

cyclic AC amplitude dependence displayed by the Bessel function is consistent with early experimental data showing that enhanced Ca^{2+} efflux caused by magnetic fields can be reversed as the AC field amplitude is increased [Liboff et al.,1987].

The prediction of the model that subharmonics of the fundamental cyclotron resonance frequency should also be effective in altering ion binding characteristics is neither supported by nor contradicted by the available experimental evidence. The model does attempt to explain curious patterns of effective higher harmonics observed in experiments, by extending the theory to include an ion able to form more than one bond with surrounding molecules. If the ion exists in a protein with 6 ligands represented by oxygen atoms of protein side groups, the total number of energy states of the seven-atom system is said to be 15. The following two conditions are then imposed:

$$\begin{aligned} n\omega &= 15\omega_c \\ \omega &= \omega_c k \end{aligned} \tag{6.44}$$

where ω is the applied frequency, ω_c is the cyclotron resonant frequency (qB_{dc}/m), and n and k are integers. The two conditions force the effective frequencies to be an integral fraction of the sum of all the 15 energy splits caused by the magnetic field, and to be a integral multiple of each individual energy split. Combining these two equations results in:

$$nk = 15 \tag{6.45}$$

Since n and k are integers, allowed values are 1,3,5 and 15. This harmonic pattern is identical to that observed in experiments with magnetic fields and diatom motility

[McLeod et al.,1987].

The author states that a primary advantage of the model over several others is that the predicted effect is independent of thermal motion. A common objection to models requiring magnetic fields to directly transfer kinetic energy to ions is that the energy in the magnetic field itself is many orders of magnitude smaller than the thermal kinetic energy of the ion. This objection does not appear to be applicable to this model, since the effect of the magnetic field is not to alter ion motion directly, but to affect its binding characteristics at some receptor site.

CHAPTER 7

NEW THEORETICAL IDEAS

Evaluating Cyclotron Resonance Models

Of the models reviewed in the previous section, those of Chiabrera and Bianco [1987], McLeod et al. [1991], Durney et al. [1988], and Lednev [1991] all attempt to provide physical rationale for the effectiveness of cyclotron resonance tuned magnetic fields in altering biological systems. As such, the models as a group can be evaluated from several perspectives, yielding insight into their plausibility.

Ion Interference

As a rule, the method followed in cyclotron resonance experiments has been to select a likely target ion, specify a DC magnetic field, and calculate the resonant frequency corresponding to the DC field for the ion. The resulting magnetic fields are created along an axis by passing electrical current through a wire coil arrangement similar to that shown in Figure 26. In Figure 26 the geomagnetic field (B_{geo}) is resolved into components parallel and perpendicular to the field generated by the coils. The DC current through the coils is adjusted so that the sum of the geomagnetic field and the DC field from the coils adds up to the desired value along the axis. Thus the DC field

created by the coils must be a function of the component of the geomagnetic field along the coil axis, as shown.

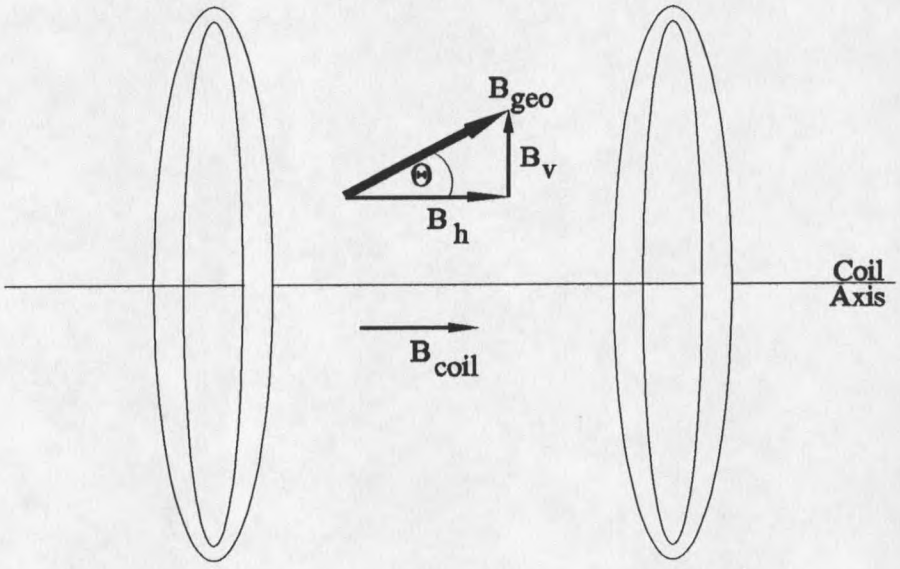

Figure 26. Helmholtz Coil Arrangement

The first difficulty which arises in such a scheme is due to the possibility of overlap between the resonance curves of the target ion and other ions which may also be biologically active. In a complex system, if multiple types of ions are affected in a resonant manner, the total effect may be unpredictable. Simply selecting a target ion and tuning the magnetic fields to its resonance conditions does not necessarily imply that all other important ions are not in resonance. This is especially true when the extra complexities of higher harmonics and direction of the DC field are considered. Hence, a clear determination of the effects of resonating one ion can only take place if the system has inherent "filtering" characteristics so that the effects of resonating other ions

can be eliminated. The diatom mobility experiments of Smith et al. [1987], are an example of one experimental system which may indeed exhibit such "filtering". The sharp resonance curves, and opposite effects of fields tuned to Ca^{2+} and K^+ ions tend to support the hypothesis that effects from other ions are minimal compared to the effects from the target ions. Figure 27 represents a simple analysis indicating the extent to which the response of ions other than the target ion can overlap with, and complicate the system's response to a target ion. The figure assumes that a system response for magnetic fields tuned to ion cyclotron resonance exhibits a "resonance curve" (as frequency is varied), similar to the curve obtained for the diatom mobility experiments [Smith et al.,1987]. A further assumption is that for each of the ions considered (Mg^{2+}, Ca^{2+}, K^+, and Na^+), harmonics 1,3 and 5 of the fundamental resonant frequency are also biologically effective. Resonance curves for each ion-harmonic combination are shown in Figure 27, assuming a DC magnetic field of .2 gauss.

The degree of overlapping of the curves demonstrates that singling out a biological response to a single ion can be difficult. As an example, an attempt to tune the magnetic fields to resonate the third harmonic of Na^+ will simultaneously create near resonant conditions for the fifth harmonic of K^+ and the third harmonic of Ca^{2+}. Thus from an ion resonance viewpoint, the response of the system to resonance tuned magnetic fields could possibly be an aggregate of the effects of several different ions. Of course, creating resonant conditions for a given ion does not guarantee that an observable biological result will ensue. Small alterations in ionic dynamics caused by the fields do not necessarily imply a biological response. Also, the creation of ion resonant magnetic

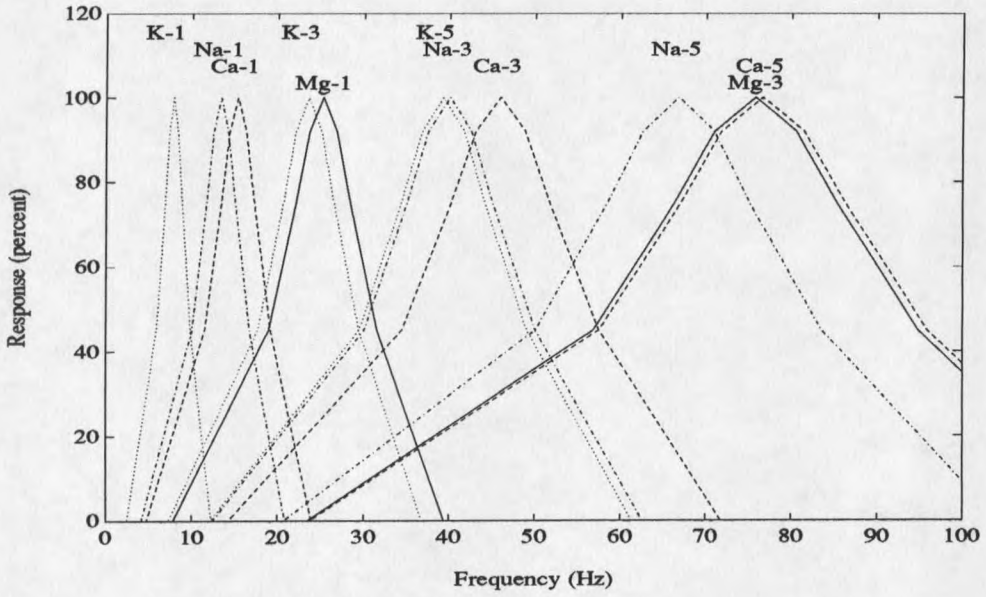

Figure 27. Harmonic resonance curves for four ions

fields does not guarantee an alteration in ion dynamics. Addressing the first point, it is well known that organisms exhibit a high degree of buffering and "negative feedback" mechanisms that tend to keep its processes at an equilibrium. Thus a real perturbation caused by an applied magnetic field may not result in a macroscopic effect unless a threshold is exceeded [Polk,1986]. Concerning the second point, it is by no means clear that tuning weak magnetic fields to cyclotron resonance conditions will affect all ion behavior in a significant way. In addition to the proper magnetic fields, specific cell sites, structures, or other biological parameters may very well be critical to the coupling of the fields to the ion. The channel structure proposed by McLeod et al. [1991], the binding sites proposed by Lednev [1991], and the cell surface properties proposed by Chiabrera and Bianco [1987] are all examples of cell structures hypothesized to be

crucial to a biological effect. If such favorable cell conditions are required, it is entirely possible that certain ions do not enjoy such favorable conditions in some biological systems. The marine diatoms may be an example of a biological system whose response to magnetic fields is dominated by effects from a very few ions (most notably Ca^{2+} and K^{+}). It may prove experimentally productive to continue to focus on such simple systems that demonstrate the inherent ability to "filter" out effects from other ions, before trying to extend the results to more complicated systems.

Resonant Surfaces

A further difficulty exists in trying to generate cyclotron resonant fields for a target ion in a biological system under laboratory conditions. As mentioned previously, the typical method of generating ion cyclotron resonant fields is to use a Helmholtz coil apparatus or solenoid to generate the desired fields along one axis. Unfortunately, this procedure leads unavoidably to the creation of resonant fields for other ions along other directions, further complicating the overlapping resonance curves mentioned in the previous section. Several of the proposed interaction models require that the resonant fields be applied in a particular direction relative to the cell or a cell structure. For instance, the model of McLeod et al. [1991], assumes the applied magnetic fields are maintained in resonant relationship along the axis of a membrane channel. Though not specifically mentioned, the assumption of ion receptor sites as the point of field-ion interaction may lead to similar "direction sensitivity" in the models of Adey [1990], and Lednev [1991], if the orientation of the fields relative to the binding structure proves important. The analysis to follow evaluates the plausibility of such "direction sensitivity"

in light of the experimental data amassed to date.

The analysis begins by assuming a cell model having a spherical shape whose membrane channels are perpendicular to the cell surface as shown in Figure 28.

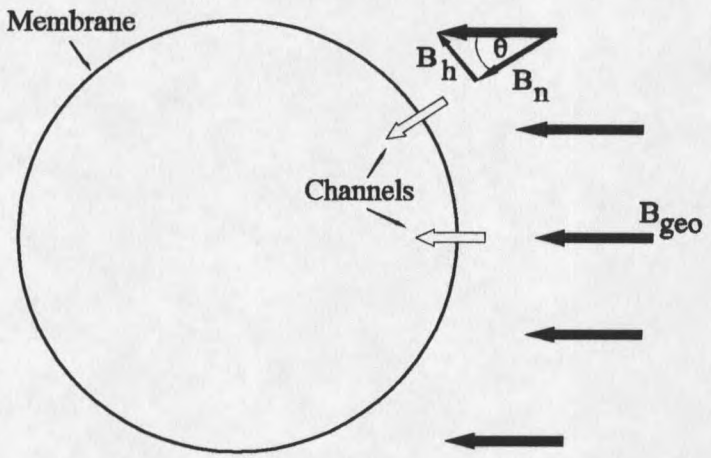

Figure 28. Spherical model of cell membrane

Assuming, in accord with the model of McLeod et al. [1991], that the resonant fields must be maintained along the axis of a channel to be effective, the figure illustrates that resonance conditions are not created over the whole cell surface. The component of the applied field along the axis of each channel, (B_n in the figure), is a function of the cosine of the angle θ between the channel axis and the vector field. Therefore resonance conditions exist only for those channels whose axis is nearly aligned with the applied field vector. The result is a resonance for the target ion which is restricted to a limited area on the cell surface. Of course, other portions of the cell surface may experience

resonance conditions for another ion, since the DC magnetic field varies continuously around the cell surface. This further enhances the possibility of the non-target ion interference effects discussed above. To illustrate this effect, a computer program was written to evaluate the resonant areas for different ions on the surface of a spherical cell. The MATLAB code listing for the program appears in Appendix E. The program allows plotting of the magnitudes of the resonant surface areas to allow a visual evaluation of the problem of ion interference.

The computer program allows the user to input the magnitude and direction of the local geomagnetic (DC) field and the desired ion resonance conditions in the form of the DC magnetic field magnitude and the AC frequency. The program then calculates the DC field that must be generated by the coils to compensate for the geomagnetic field and create the desired net DC field along the coil axis. Next, the component of each of the magnetic fields (coil and geomagnetic) perpendicular to the cell surface is calculated at a large number of points arranged in grid-like fashion on the surface. The resultant fields at each point are tested to see if they fall within the resonance bandwidths for each of 14 different ions. In this way a picture of the resonant surface areas for each of the ions is developed. In order to qualify for resonance, the DC amplitude of the normal magnetic field must be within 12.5% of the cyclotron resonant value corresponding to the applied frequency, and the AC magnetic field amplitude must be within 40% of the DC field amplitude. These numbers were chosen to coincide approximately with the resonant bandwidths demonstrated for the diatom experiments [Smith et al.,1987]. The program checks for resonance conditions for harmonics 1,3,5 and 15 of the fundamental

cyclotron resonance conditions. The total resonant surface area for a given ion is taken to be the sum of the resonant areas for each of the harmonics for that ion, expressed as a percentage of the total surface area of the sphere. Figure 29 is an example of the program output with the parameters listed in the figure. In the legend, Bgeo represents the DC geomagnetic field magnitude and ϕ and θ represent the angles of the geomagnetic field with respect to the coil axis, as shown in Figure 30. Bdc represents the total static magnetic field due to the sum of the coil field and the geomagnetic field in the direction of the coil axis.

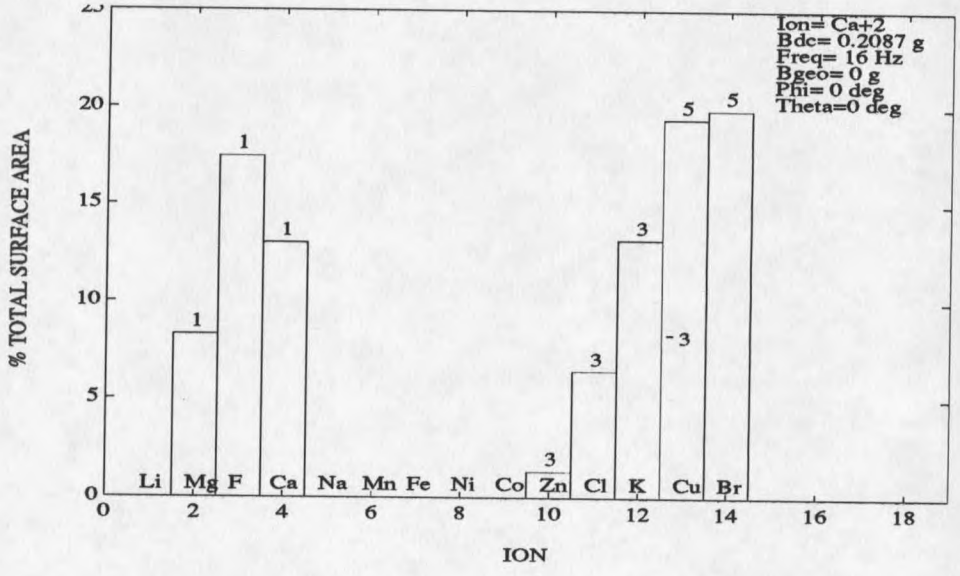

Figure 29. Resonant surface percentage.

Figure 29 illustrates the complications observed in resonance conditions assuming the system is sensitive to the direction of the applied fields. Though the fields are tuned specifically to create resonance conditions for the Ca^{2+} ion, only about 13% of the surface area of a spherical cell is in resonance for Ca^{2+}. Several other ions exhibit

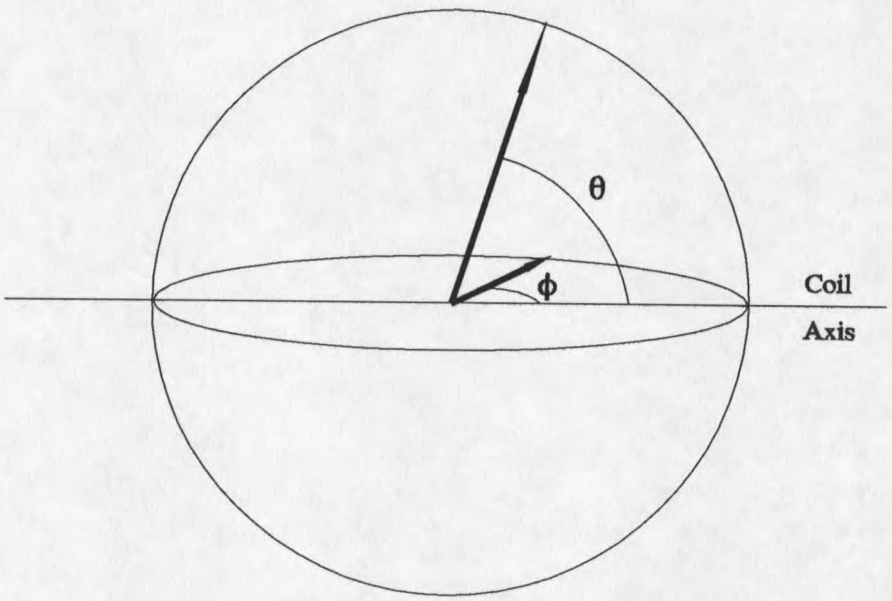

Figure 30. Definition of ϕ and θ angles.

significantly greater resonant surface areas than Ca^{2+}. The phenomenon is further clarified by observing a map of the surface of the cell with the resonant areas marked, as in Figure 31. The figure consists of the top half of the cell surface mapped onto a rectangular space. Figure 31 shows that the resonant surface area for the Ca^{2+} ion consists of two semispheres centered where the coil axis intersects the sphere.

For comparison, Figure 32 shows similar resonant surface areas for the K^+ ion under the same field conditions. The resonant area is an annulus centered around the coil axis.

Figures 29, 31 and 32 show that the resonant surface areas for Ca^{2+} and K^+ are nearly equal in magnitude although they exist on different parts of the spherical cell surface. In at least two experiments [Smith et al.,1987; Smith et al.,1991], tuning of

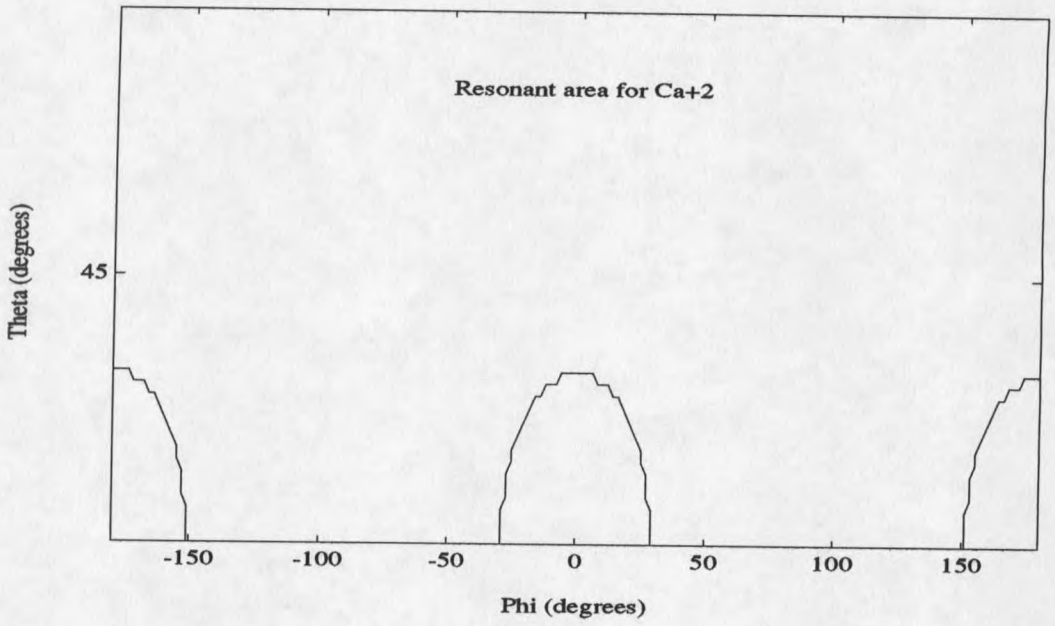

Figure 31. Calcium resonant area under Ca^{2+} CR conditions.

magnetic fields to resonance conditions for K^+ has produced the opposite biological effect from fields tuned to resonance conditions for Ca^{2+}. The above analysis illustrates that simply tuning magnetic fields for ion cyclotron resonant conditions along one axis may not guarantee that the resulting biological effect, if any, is necessarily due to altered ion dynamics for the target ion. Rather, the nature of the cell surface, the geomagnetic field, and the effective harmonic patterns may combine to confuse the resonance picture so that ions other than the target ion could enjoy more favorable resonance conditions than the target ion itself. Of course, the extent of the ion interference problem is unknown. The foregoing analysis of the problem is based on three assumptions: 1) that the cell system is sensitive to the direction of the applied fields, 2) that the effective resonance window for the AC frequency is plus or minus 12.5% from the cyclotron resonant peak

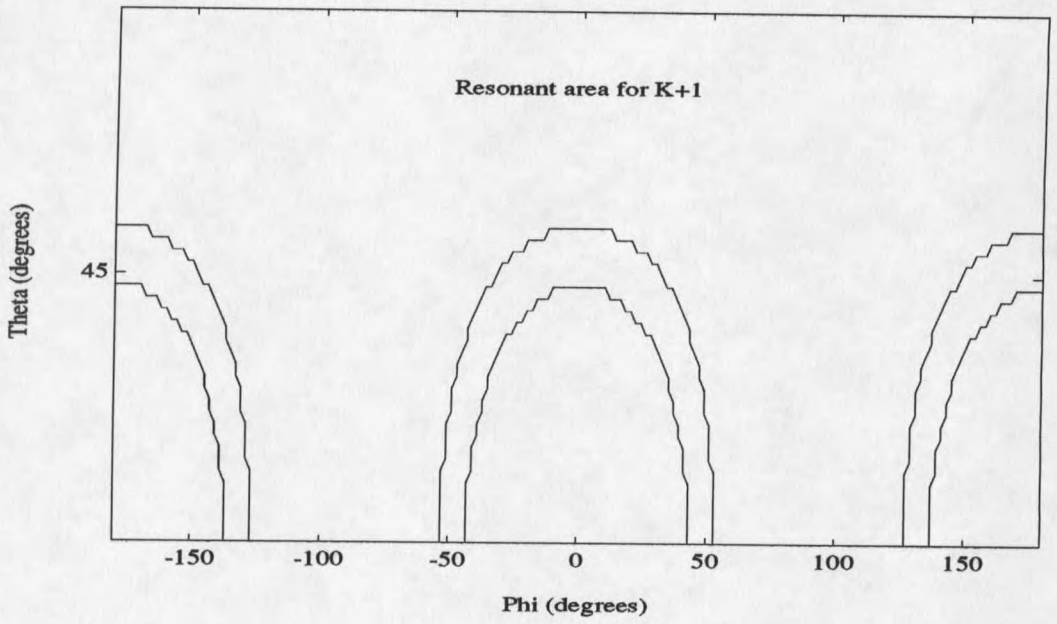

Figure 32. Potassium resonance area under Ca^{2+} CR conditions.

frequency, and, 3) that the effective resonance window for the AC amplitude is plus or minus 40% from the DC magnetic field amplitude. None of the assumptions has been proven for all biological systems. In particular, the first assumption is only a hypothesis whose experimental vindication or rejection remains for future work. In fact, further analysis reveals an apparent inconsistency of the predictions of this assumption with the current experimental evidence. Analyzing resonant surface areas for different DC field amplitudes at the same frequency reveals that the maximum resonant surface area for a target ion is not obtained by tuning to exact cyclotron resonance conditions.

Figure 33 shows the resonant surface for the Ca^{2+} ion for the same conditions as Figure 29 except that the DC field is .23 gauss, which is slightly greater than the .209 gauss predicted by the cyclotron resonance equation.

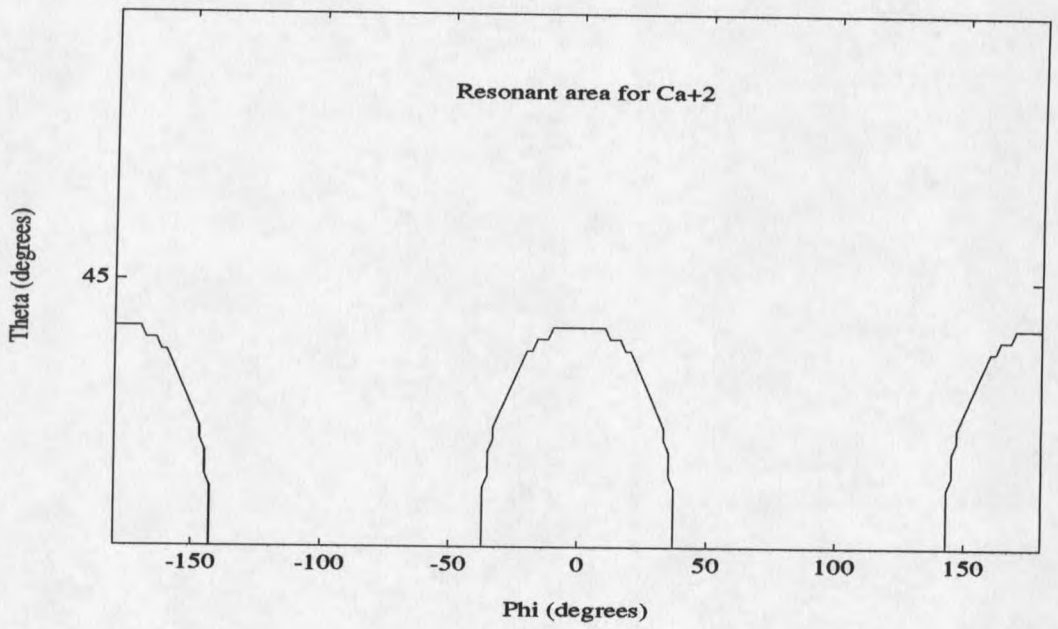

Figure 33. Ca^{2+} resonant area with altered DC field.

Comparison of Figures 29 and 33 reveals that the resonant surface area is greater when the DC magnetic field is slightly greater than the value predicted by the cyclotron resonance equation. The reason for this phenomenon follows from the assumption that the cell system is sensitive only to the component of the DC field which is normal to the cell surface (i.e. parallel to membrane channel axes) at any given point on the surface, and from the assumption that the resonance can occur for DC fields within a percentage tolerance (in this case plus or minus 12.5%), of the calculated cyclotron resonance value. A profile of the resonant surface area for the Ca^{2+} ion as a function of the DC magnetic field for an AC frequency of 16 Hz is shown in Figure 34.

Figure 34 reveals that the resonant surface area reaches a peak at a DC magnetic field value of .235 gauss. Note that this value is 12.5% greater than the calculated

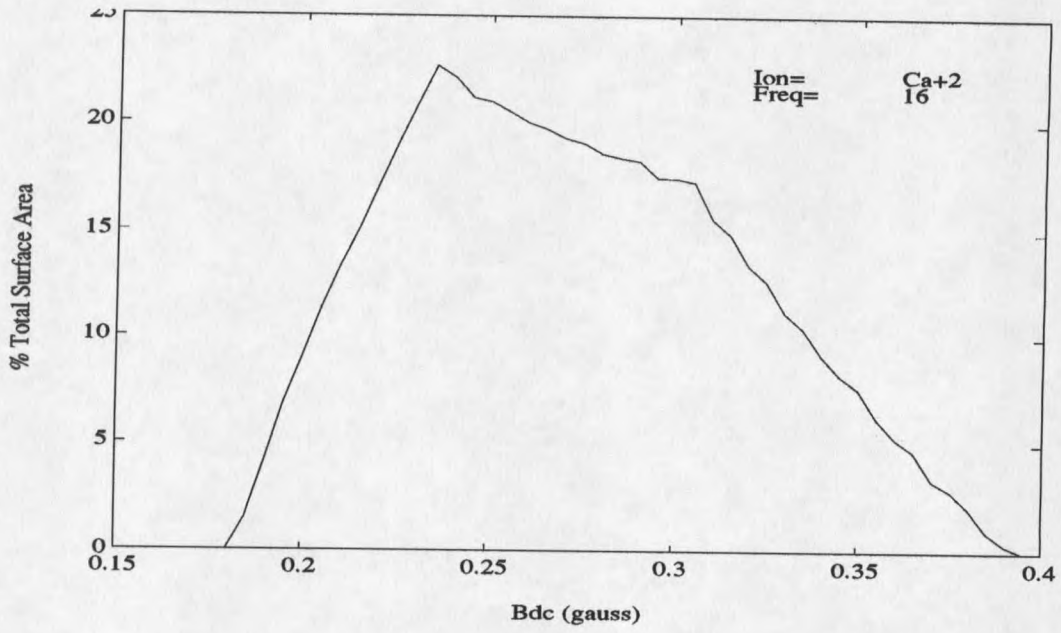

Figure 34. Resonant surface area versus DC field

cyclotron resonance value of .209 gauss for a 16 Hz AC frequency. This result illustrates that under the assumptions of the model, the maximum resonant surface area for a target ion is not achieved at the exact cyclotron resonance conditions, but rather when the DC magnetic field is increased so that it is just at the upper limit of its resonant "window" for the given AC frequency.

Several experiments demonstrating the effectiveness of cyclotron resonant fields on biological systems have shown peak responses exactly at cyclotron resonance conditions [Smith et al.,1987; Liboff et al.,1987]. These experimental results call into question one or more of the assumptions under which the above analysis was performed. In particular, the assumption of system sensitivity to the direction of the applied fields might be challenged since it arose from a theoretical model instead of experimental data.

If the interaction mechanism was not sensitive to the direction of the applied fields, then setting up cyclotron resonant fields in one direction could in essence create resonant conditions along the whole surface, instead of just small portions. This direction-insensitivity would occur if the resonant mechanism could make use of the total DC field at all points on the surface, rather than just the DC field component perpendicular to the cell membrane. In this event, one would expect the effect to occur exactly at cyclotron resonance conditions, agreeing with the experimental results.

One last complication created by the assumption of a system sensitive to the direction of the applied fields is that the resonant surface area for a given ion can be affected dramatically by the presence of an external (geomagnetic) DC field at some angle to the direction of the fields created by the coil apparatus. As an example, Figure 35 shows the Ca^{2+} resonant surface area under Ca^{2+} cyclotron resonant conditions as does Figure 29, but with an added geomagnetic field of .5 gauss directed at an angle 30° from the coil fields.

Comparison of Figures 29 and 35 reveals the dramatic difference in resonant surface area that the presence of a geomagnetic field can make. In each case, the field along the coil axis is adjusted to give exact cyclotron resonance conditions. The presence of the geomagnetic field in the second case significantly alters the normal DC component of the total magnetic field at all points along the cell surface, resulting in completely different resonant surface areas. Several experiments have reported a sensitivity of the biological response to the total DC magnetic field at the exposure site [Blackman et al.,1985; Thomas et al.,1986; McLeod et al.,1987; Liboff et al.,1987], but

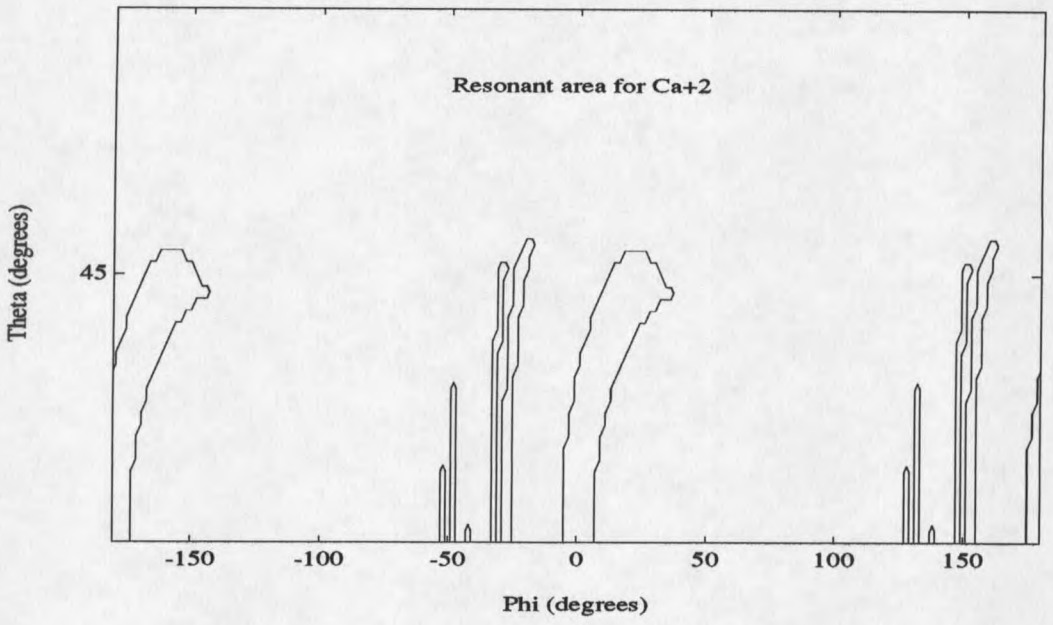

Figure 35. Ca^{2+} resonant area with .5 g geomagnetic field

to date none have implicated separate roles for the background geomagnetic and applied coil DC fields, as predicted by the above analysis. This fact once again raises questions about the validity of the assumption of the sensitivity of the cell systems to the direction of the applied magnetic fields.

Cyclotron Resonance and Thermal Collisions

The results of experiments involving low frequency electromagnetic fields and biological organisms have created real difficulties for those attempting to propose theories explaining the interaction. On the one hand, sharp resonance response curves, and the predictable relationship between the DC magnetic field and effective AC frequencies suggest that the interaction between the fields and the organism should be

rather clear cut and well ordered. On the other hand, the effective fields have exhibited extremely low frequencies and weak amplitudes, leaving simple, clear cut theories open to criticism from a physical standpoint. One of the most common criticisms of cyclotron resonance theories involves noise from thermal collisions of ions with other particles in the biological milieu [Halle,1988]. In several proposed models [McLeod et al.,1991; Chiabrera and Bianco,1987], the effect of the magnetic field on the organism follows directly from an effect on the motion of ions under the influence of the magnetic field. In order for low frequency fields to have a coherent effect on the ion motion, however, it would appear that the ion must be free to travel for long periods of time (several cycles of the applied field), with relatively few thermal collisions. Mean time between collisions for affected ions would then be on the order of tens of milliseconds, orders of magnitude greater than the collision times normally experienced by particles in a biological setting. The models of McLeod and Chiabrera both attempt to solve the thermal collision problem by hypothesizing an interaction site which affords the longer collision times required. McLeod suggests that membrane channels may offer such an environment, while Chiabrera suggests that the immediate vicinity of the cell surface may be sufficiently depleted to allow for reduced thermal collisions.

In this section, a new hypothesis will be presented which attempts to describe a resonant effect on ion motion which can take place in environments where thermal collisions are high. In this model, thermal collisions, rather than being a hindrance which must be eliminated, prove to be an essential part of the conditions creating the ion resonance. The model is admittedly rudimentary, but may serve to stimulate more

thinking about the mechanism by which extremely low frequency fields can elicit the well ordered biological responses that have appeared in the results of numerous experiments.

A first approach to the concept behind the model can be made by considering ion motion which is constrained within a boundary. In the analysis to follow, attention will be focused on the two-dimensional ion motion in the plane of the boundary. The boundary itself is idealized at the outset to be a circle. Real cellular structures which may approximate the circular boundary include the interior of membrane channels and ion binding sites. The ion trapped within the circular boundaries is assumed to travel at a mean thermal velocity determined by temperature. As it collides with the boundary, the ion ricochets back into the interior in a random direction. The process is illustrated in Figure 36.

Now consider the effect of a DC magnetic field on the path of the ion as it oscillates within the boundary. In the absence of a magnetic field, the ion paths between collisions will be approximated by straight lines. If a DC magnetic field is applied in a direction perpendicular to the plane of the ion motion, the force on the ion is given by the Lorentz force equation:

$$\overline{F} = q(\overline{v}\times\overline{B}) \tag{7.1}$$

The force on the ion is perpendicular to the ion velocity and the magnetic field, and results in a very small deflection of the ion in this direction. An exaggerated illustration of this deflection is shown in Figure 37.

In Figure 37, the h direction is defined to be the direction of the cross product

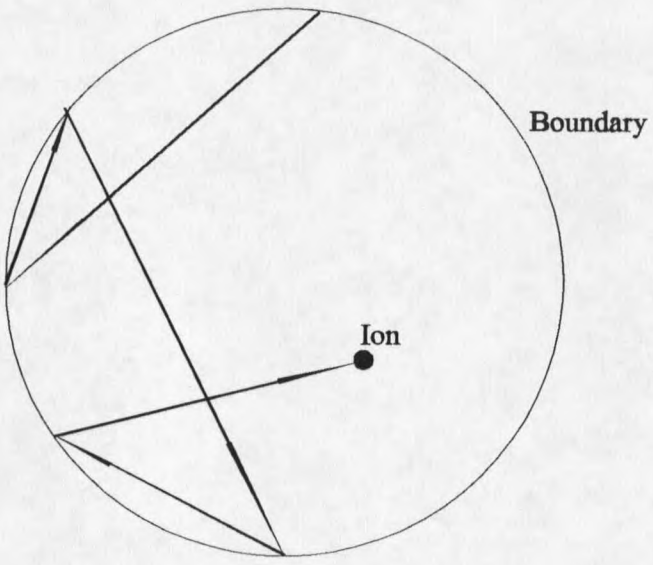

Figure 36. Ion motion within circular boundary

between the velocity vector and magnetic field vectors, as illustrated. To determine the magnitude of the small deflection (Δh), in Figure 37, the component of the equation of motion in the direction perpendicular to the original path p can be written:

$$\ddot{h} = \frac{qvB}{m} \tag{7.2}$$

where q is the ion charge, v is the magnitude of its velocity, B is the magnetic field magnitude, and m is the ion mass. As defined, the displacement and velocity of the ion in the y direction are both zero as the traverse begins. Use of these initial conditions results in a solution for the deflection in the y direction:

$$h = \frac{qvBt^2}{2m} \tag{7.3}$$

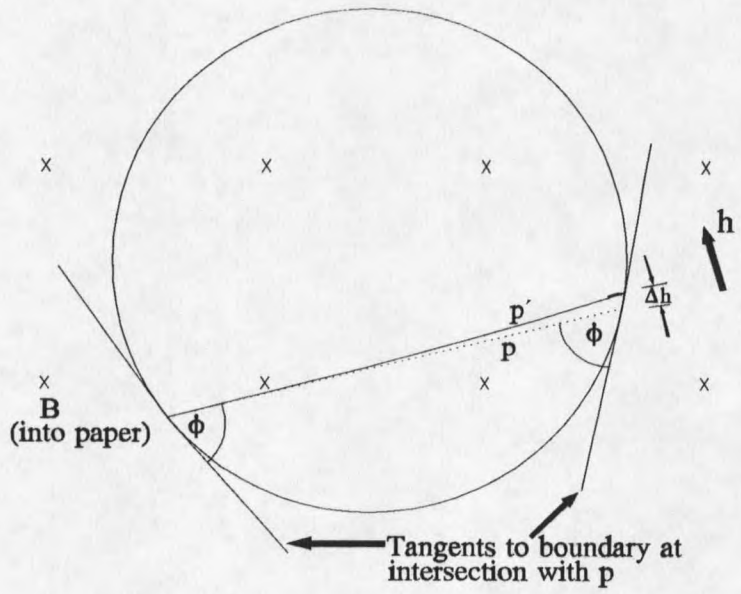

Figure 37. Ion deflection under magnetic field influence

where t is the elapsed time since the beginning of the traverse. If the total transit time is designated Δt, then the deflection Δh is easily obtained by substituting Δt for t in Equation (7.3):

$$\Delta h = \frac{qvB(\Delta t)^2}{2m} \tag{7.4}$$

If the total traverse time is small, the resulting deflection will also be very small, so that the original path and the deflected paths coincide almost exactly. Typical mean time between collisions in biological systems is on the order of picoseconds or less, so an assumption of small traverse times appears quite plausible when viewed from a physical standpoint. Equation (7.4) can be rewritten using the fact that the ion velocity v can be expressed as $p/\Delta t$:

$$\Delta h = \frac{qpB(\Delta t)}{2m} \tag{7.5}$$

If the deflection Δh is small, the paths p and p′ approximate parallel lines as illustrated in Figure 38.

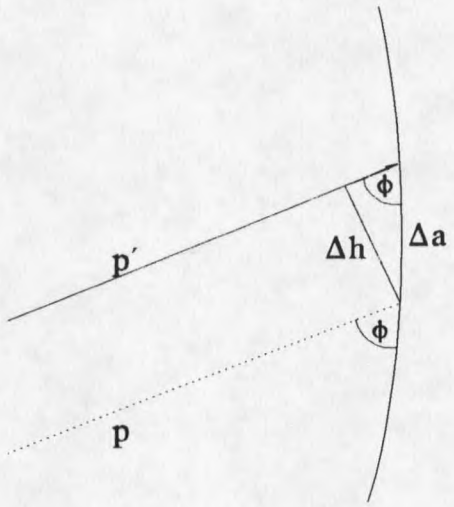

Figure 38. Deflected ion path at boundary.

The arc length Δa in Figure 38 is simply Δh divided by the factor sin(ϕ):

$$\Delta a = \frac{qpB(\Delta t)}{2m \sin(\phi)} \tag{7.6}$$

The path length p can also be expressed as a function of the radius r and the angle ϕ:

$$p = 2r \sin(\phi) \tag{7.7}$$

Using this expression for p, the arc length can be rewritten:

$$\Delta a = \frac{qrB(\Delta t)}{m} \tag{7.8}$$

Note that the arc length is not a function of the direction of the ion velocity as it begins its traverse (angle ϕ). It depends only on the transit time Δt. It is clear from Equation (7.8) that the magnetic field causes a deflection of the ion which results in a net displacement of the ion position around the circumference of the boundary. As the ion executes many random transits across the interior of the circular boundary, the circumferential velocity associated with each transit is given by:

$$\frac{\Delta a}{\Delta t} = \frac{qrB}{m} \tag{7.9}$$

This circumferential velocity results in a net angular motion of the ion with a frequency equal to the circumferential velocity divided by the circumference:

$$f = \frac{qrB}{m(2\pi r)} = \frac{qB}{2\pi m} \tag{7.10}$$

This frequency is identical to the cyclotron resonance frequency defined by Equation (1.10) for an ion in a DC magnetic field. It should be noted that Equation (7.10) does not predict the position of the oscillating ion at any given time. Rather, it defines a net angular velocity that will manifest itself over a great many oscillations of the ion. This angular velocity is independent of the speed at which the ion moves as it traverses from boundary to boundary, and of the number of "bounces" it makes off the boundary walls. It is also independent of the size of the circular boundary. The result given by (7.10) therefore holds for ions undergoing a great many thermal collisions at arbitrarily large

collision frequencies. The circular boundary provides a structure which constrains the ion motion in such a way as to create the low frequency net circular motion. The clear advantage of the model is that ions are no longer required to undergo long periods of time free from thermal collisions. Instead, organization of the thermal collisions into boundaries allows retention of the cyclotron resonant angular motion while placing no restriction on the number of thermal collisions the ion undergoes.

The Beginning of a Model

The possibility of ion cyclotron resonant motion in the face of thermal collisions as outlined above raises the possibility of several mechanisms by which combined DC and AC magnetic fields might affect ion dynamics and ionic flux in such a way as to induce biological effects. Applying an AC magnetic field at the cyclotron resonant frequency to an ion trapped within a circular boundary raises the possibility of displacing the overall ion position in a resonant manner, if the boundaries are not completely rigid. Such ion displacement might prove important in the ability of an ion to traverse a "slow" channel, similar to the hypothesis of McLeod et al. [1991]. Alternatively, such an ion displacement might affect ion binding characteristics at binding sites that are important in transmembrane ionic flux. The models of Chiabrera and Bianco [1987], and Lednev [1991], hypothesize effects due to altered binding characteristics, though the mechanisms causing the altered binding are different from that proposed above.

A third possibility may also explain why small displacements of bound ions might induce cellular changes sufficient to cause significant alteration of transmembrane ionic

flux. One can conceive of a cell structure which has a large number of ions at similar binding sites along its surface. A DC magnetic field applied to the surface could cause a small resonant displacement of the ions oscillating at the cyclotron resonant frequency. The key fact in this model is that since all the ions are subject to the same magnetic field, their displacements will be synchronized, as illustrated in Figure 39.

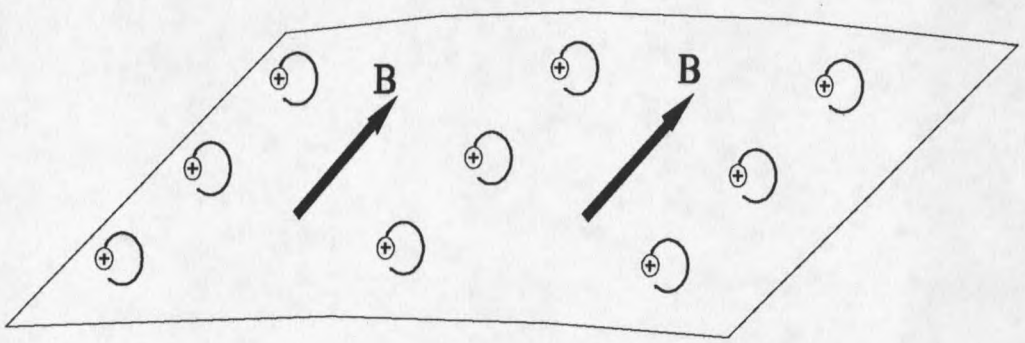

Figure 39. Resonant displacement of ions along membrane surface.

Adey [1990], has hypothesized that some such form of cooperativity is required to explain the phenomenon of amplification which allows low-energy electromagnetic fields to induce biological effects. The possible synchronization of the displacements of many ions suggests a mechanism by which this cooperativity might be achieved. In this model, the magnetic field serves as an agent causing cooperative motion of many ions. The resulting cooperative ion displacement could cause a large magnification of the

electrostatic forces created by the bound ions. Such a shift in the electrostatic environment of the membrane surface might in turn affect transmembrane ion transport by altering the gating characteristics of transmembrane channels. The altered electrostatic environment caused by the magnetic fields could conceivably affect membrane gating characteristics directly or indirectly by inducing a structural phase transition in the membrane.

If such a mechanism does in fact exist, it could facilitate coupling of extremely weak electromagnetic fields to biological systems on three fronts. First, the cyclotron resonance phenomenon inherently exhibits a narrow band of effective AC frequencies, determined by the DC magnetic field. This frequency band limiting reduces the system noise threshold as described in Chapter 5. Second, the possibility of signal averaging over multiple cycles exists in the model. Tiny resonant ion displacements could accumulate over several cycles before achieving amplitudes large enough to trigger larger effects. Third, an inherent mechanism for cooperativity is included, which could result in an amplification of the desired signal without a corresponding amplification of system noise.

Considering the body of experimental data that has been gathered to date, at least one shortcoming of this proposed model is evident. As it stands, there is nothing in the model to explain the existence of the curious 1,3,5 and 15 harmonic pattern observed in at least one experiment [McLeod et al.,1987]. The effectiveness of odd harmonics in this model is expected to be similar to that described in an early cyclotron resonance model [McLeod and Liboff,1987]. Briefly stated, all odd harmonics should prove effective in

imparting energy to the ion in a resonant manner, though each successive one less so than the previous one. It would perhaps require the existence of special structures in the ion-boundary system to account for the ineffectiveness of some of the odd harmonics.

CHAPTER 8

CONCLUSIONS AND FUTURE WORK

Obstacles to the Discovery of an Interaction Mechanism

The fact that very weak, low frequency electromagnetic fields can significantly alter the processes of living organisms has now been well established. Unfortunately, the reasons behind the effects are not well understood. The lack of a definitive model explaining low frequency electromagnetic field effects is a result of several factors. First, the interaction of the fields with the organism takes place on such a small scale that it is impossible to "see" the interaction taking place. Though the macroscopic effects of the interaction are plainly evident, the microscopic mechanisms are not. Another obstacle to discovery of the mechanism of field-organism interaction is the very nature of the electromagnetic fields themselves. The magnitudes of the effective fields are often miniscule compared to the forces inherently present in the biological target system. Similarly, the cycle periods of extremely low frequency fields are often many orders of magnitude longer than the microscopic biological processes they are presumed to affect. A further difficulty arises from the wide diversity of the biological systems that have proven to be susceptible to electromagnetic field effects. Effects have been observed on many systems ranging from one-celled organisms to complex brain tissue.

The diversity of these systems raises the possibility that more than one mechanism of interaction may exist.

Experimental Evidence

Though the goal of discovering the mechanism or mechanisms by which low frequency electromagnetic fields affect biological organisms has not been reached, various experiments have uncovered several clues that may help lead to the discovery. One of the most important of these clues is the apparent involvement of ions and ionic flux in many or all of the effects [Blackman et al.,1979; Bawin and Adey,1976; Liboff et al.,1987]. The cell membrane surface has been identified as the likely site of field interaction by various studies employing membrane blocking agents [Bawin et al.,1978; Lin-Liu and Adey,1982; Dixey and Rein,1982]. Further experimental evidence indicates that applied fields must be within certain frequency and amplitude "windows" to be effective, and that these windows may be quite narrow [Blackman et al.,1985; Bawin et al.,1975; Smith et al.,1987; Liboff et al.,1987]. Some experiments have demonstrated an effect from an electric field [Bawin and Adey,1976], and others have shown that a magnetic field is indispensable [Blackman et al.,1985; Smith et al.,1987; Liboff et al.,1987]. The DC magnetic field in the region of the experiment has been shown to affect the location of the frequency windows in an orderly way [Blackman et al.,1985]. Magnetic fields tuned to cyclotron resonance conditions for various ions have produced convincing evidence that at least some of the effects may be due to some sort of cyclotron resonance mechanism [Smith et al.,1987; Liboff et al.,1987; Deibert et

al.,1991]. In general, only odd harmonics of a fundamental resonant frequency have proven effective [Blackman et al.,1985], while a distinct harmonic pattern (1,3,5 and 15) has been observed in at least one system [McLeod et al.,1987].

New Experiments

The experimental results recorded in this thesis demonstrate the ability of calcium cyclotron resonance tuned magnetic fields to enhance the growth of bean plants. The plant roots appear to be especially sensitive to the application of the magnetic fields. The effect of the fields is modified by the temperature at which the experiments are carried out. The effect is more pronounced at temperatures significantly less than the optimal growing temperature for the plants. This result suggests that temperature may serve as a stress factor that predisposes the plants to the magnetic field effects. It is not known if the lower temperature alters the plant to make it more susceptible to the magnetic fields or if it simply provides an environment in which the microscopic field effects are expressed more dramatically in macroscopic form.

There is much room to expand on the plant growth results that have been obtained to date. One specific opportunity lies in varying the frequency of the AC magnetic field around the cyclotron resonant value. In several reports on other systems, a "resonance curve" resulted from such experiments, showing a peak effect at the cyclotron resonant frequency [McLeod et al.,1987; Liboff et al.,1987]. Additional experiments which may prove enlightening include varying the AC amplitude, tuning to higher harmonics, and tuning to ions besides calcium. Certainly, the effect of

temperature on the results deserves better characterization. A complete curve showing the dependence of the effect on temperature is desirable. Finally, the experiments may be extended to include other plant systems.

Theoretical Models

The need for a verified theoretical model describing the effects of low frequency electromagnetic fields on biological organisms is rapidly becoming more acute. Several epidemiological studies have uncovered a possible link between such fields and adverse health effects such as cancer [Wertheimer and Leeper,1979; Savitz et al.,1988]. At the same time, beneficial effects such as bone growth enhancement are well documented. Clearly, an understanding of the underlying mechanism behind the effects is necessary. Only with this knowledge can safety standards concerning electromagnetic field exposure be established with confidence. Such an understanding may also point the way toward many new beneficial applications of low frequency electromagnetic fields.

The discovery that cyclotron resonant magnetic fields can induce dramatic effects in several biological systems is undoubtedly a big step forward in the effort to establish a model of interaction. However, the reason why such fields are effective is still a matter of debate. Several widely different theories have already been proposed. Much future experimental work should be devoted toward discovering the mechanism by which cyclotron resonant fields have their effect. Given the past successes in demonstrating such effects on different systems, it is tempting to focus on extending the same results to other systems, with a view toward the many practical applications which may be

possible. Such experiments are necessary, but should be increasingly accompanied by experiments designed specifically to establish, test and refine hypotheses concerning the actual interaction mechanism.

The particular theoretical model proposed in this thesis concerns the synchronous resonant displacement of many ions along the surface of a cell membrane. The hypothesis included in this model is that cyclotron resonant fields can induce such a cooperative synchronous displacement of many ions, and that a corresponding change in the electrostatic environment of the membrane will result. It is further proposed that the electrostatic shift may be sufficient to cause alteration of the gating characteristics of ionic channels either directly or by means of an intermediate phase transition in the membrane itself. Such a hypothesis might be tested on an artificial membrane known to have many similar ionic binding sites along its surface. If the membrane conductivity can be altered using cyclotron resonant fields, or if a phase transition can be induced by such fields under certain conditions, then this hypothesis deserves further consideration.

Future Potential

If experimental history is any indication, the ramifications of electromagnetic effects on living organisms may be far reaching. Without doubt, many more effects will be uncovered as research continues. However, until the mechanism behind the effects is discovered the work will be slow going, and the full extent both of potential health problems and potential benefits will remain a mystery.

REFERENCES CITED

1. Adey, W. R. (1990), "Nonlinear Electrodynamics in Cell Membrane Transductive Coupling", in Membrane Transport and Information Storage, Alan R. Liss, Inc., New York

2. Barinaga, M. (1990), "Playing Tetherball in the Nervous System", Science, 250:506-507

3. Barnes, F. S. and M. Seyed-Madani (1987), "Some Possible Limits on the Minimum Electrical Signals of Biological Significance", In Mechanistic Approaches to Interactions of Electric and Electromagnetic Fields with Living Systems, M. Blank and E. Findl, Eds., Plenum, New York

4. Bassett, C. A. L., R. J. Pawluk and A. A. Pilla (1974), "Augmentation of Bone Repair by Inductively Coupled Electromagnetic Fields, Science, 184:575-577

5. Bassett, C. A. L. (1971), "Biophysical Principles Affecting Bone Structure", in The Biochemistry and Physiology of Bone, G. H. Bourne, Ed., Academic Press, New York

6. Bawin, S. M., R. J. Gavalas-Medici and W. R. Adey (1973), "Effects of Modulated Very High Frequency Fields on Specific Brain Rhythms in Cats", Brain Research, 58:365-384

7. Bawin, S. M., L. K. Kaczmarek and W. R. Adey (1975), "Effects of Modulated VHF Fields on the Central Nervous System", Annals of the New York Academy of Sciences, 247:74-81

8. Bawin, S. M. and W. R. Adey (1976), "Sensitivity of Calcium Binding in Cerebral Tissue to Weak Environmental Electric Fields Oscillating at Low Frequency", Proceedings of the National Academy of Sciences, 73:1999-2003

9. Bawin, S. M., W. R. Adey and I. M. Sabbot (1978), "Ionic Factors in Release of $^{45}Ca^{2+}$ from Chicken Cerebral Tissue by Electromagnetic Fields", Proceedings of the National Academy of Sciences, 75:6314-6318

10. Blackman, C. F., J. A. Elder, C. M. Weil, S. G. Benane, D. C. Eichinger and D. E. House (1979), "Induction of Calcium-Ion Efflux from Brain Tissue b Radio Frequency Radiation: Effects of Modulation Frequency and Field Strength", Radio Science, 14(6S):93-98

11. Blackman, C. F., S. G. Benane, J. A. Elder, D. E. House, J. A. Lampe and J. M. Faulk (1980a), "Induction of Calcium-Ion Efflux from Brain Tissue by Radiofrequency Radiation: Effect of Sample Number and Modulation Frequency on the Power-Density Window", Bioelectromagnetics, 1:35-43

12. Blackman, C. F. S. G. Benane, W. T. Joines, M. A. Hollis and D. E. House (1980b), "Calcium-Ion efflux from Brain Tissue: Power-Density Versus Internal Field-Intensity Dependencies at 50-MHz RF Radiation", Bioelectromagnetics, 1:277-283

13. Blackman, C. F., S. G. Benane, L. S. Kinney, W. T. Joines and D. E. House (1982), "Effects of ELF Fields on Calcium-Ion Efflux from Brain Tissue In Vitro", Radiation Research, 92:510-520

14. Blackman, C. F., S. G. Benane, J. R. Rabinowitz, D. E. House and W. T. Joines (1985), "A Role for the Magnetic Field in the Radiation-Induced Efflux of Calcium Ions from Brain Tissue In Vitro", Bioelectromagnetics, 6:327-337

15. Blackman, C. F., S. G. Benane, D. J. Elliott, D. E. House and M. M. Pollack (1988a), "Influence of Electomagnetic Fields on the Efflux of Calcium Ions from Brain Tissue In Vitro: A Three-Model Analysis Consistent With the Frequency Response Up to 510 Hz", Bioelectromagnetics, 9:215-227

16. Blackman, C. F., D. E. House, S. G. Benane, W. T. Joines and R. J. Spiegel (1988b), "Effect of Ambient Levels of Power-Line-Frequency Electric Fields on a Developing Vertebrate", Bioelectromagnetics, 9:129-140

17. Blank, M. (1987), "Ionic Processes at Membrane Surfaces: The Role of Electrical Double Layers in Electrically Stimulated Ion Transport", in Mechanistic Approaches to Interactions of Electric and Electromagnetic Fields with Living Systems, M. Blank and E. Findl, Eds., Plenum, New York

18. Botstein, D. and G. R. Fink (1988), "Yeast: An Experimental Organism for Modern Biology", Science, 240:1439-1443

19. Brisson, A. and P. N. T. Unwin (1985), "Quaternary Structure of the Acetylcholine Receptor", Nature, 315:474-477

20. Campbell, A. K. (1983), Intracellular Calcium, John Wiley and Sons, New York

21. Campbell, N. A. (1987), Biology, Benjamin/Cummings Publishing Company, Inc., Menlo Park, California

22. Cheung, W. Y. (1980), "Calmodulin Plays a Pivotal Role in Cellular Regulation", Science, 207:19-27

23. Chiabrera, A. and B. Bianco (1987), "The Role of the Magnetic Field in the EM Interaction with Ligand Binding", in Mechanistic Approaches to Interactions of Electric and Electromagnetic Fields with Living Systems, M. Blank and E. Findl, Eds., Plenum, New York

24. Conti, P., G. E. Gigante, M. G. Cifone, E. Alesse, G. Ianni, M. Reale and P. U. Angeletti (1983), "Reduced Mitogenic Stimulation of Human Lymphocytes by Extremely Low Frequency Electromagnetic Fields", Federation of European Biochemical Societies Letters, 162:156-160

25. Conti, P., G. E. Gigante, M. G. Cifone, C. Fieschi, M. Reale and P. U. Angeletti (1985), "A Role for Ca^{2+} in the Effect of Very Low Frequency Electromagnetic Fields on the Blastogenesis of Human Lymphocytes", Federation of European Biochemical Societies Letters, 181:28-31

26. Cooksey, B. and K. E. Cooksey (1980), "Calcium is Necessary for Mobility in the Diatom Amphora Coffeaeformis", Plant Physiology, 65:129-131

27. Deibert, M. C., B. R. McLeod, S. D. Smith and A. R. Liboff (1991), "Ion Magnetic Resonance Stimulation of Fracture Healing in Rabbits with Fibular Ostectomies", in review

28. Delgado, J. M. R., J. Leal, J. L. Monteagudo and M. G. Gracia (1982), "Embryological Changes Induced by Weak, Extremely Low Frequency Electromagnetic Fields", Journal of Anatomy, 134:533-551

29. Dixey, R. and G. Rein (1982), "^{3}H-Noradrenaline Release Potentiated in a Clonal Nerve Cell Line by Low-Intensity Pulsed Magnetic Fields", Nature, 296:253-256

30. Durney, C. H., C. K. Rushforth and A. A. Anderson (1988), "Resonant AC-DC Magnetic Fields: Calculated Response",Bioelectromagnetics,9:315-336

31. Dutta, S. K., A. Subramoniam, B. Ghosh and R. Parshad (1984), "Microwave Radiation-Induced Calcium Ion Efflux from Human Neuroblastoma Cells in Culture", Bioelectromagnetics, 5:71-78

32. Dutta, S. K., B. Ghosh and C. F. Blackman (1989), "Radiofrequency Radiation-Induced Calcium Ion Efflux Enhancement from Human and Other Neuroblastoma Cells in Culture", Bioelectromagnetics, 10:197-202

33. Findl, E. (1987), "Membrane Transduction of Low Energy Level Fields and the Ca^{++} Hypothesis", in Mechanistic Approaches to Interactions of Electric and Electromagnetic Fields with Living Systems, M. Blank and E. Findl, Eds., Plenum, New York

34. Fischer, W., J. Brickmann and P. Lauger (1981), "Molecular Dynamics Study of Ion Transport in Transmembrane Protein Channels", Biophysical Chemistry, 13:105-116

35. Fischer, W. and J. Brickmann (1983), "Ion-Specific Diffusion Rates Through Transmembrane Protein Channels- A Molecular Dynamics Study", Biophysical Chemistry, 18:323-327

36. Foster, K. R. and H. P. Schwan (1986), "Dielectric Permittivity and Electrical Conductivity of Biological Materials", in CRC Handbook of Biological Effects of Electromagnetic Fields, C. Polk and E. Postow, Eds., CRC Press Inc., Boca Raton, Florida

37. Fox, J. A. (1987), "Ion Channel Subconductance States", Journal of Membrane Biology, 97:1-8

38. Friedman, H., R. O. Becker and C. H. Bachman (1967), "Effect of Magnetic Fields on Reaction Time Performance", Nature, 213:949-950

39. Gavalas-Medici, R. and S. R. Day-Magdaleno (1976), "Extremely Low Frequency, Weak Fields Affect Schedule-Controlled Behaviour of Monkeys", Nature, 261:256-259

40. Goodman, R., C. A. L. Bassett and A. S. Henderson (1983), "Pulsing Electromagnetic Fields Induce Cellular Transcription", Science, 220:1283-1285

41. Goodman, R., and A. S. Henderson (1986), "Sine Waves Enhance Cellular Transcription", Bioelectromagnetics, 7:23-29

42. Grundler, W., F. Keilman and H. Frölich (1977), "Resonant Growth Rate Response of Yeast Cells Irradiated by Weak Microwaves", Physics Letters, 62A:463-466

43. Halle, B. (1988), "On the Cyclotron Resonance Mechanism for Magnetic Field Effects on Transmembrane Ion Concuctivity", Bioelectromagnetics, 9:381-385

44. Hoshi, T., W. N. Zagotta and R. W. Aldrich (1990), "Biophysical and Molecular Mechanisms of Shaker Potassium Channel Inactivation", Science, 250:533-538

45. Kaczmarek, L. K. and W. R. Adey (1974), "Weak Electric Gradients Change Ionic and Transmitter Fluxes in Cortex", Brain Research, 66:537-540

46. Halliday, D. and R. Resnick (1962), Physics for Students of Science and Engineering, John Wiley and Sons, Inc., New York

47. Hasselbach, W., J. Suko, M. H. Stromer and R. The (1975), "Mechanism of Calcium Transport in Sarcoplasmic Reticulum", Annals of the New York Academy of Sciences, 264:335-349

48. Hille, B. (1984), Ionic Channels of Excitable Membranes, Sinauer Associates, Inc., Sunderland, Massachusetts

49. Hucho, F., W. Oberthür and F. Lottspeich (1986), "The Ion Channel of the Nicotinic Acetylcholine Receptor is Formed By the Homologous Helices MII of the Receptor Subunits", Federation of European Biochemical Societies Letters, 205:137-142

50. Jordan, P. C. (1984), "The Total Electrostatic Potential in a Gramicidin Channel", Journal of Membrane Biology, 78:91-102

51. Koeppe, R. E. II, J. M. Berg, K. O. Hodgson and L. Stryer (1979), "Gramicidin A Crystals Contain Two Cation Binding Sites Per Channel", Nature, 279:723-725

52. Krouse, M. E., G. T. Schneider and P. W. Gage (1986), "A Large Anion-Selective Channel Has Seven Conductance Levels", Nature, 319:58-60

53. Kwang, S. K., H. L. Nguyen, P. K. Swaminathan and E. Clementi (1985), "Ion Transport Through a Solvated Gramicidin A Transmembrane Channel: Molecular Dynamics Studies Using Parallel Processors", Journal of Physical Chemistry, 89:2870-2876

54. Lednev, V. V. (1990), "Interaction of Modulated Electromagnetic Radiation with Biological Systems: Theoretical Predictions and Experimental Data", presented at the Twelfth Annual Meeting of the Bioelectromagnetics Society, Abstract A-1-4

55. Lednev, V. V. (1991), "Possible Mechanism for the Influence of Weak Magnetic Fields on Biological Systems", Bioelectromagnetics, 12:71-75

56. Levitt, D. G. (1978), "Electrostatic Calculations for an Ion Channel", Biophysical Journal, 22:209-219

57. Lewis, R. S. and M. D. Cahalan (1989), "Mitogen-Induced Oscillation of Cytosolic Ca^{2+} and Transmembrane Ca^{2+} Current in Human Leukemic T Cells", Cell Regulation, 1:99-112

58. Liboff, A. R., T. Williams Jr., D. M. Strong and R. Wistar Jr. (1984), "Time-Varying Magnetic Fields: Effect on DNA Synthesis", Science, 223:818-820

59. Liboff, A. R. (1985), "Cyclotron Resonance in Membrane Transport", in Interactions Between Electromagnetic Fields and Cells, A. Chiabrera, C. Nicolini and H. P. Schwan, Eds., Plenum, New York

60. Liboff, A. R., R. J. Rozek, M. L. Sherman, B. R. McLeod and S. D. Smith (1987), "Ca^{2+}-45 Cyclotron Resonance in Human Lymphocytes", Journal of Bioelectricity, 6:13-22

61. Liboff, A. R. and B. R. McLeod (1988), "Kinetics of Channelized Membrane Ions in Magnetic Fields", Bioelectromagnetics, 9:39-51

62. Liboff, A. R., J. R. Thomas and J. Schrot (1989), "Intensity Threshold for 60-Hz Magnetically Induced Behavioral Changes in Rats", Bioelectromagnetics, 10:111-113

63. Liboff, A. R. and W. C. Parkinson, "Search for Ion-Cyclotron Resonance in an Na^+-Transport System", Bioelectromagnetics, 12:77-83

64. Lin-Liu, S. and W. R. Adey (1982), "Low Frequency Amplitude Modulated Microwave Fields Change Calcium Efflux Rates from Synaptosomes", Bioelectromagnetics, 3:309-322

65. Luben, R. A., C. D. Cain, M. C. Chen, D. M. Rosen and W. R. Adey (1982), "Effects of Electromagnetic Stimuli on Bone and Bone Cells In Vitro: Inhibition of Responses to Parathyroid Hormone by Low-Energy Low-Frequency Fields", Proceedings of the National Acacemy of Sciences, 79:4180-4184

66. Lyle, D. B., R. D. Ayotte, Z. Wang, A. R. Sheppard and W. R. Adey (1989), "Activation and Proliferation of Normal and Leukemic T-Lymphocytes Exposed to Magnetic Fields Under Calcium Cyclotron Resonance Conditions", Presented at the Eleventh Annual Meeting of the Bioelectromagnetics Society, Abstract B-3-3

67. Lyle, D. B., X. Wang, R. D. Ayotte, A. R. Sheppard and W. R. Adey (1990), "Modulation of Calcium Uptake by Concanavalin A and Ouabain in Normal and Leukemic T-Lymphocytes Exposed to Magnetic Fields Under Calcium Cyclotron Resonance Conditions", Presented at the Twelfth Annual Meeting of the Bioelectromagnetics Society, Abstract E-3-4

68. Mackay, D. H. J., P. H. Berens, K. R. Wilson and A. T. Hagler (1984), "Structure and Dynamics of Ion Transport Through Gramicidin A", Biophysical Journal, 46:229-248

69. Marron, M. T., E. M. Goodman and B. Greenebaum (1975), "Mitotic Delay in the Slime Mould Physarum Polycephalum Induced by Low Intensity 60 and 75 Hz Electromagnetic Fields", Nature, 254:66-67

70. Martin, A. H. (1988), "Magnetic Fields and Time Dependent Effects on Development", Bioelectromagnetics, 9:393-396

71. McLeod, B. R., S. D. Smith and A. R. Liboff (1987), "Calcium and Potassium Cyclotron Resonance Curves and Harmonics in Diatoms (A. Coffeaeformis)", Journal of Bioelectricity, 6:153-168

72. McLeod, B. R. and A. R. Liboff (1987), "Cycolotron Resonance in Membrane Transport: The Theory of the Mechanism", in Mechanistic Approaches to Interactions of Electric and Electromagnetic Fields with Living Systems, M. Blank and E. Findl, Eds., Plenum Press, New York

73. McLeod, B. R., A. R. Liboff and S. D. Smith (1990), "Cell Channel Model Suggested by Data Linking Biological Systems and ELF Fields", presented at the twelfth annual meeting of the Bioelectromagnetics Society, Abstract D-1-5

74. McLeod, B. R., A. R. Liboff and S. D. Smith (1991), "Electromagnetic Gating in Ion Channels", in review

75. Merritt, J. H., W. W. Shelton and A. F. Chamness (1982), Attempts to Alter $^{45}Ca^{2+}$ Binding to Brain Tissue With Pulse-Modulated Microwave Energy", Bioelectromagnetics, 3:475-478

76. Michaelson, S. M. (1985), "Perspective on Windows and Calcium Efflux Studies", in Interactions Between Electromagnetic Fields and Cells, A. Chiabrera, C. Nicolini and H. P. Schwan, Eds., Plenum Press, New York

77. Morris, E. O. (1958), "Yeast Growth", in The Chemistry and Biology of Yeasts, A. H. Cook, Ed., Academic Press, London

78. Oppenheim, A. V. and R. W. Schafer (1975), Digital Signal Processing, Prentice-Hall, London

79. Ott, H. W. (1988), Noise Reduction Techniques in Electronic Systems, John Wiley and Sons, Inc., New York

80. Parkinson, W. C. and C. T. Hanks (1989), "Search for Cyclotron Resonance in Cells In Vitro", Bioelectromagnetics, 10:129-145

81. Parsegian, A. (1969), "Energy of an Ion Crossing a Low Dielectric Membrane: Solutions to Four Relevant Electrostatic Problems", Nature, 221:844-846

82. Phillips, J. L., W. D. Winters and L. Rutledge (1986), "In Vitro Exposure to Electromagnetic Fields: Changes in Tumour Cell Porperties", Int. J. Radiat Biol., 49:463-469

83. Poenie, M., J. Alderton, R. Y. Tsien and R. A. Steinhardt (1985), "Changes of Free Calcium Levels With Stages of the Cell Division Cycle", Nature, 315:147-149

84. Polk, C. (1986), "Introduction", in CRC Handbook of Biological Effects of Electromagnetic Fields, C. Polk and E. Postow, Eds., CRC Press, Inc., Boca Raton, Florida

85. Polymeropoulos, E. E. and J. Brickmann (1985), "Molecular Dynamics of Ion Transport Through Transmembrane Model Channels", Annual Review of Biophysics and Biophysical Chemistry, 14:315-330

86. Ramirez, E., J. L. Monteagudo, M. García-Gracia and J. M. R. Delgado (1983), "Oviposition and Development of Drosophila Modified by Magnetic Fields", Bioelectromagnetics, 4:315-326

87. Reese, J. A., M. E. Frazier, J. E. Morris, R. L. Buschbom and D. L. Miller (1991), "Evaluation of Changes in Diatom Mobility After Exposure to 16-Hz Eletromagnetic Fields", Bioelectromagnetics, 12:21-25

88. Sagan, P. M. and R. G. Medici (1979), "Behavior of Chicks Exposed to Low-Power 450-MHz Fields Sinusoidally Modulated at EEG Frequencies", Radio Science, 14(6S):239-245

89. Sakmann, B. and E. Neher, Eds. (1983), Single Channel Recording, Plenum, New York

90. Savitz, D., H. Wachtel, F. Barnes, E. John and J. Tvrdik (1988), "Case Control Study of Childhood Cancer and Exposure to 60-Hz Magnetic Fields", American Journal of Epidemiology, 128:21-38

91. Schatzmann, H. J. (1983), "The Red Cell Calcium Pump", Annual Review of Physiology, 405:303-312

92. Shelton, W. W. Jr. and J. H. Merritt (1981), "In Vitro Study of Microwave Effects on Calcium Efflux in Rat Brain Tissue", Bioelectromagnetics, 2:161-167

93. Sheppard, A. R., S. M. Bawin and W. R. Adey (1979), "Models of Long-Range Order in Cerebral Macromolecules: Effects of Sub-ELF and of Modulated VHF and UHF Fields", Radio Science, 14(6S):141-145

94. Shirakawa, F., U. Yamashita, S. Oda, S. Chiba, S. Eto and H. Suzuki (1986), "Calcium Dependency in the Growth of Adult T-Cell Leukemia Cells In Vitro", Cancer Research, 46:658-661

95. Silver, R. A., A. G. Lamb and S. R. Bolsover (1990), "Calcium Hotspots Caused by L-Channel Clustering Promote Morphological Changes in Neuronal Growth Cones", Nature, 343:751-754

96. Skerra, A. and J. Brickmann (1987), "Simulation of Voltage-Driven Hydrated Cation Transport Through Narrow Transmembrane Channels", Biophysical Journal, 51:977-983

97. Smith, R. F. (1988), "Lithium as a Normal Metabolite: Some Implications for Cyclotron Resonance of Ions in Magnetic Fields", Bioelectromagnetics, 9:387-391

98. Smith, S. D., B. R. McLeod, A. R. Liboff and K. E. Cooksey (1987a), "Calcium Cyclotron Resonance and Diatom Mobility", Bioelectromagnetics, 8:215-227

99. Smith, S. D., B. R. McLeod, A. R. Liboff and K. E. Cooksey (1987b), "Calcium Cyclotron Resonance and Diatom Motility", Studia Biophysica, 119:131-136

100. Smith, S. D., B. R. McLeod and A. R. Liboff (1991), "Control of Embryonic Chick Bone Growth by Resonant Electromagnetic Fields",in review

101. Smith, S. J., A. B. MacDermott and F. F. Weight (1983), "Detection of Intracellular Ca^{2+} Transients in Sympathetic Neurones Using Arsenazo III", Nature, 304:350-352

102. Stein, W. D. (1986), Transport and Diffusion Across Cell Membranes, Academic Press, Inc., Orlando

103. Swierenga, S. H. H., J. F. Whitfield and S. Karasaki (1978), "Loss of Proliferative Calcium Dependence: Simple In Vitro Indicator of Tumorigenicity", Proceedings of the National Academy of Sciences, 75:6069-6072

104. Taylor, D. L., J. R. Blinks and G. Reynolds (1980), "Contractile Basis of Ameboid Movement", The Journal of Cell Biology, 86:599-607

105. Thomas, J. R., J. Schrot and A. R. Liboff (1986), "Low-Intensity Magnetic Fields Alter Operant Behavior in Rats", Bioelectromagnetics, 7:349-357

106. Toyoshima, C. and N. Unwin (1988), "Ion Channel of Acetylcholine Receptor Reconstructed from Images of Postsynaptic Membrane", Nature, 336:247-250

107. Unwin, N. (1986), "Is there a Common Design for Cell Membrane Channels?", Nature, 323:12-13

108. Unwin, P. N. T. and G. Zampighi (1980), "Structure of the Junction Between Communicating Cells", Nature, 283:545-549

109. Walleczek, J. and R. P. Liburdy (1990), "Combined DC/AC Magnetic Fields Alter Ca^{2+} -Metabolism in Activated Rat Thymic Lymphocytes", Presented at the Twelfth Annual Meeting of the Bioelectromagnetics Society, Abstract E-3-2

110. Weaver, J. C. and R. D. Astumian (1990), "The Response of Living Cells to Very Weak Electric Fields: The Thermal Noise Limit", Science, 247:459-462

111. Wertheimer, N. W. and L. Leeper (1979), "Electrical Wiring Configuration and Childhood Cancer", American Journal of Epidemiology, 109:273-284

112. Zagotta, W. N., T. Hoshi and R. W. Aldrich (1990), "Restoration of Inactivation in Mutants of Shaker Potassium Channels by a Peptide Derived from ShB", Science, 250:568-571

113. Zahn, M. (1979), Electromagnetic Field Theory, John Wiley and Sons, Inc., New York

APPENDICES

APPENDIX A

SUMMARY OF REVIEWED EXPERIMENTS

Table 2. Summary of Experimental Results

Author	Biosystem	Field Strength	Freq	Exposure Period	Results	Comments
Bassett et al.,1974	Bone strength (canines)	E=2 mV/m or 20 mV/m	1 Hz or 65 Hz	28 days	1 Hz- no effect 65 Hz- increased load bearing	Pulsed magnetic field effects bone growth
Bawin et al.,1973	Cat brain rhythms	1 mW/cm^2	1-16 Hz	unknown	EEG patterns grouped around applied frequency	147 MHz RF. Effects at EEG frequencies.
Bawin et al.,1975	Ca^{2+} efflux & chick brain tissue	1-2 mW/cm^2	0-35 Hz	20 mins	Peak enhanced efflux at 16 Hz.	147 MHz RF. Freq window. 10-20% shift.
Bawin et al.,1976	Ca^{2+} efflux & chick brain tissue	5-100 V/m, (10^{-5} V/m in tissue)	1-32 Hz	20 mins	Decreased efflux at some power- frequency combinations	No RF. Less efflux. Freq and power windows.
Bawin et al.,1978	Ca^{2+} efflux & chick brain tissue	.75 mW/cm^2 5-10 V/m in tissue	16 Hz	20 mins	$[Ca^{2+}]_o$ had no effect on efflux. Other ions did.	450 MHz RF. Ionic results point to cell membrane as interaction site
Blackman et al., 1979	Ca^{2+} efflux & chick brain tissue	.5-2.0 mW/cm^2	0-30 Hz	20 mins	Some power-frequency combinations enhanced efflux.	147 MHz RF. Power & frequency windows.
Blackman et al, 1980a	Ca^{2+} efflux & chick brain tissue	.11-1.66 mW/cm^2	9,16 Hz	20 mins	Peak enhanced efflux at .83 mW/cm^2.	147 MHz RF. Results unaffected by freq change

Table 2 - Continued

Author	Biosystem	Field Strength	Freq	Exposure Period	Results	Comments
Blackman [Ref]	Ca^{2+} efflux & chick brain tissue	.37-4.32 mW/cm^2	16 Hz	20 mins	Peak enhancment at .55,1.38 mW/cm^2 powers.	50 MHz RF. Effective power density depends on RF frequency
Blackman [Ref]	Ca^{2+} efflux & chick brain tissue	1-70 V/m .033-2.33 mg	16,30 Hz	20 mins	Enhanced efflux peaks at 16 Hz, 6 and 40 V/m	No RF. Two power density peaks.
Blackman [Ref]	Ca^{2+} efflux & chick brain tissue	6-40 V/m 0-.83 mg	15,30 Hz	20 mins	No effect without B field. Effective freqs depend on geomagnetic field.	Effect from extremely small B field. Effective freq proportional to odd harmonic of geomagnetic B.
Blackman [Ref]	Ca^{2+} efflux & chick brain tissue	15 V/m RMS, .6 mg	1-510 Hz	20 mins	All odd harmonics of 15 Hz enhanced efflux except #11. Harmonics 4,6,12, 27 also effective.	Large number of harmonics effective.
Conti [Ref]	Human lymphocyte mitogenic stimulation	Pulsed .1-1 V/m B not given.	1-200 Hz	6-72 hrs	Decreased mitogenic stimulation for some combinations	Reduction of number of cells reproducing.
Conti [Ref]	Human lymphocyte mitogenic stimulation	Pulsed 60 g. E not given.	3 Hz	72 hrs	Decrease in Ca^{2+} uptake.	Effect due to altering Ca^{2+} flux across membrane.

Table 2 - Continued

Author	Biosystem	Field Strength	Freq	Exposure Period	Results	Comments
Deibert [Ref]	Rabbit fibular ostectomy healing	CR fields for Ca^{2+}, Mg^{2+}. .3g pk-pk AC	CR freqs	28 days, .5-24 hrs per day	Growth and stiffness increases.	CR tuning effect on bones in vivo.
Delgado [Ref]	Chick embryos	Pulsed .0012 to .12 g	10-1000 Hz	48 hrs	Embryo abnormalities at some combinations.	Frequency & amplitude windows.
Dixey [Ref]	Noradrenaline release in nerve cells	Pulsed .038 V/m	500 Hz	2 hrs	Noradrenaline release stimulated. Effect inhibited by adding Mg^{2+}	Ca^{2+} ion flux suggested cause.
Dutta [Ref]	Ca^{2+} efflux from human neuroblastoma cells in vitro	0-5 mW/g (μwave carrier)	16 Hz	30 mins	.05, & 1.0 mW/g enhanced efflux. No modulation needed for effect at 1 mW/g	Human cells. Amplitude windows. Ca^{2+} ion flux.
Friedman [Ref]	Human reaction time	5-17 g	0-.2 Hz	Through-out 50 trials	.2 Hz slowed reaction time. 0 and .1 Hz ineffective.	Human behavior. Frequency critical.
Gavalas-Medici [Ref]	Monkey schedule control	1-56 V/m	7-75 Hz	Not given	Shortened inter-response times for 10 V/m, 7 Hz & 56 V/m, at 7 and 75 Hz.	Amplitude threshold effect suggested.

Table 2 - Continued

Author	Biosystem	Field Strength	Freq	Exposure Period	Results	Comments
Goodman [Ref]	RNA transcription in dipteran salivary gland cells	Pulsed .15 V/m	15,72 Hz	15-45 mins	15, 45 min exposure time increased transcription. 30 min did not.	Exposure period "window".
Kacz-marek [Ref]	Ionic flux from cat cortex	Pulsed 5 V/m implants	200 Hz	10-20 mins	Increased GABA and Ca^{2+} efflux	Ion flux again.
Liboff [Ref]	Ca^{2+} uptake by human lymphocytes	.209 g DC, 0-1.5 g AC	0-30 Hz	1 hr	Enhanced uptake resonance curve centered at 14.27 Hz. AC amplitude window	CR conditions for $^{45}Ca^{2+}$. Results depend on AC amplitude.
Liboff [Ref]	DNA synthesis in human fibroblasts	.16-.4 g RMS	15 Hz to 4 kHz	18-96 hrs	Increased synthesis at nearly all combinations.	
Lin-Liu [Ref]	Ca^{2+} efflux from synaptosomes	43 V/m (.5 mW/cm^2)	0-60 Hz	10 mins	No effect from 0,60 Hz. 38% increase in efflux for 16 Hz	Not whole cells. Normal cell processes not necessary. Suggest surface interaction.
Luben [Ref]	Bone cells in vitro	Pulsed 20 g, .1-1 V/m	15, 72 Hz	72 hrs	Decrease in cAMP accumulation. Decreased activation of cyclase activity by some hormones	Results point to cell surface as interaction site.

Table 2 - Continued

Author	Biosystem	Field Strength	Freq	Exposure Period	Results	Comments
Marron [Ref]	Slime mold mitotic interval	2 g, .7 V/m	60,75 Hz	100 days	Mitotic delay. Returned to normal after fields removed.	Long exposure period. Reversible effect.
McLeod [Ref]	Diatom mobility	.21, .41 gauss.	8-136 Hz	1 hr	8 resonance curves at CR conditions. Harmonics 1,3,5,15 enhance mobility	Strong evidence for CR effect. Curious harmonic pattern.
Merritt [Ref]	Ca^{2+} efflux from rat brain tissue	Pulsed 1,10 mW/cm^2	16 Hz	20 mins	No significant efflux changes.	1,2.45 GHz RF frequencies. May have missed windows.
Phillips [Ref]	Human colon cancer cells in vitro.	1 g RMS, E induced 300 mA/m^2	60 Hz	24 hrs	Increased antibody binding & clonogenic capacity when B present.	Cancer cells. Membrane surface likely interaction site.
Ramirez [Ref]	Oviposition & development of drosophila	10-45 g	0-100 Hz	1-14 days	Egg-laying avoidance & increased mortality in exposed areas	Effect on developing embryonic system.
Sagan [Ref]	Chick behavior	1,5 mW/cm^2	3, 16 Hz	20 mins	No significant effects	450 MHz carrier.

Table 2 - Continued

Author	Biosystem	Field Strength	Freq	Exposure Period	Results	Comments
Shelton & Merritt, 1981	Ca^{2+} efflux from rat brain tissue	.5-15 mW/cm^2	16,32 Hz	20 mins	No significant effects.	1 GHz carrier
Sheppard et al., 1979	Ca^{2+} efflux from chick brain tissue	.05-5 mW/cm^2	16 Hz	20 mins	Increased Ca^{2+} efflux at .1, 1 mW/cm^2	Power density windows. Cooperative behavior suggested.
Smith et al., 1990	Embryonic chick bone growth	.21-.41 g DC, .4g pk-pk AC	16 Hz	7 days	CR tuning for Ca^{2+} & Mg^{2+} stimulated growth. K^+ tuning stunted growth. Na^+ tuning no effect	Cyclotron resonance tuning affects bone tissue.
Smith et al., 1987	Diatom mobility	.21 g DC 0-.63 g pk AC	0-32 Hz	1 hr	CR Ca^{2+} tuning ehnanced motion. DC, AC fields had to be collinear. Odd harmonics effective. Resonance curve centered at CR frequency.	Cyclotron resonance model evidence. Odd harmonics similar to Blackman et al., 1985

APPENDIX B

BONE DEVICE ASSEMBLY LANGUAGE CODE

```
* Program for bone healing device. Code is written in Motorola 68HC11 assembly
*language

*****************************************************************
*memory locs
                        org     $0

trans_ptr               rmb     2
filt_in                 rmb     2
z_minus_1               rmb     2
z_minus_2               rmb     2
filt_out                rmb     2

mlights                 rmb     1
light_count             rmb     1
cal_out_count           rmb     2
three_day_count         rmb     1
one_minutes             rmb     1
five_minutes            rmb     1
holding_count           rmb     1
first5_flag             rmb     1
log_full_flag           rmb     1
button_count            rmb     1
old_sec                 rmb     1
old_min                 rmb     1
cum15_count             rmb     1
break_count             rmb     1
cerr_count              rmb     1
cerr_flag               rmb     1
new_day_flag            rmb     1

power_flag              rmb     1
day_count               rmb     1
sec_count1              rmb     1
ppeak                   rmb     2
npeak                   rmb     2
sine                    rmb     2
pktopk                  rmb     1
```

Figure 40. Bone device assembly language code

```
sine_peak           rmb   2
feedback            rmb   2

clock_data
sec1                rmb   1
sec10               rmb   1

min1                rmb   1
min10               rmb   1
hour1               rmb   1
hour10              rmb   1
day1                rmb   1
day10               rmb   1
month1              rmb   1
month10             rmb   1

pclock_data         rmb   10

temp                rmb   1
event_id            rmb   2
prog                rmb   70
endprog


*************************************************************************
*control regs

tcnt        equ     $100e
toc2        equ     $1018
toc3        equ     $101a
porta       equ     $1000
portb       equ     $1004
portc       equ     $1003
portd       equ     $1008
adctl       equ     $1030
adr2        equ     $1032
option      equ     $1039
coprst      equ     $103a
```

Figure 40 - Continued

```
tflg1           equ     $1023
tmsk1           equ     $1022
ddrc            equ     $1007
ddrd            equ     $1009
spcr            equ     $1028
pprog           equ     $103b
sccr1           equ     $102c
sccr2           equ     $102d
scsr            equ     $102e
scdr            equ     $102f
baud            equ     $102b
tctl2           equ     $1021
pactl           equ     $1026
tmsk2           equ     $1024
tflg2           equ     $1025
bprot           equ     $1035

fifteen_msec    equ     $0
one_sec         equ     $4
one_min         equ     $8
end_log         equ     $0
programmed      equ     $f000
doc_visit       equ     $20
low_batt        equ     $f040
control_err     equ     $f060
shutdown        equ     $f080
cable_dis       equ     $f0a0

all             equ     $b0
red             equ     $10
green           equ     $20
beep            equ     $40
yellow          equ     $80
grandyellow     equ     $a0
only            equ     $e0

perr_thresh     equ     450
nerr_thresh     equ     -450
```

Figure 40 - Continued

```
min1adr     equ   $f2
clocksel    equ   $bf
notclock    equ   $40
writesel    equ   $f7
readsel     equ   $fb
busy        equ   $2

*************************************************************************
*interrupt vector locations

        org   $ffe6
eeoc2_vector fdb   #oc2_vector

        org   $fff4
xirq_vector  fdb   #clock_isr

        org   $fffa
cop_vector   fdb   #begin

        org   $fffe
reset_vector fdb   #begin


*************************************************************************
*ram interrupt vector for oc2 (sine wave ) interrupt
        org   $dc
oc2_vector   rmb   3



*************************************************************************
*Program begins
*************************************************************************
        org   $f800
begin

*a/d converter and cop timeout intialization
        ldaa  #$93          *power up converter,cop timeout 2sec
        staa  option
```

Figure 40 - Continued

```
*eeprom block protect initialization
        ldaa    #$17
        staa    bprot

*stack ptr, port c output init
        lds     #$c0
        ldaa    #$ff
        staa    ddrc

*write eeprom programming routine to ram
        ldd     #progr
        xgdx
        ldy     #prog
epp1    ldaa    0,x
        staa    0,y
        inx
        iny
        cpy     #endprog+1
        bne     epp1

* initialization
*sine wave interrupt vector
        ldaa    #$7e
        staa    oc2_vector
        ldd     #sine1
        std     oc2_vector+1

*serial port initialization
        clra
        staa    sccr1
        ldaa    #$0c            *enable rx,tx
        staa    sccr2
        ldaa    #$31            *2400 baud (1 Mhz clock)
        staa    baud

*parallel ports initialization
        clra                    *turn off spi so port d can be used
        staa    spcr
        coma
```

Figure 40 - Continued

```
        staa    ddrd            *port d output
        staa    portd           *turn off read, write signals

*timer initialization
        ldaa    #$40            *enable oc2 interrupt
        staa    tmsk1
        ldaa    #$60            *and oc3 (but oc3 not interrupt)
        staa    tflg1

        ldaa    #$88            *porta-7 output
        staa    pactl

*flags and misc initialization
        clra
        ldx     #filt_in
inzr
        staa    0,x
        inx
        cpx     #sine+2
        blt     inzr
        ldd     #sineconsts
        std     trans_ptr       *trans_ptr at start of sineconst buff
        jsr     power_down      *start out without analog power

*clear op flag and disable sine interrupt
nopyt
        ldaa    #$10            *sine intrpt disabled, 1min intrpt enabled
        tap
stnpy
        stop
        ldaa    status
        bita    #1
        bne     stnpy

*calculate sine_peak based on programmed data
pgrmd
        ldd     sine_skip
        ldaa    sine_count+1
        lsra
```

Figure 40 - Continued

```
        mul
        std     sine_peak
        clr     sec_count1

*enable all interrupts
        ldaa    #0
        tap

*check if power on
wtlp
        ldaa    power_flag
        bne     pwfon
        stop                    *if analog power off stopi
        bra     wtlp
pwfon
        wai                     *if analog power on wait
        bra     wtlp

*****************************************************************

*real-time clock interrupt service routine
clock_isr

*clear rtc interrupt flag
        jsr     select_clock
        clra
        ldab    #$d
        jsr     cwrite
        jsr     deselect_clock

*reset watchdog timer
        jsr     reset_watchdog

*check if button pushed or clock interrupt
        jsr     clockread
        ldaa    power_flag
        bne     trymin
        ldaa    sec10
        jsr     mult10
```

Figure 40 - Continued

```
        adda    sec1
        cmpa    old_sec
        beq     butn
        staa    old_sec
        bra     nobutt
trymin
        ldaa    min10
        jsr     mult10
        adda    min1
        cmpa    old_min
        beq     butn
        staa    old_min
        bra     nobutt

*make sure button is down for certain time
butn
        inc     button_count
        ldaa    button_count
        cmpa    #2
        bge     nobz
        rti

*if yellow-light mode start treatment
nobz
        clr     button_count
        ldaa    mlights
        cmpa    #yellow
        bne     ntyo
        ldy     #1
        jsr     flashb
        jsr     power_up
        ldaa    #-2
        staa    one_minutes
        clra
        staa    mlights
        staa    cum15_count
        coma
        staa    first5_flag
        rti
```

Figure 40 - Continued

```
*check if waiting for button after treatment block
ntyo
        ldaa    holding_count
        beq     hldf
        clr     holding_count
        jsr     done_for_day *log time and shut down for day
hldf
        rti

*Check to see if holding after treatment blk with no motion
nobutt
        ldaa    holding_count
        beq     now
        inc     holding_count
        ldaa    holding_count
        cmpa    #60
        blo     hcck
        inc     break_count
        jsr     done_for_day
        clr     holding_count
hcck
        rti

*inc second count var
now
        ldaa    power_flag
        bne     cbuc
        inc     sec_count1
        ldaa    sec_count1
        cmpa    #3
        bge     cbuc
okex
        rti

*check to see if base unit connected
cbuc
        clr     sec_count1
        ldaa    #$ff            *write ff to serial port
        jsr     send_char
```

Figure 40 - Continued

```
        ldx     #1666           *delay 10 msec (1 Mhz clock)
ciwt
        dex
        bne     ciwt
        ldaa    scsr            *check if char recvd on serial port
        anda    #$20
        beq     coloop                  *if no, wait for command
        ldaa    scdr            *check if char is $ff
        cmpa    #$ff
        beq     tdfd            *if so, continue
        jsr     base_serv       *if not go to base_serv
coloop
        ldx     #26300                  *if no, wait for command ( 1 sec)
cidx
        jsr     reset_watchdog          *keep watchdog timer happy
        ldaa    scsr
        anda    #$20
        beq     eecc
        jsr     base_serv       *when command recvd go to base_serv
        bra     cbuc
eecc
        dex
        bne     cidx
        bra     cbuc            *after timeout start over

tdfd
        ldaa    scdr

*check if non_recoverable error condition
minp
        ldaa    status          *error indicated by status bit 3
        bita    #8
        beq     itdf
        ldaa    #red
        staa    mlights
        jmp     nost
```

Figure 40 - Continued

```
*check if unit programmed yet
itdf
        ldaa    status
        bita    #1
        beq     tdf1
        rti                     *if not operational exit routine

*treatment done for day?
tdf1
        ldaa    end24_flag
        beq     ccc
        ldaa    #green
        staa    mlights
        jmp     omex

*check if cable connected
ccc
        ldaa    porta
        bita    #2
        beq     mortr
        ldaa    power_flag      *if cable disconnect is during treatment
        beq     cdis            *(excluding first 5 mins of treatment
        ldaa    first5_flag     *block), record in log
        bne     cdis
        ldd     #cable_dis
        std     event_id
        jsr     log_event
cdis
        jsr     power_down      *if not, power down and set red light bit
        ldaa    #red
        staa    mlights
        jmp     omex

*check if power on
mortr   ldaa    power_flag
        bne     mprok
        jmp     nopwr
mprok
        clra
        staa    mlights
```

Figure 40 - Continued

```
*check if control error
        ldaa    cerr_flag
        beq     nocflg
        clr     cerr_flag
        inc     cerr_count

*if control err, restart control loop by zeroing dig filt locs
        ldx     #filt_in        *zero digital filter
        clra
zdf
        staa    0,x
        inx
        cpx     #filt_out+2
        bne     zdf

*check if 5 min block of treatment passed
nocflg
        inc     one_minutes
        ldaa    one_minutes
        cmpa    #5
        beq     m5b
        jmp     omex

*mark 5 min treatment block
m5b
        clr     one_minutes
        inc     five_minutes
        clr     first5_flag

*check if 15 mins of treatment fulfilled
mo5
        ldaa    five_minutes
        cmpa    #3
        beq     c15b
        jmp     omex
```

Figure 40 - Continued

```
*mark 15 min block
c15b
        inc     cum15_count
        clr     five_minutes
        clr     cerr_count

*check if treat period for day complete
        ldaa    cum15_count
        cmpa    on_time_per_day
        bge     lshu
        jmp     omex

* shut off analog power
lshu
        jsr     power_down

*check out of cal total
        ldd     cal_out_count
        cpd     #300
        bhi     ckoc3d
        clr     three_day_count
        bra     cc3d
ckoc3d
        ldd     #control_err
        std     event_id
        inc     three_day_count
        ldaa    three_day_count
        cmpa    #3
        blo     nopey
        jmp     lgerr
nopey
        jsr     log_event

*beep 5x and hold for button push
cc3d
        ldy     #5              *if not, beep 5x, set holding_count
        jsr     flashb
        ldaa    #1
        staa    holding_count
        bra     omex
```

Figure 40 - Continued

```
*flash yellow light
nopwr
        ldaa    #yellow
        staa    mlights

*check for low battery
omex
        ldaa    porta
        anda    #1
        beq     nocer
        ldd     #low_batt
        std     event_id
        bra     lgerr           *log low batter error

*check for new 24-hr period beginning
nocer
        jsr     clockread       *read hrs from real time clock
        ldaa    hour10
        jsr     mult10
        adda    hour1
        cmpa    start_time      *check for new day
        beq     sstt
        clr     new_day_flag
        bra     nost
sstt
        ldaa    new_day_flag
        bne     nost
        ldaa    #$ff
        staa    new_day_flag

*remove shutdown feature
*check for device shutdown time
*       ldaa    day_count
*       inca
*       cmpa    total_treat     *check for shutdown time
*       bne     nody
*       ldd     #shutdown       *log shutdown event
*       std     event_id
*       bra     lgerr
```

Figure 40 - Continued

```
*nody
*       staa    day_count
        jsr     power_down  *analog powr off
        clra                *initialize for new day
        staa    break_count
        ldx     #end24_flag
        jsr     prog
        bra     nost

lgerr
        jsr     log_event       *portion to log err event
        ldaa    status
        oraa    #$8
        ldx     #status
        jsr     prog
        jsr     power_down

*exit
nost
        ldaa    mlights             *flash lights specified
        staa    portc
        ldx     #10000
bd9
        dex
        bne     bd9
        clra
        staa    portc
        rti

*****************************************************************
*subroutine to end treatment for day
done_for_day
        ldy     #1
        jsr     flashb
        clra
        coma
        ldx     #end24_flag
        jsr     prog
        jsr     log_time_block
        rts
*****************************************************************
```

Figure 40 - Continued

```
*subroutine to reset watchdog timer
reset_watchdog
        ldaa    #$55
        staa    coprst
        ldaa    #$aa
        staa    coprst
        rts

*****************************************************************
*serial port routine to communicate with base unit
base_serv

*called from clock_isr routine
        ldaa    scdr
        cmpa    #'N
        bne     nx0
        ldy     #6
        ldx     #id
        jsr     get_msg
        jmp     rx_quit

nx0
        cmpa    #'S             *status request
        bne     nx1
        ldy     #7
        ldx     #id
        jsr     send_msg
       ldaa    sine_skip_low
        jsr     send_char
        jmp     rx_quit

nx1     cmpa    #'L             *log request?
        bne     nx2
        ldd     #end_log
        std     event_id
        jsr     log_event
        ldd     log_ptr
        subd    #log
        xgdy
        ldx     #log
```

Figure 40 - Continued

```
        jsr     send_msg

        ldaa    log_full_flag  *change log entry to doc visit if log not full
        beq     rdv
        jmp     rx_quit
rdv
        ldx     log_ptr
        dex
        ldaa    0,x
        oraa    #doc_visit
        jsr     prog
        dex
        ldaa    0,x
        oraa    #$f0
        jsr     prog
        jmp     rx_quit

nx2     cmpa    #'P             *reprogramming request?
        bne     nx3
        ldy     #10
        ldx     #pclock_data
        jsr     get_msg
        ldx     #10
        ldab    #2
        jsr     clockwrite

        ldy     #6
        ldx     #ref
        jsr     get_msg
        ldx     #sineconsts
        ldy     sine_count
        jsr     get_msg
        ldd     #log            *log_ptr at start of log buff
        ldx     #log_ptr
        jsr     prog
        tba
        inx
        jsr     prog
        ldd     #programmed
        std     event_id
```

Figure 40 - Continued

```
        jsr     log_event
        ldaa    status
        anda    #$fe
        ldx     #status
        jsr     prog
        clra
        staa    cerr_count
        ldx     #end24_flag
        jsr     prog
        bra     rx_quit

nx3     cmpa    #'R             *request for current programmed info?
        bne     nx4
        ldy     #10
        ldx     #pclock_data
        jsr     send_msg
        ldy     #6
        ldx     #ref
        jsr     send_msg
        ldx     #sineconsts
        ldy     sine_count
        jsr     send_msg
        bra     rx_quit

nx4
        cmpa    #'I
        bne     nx5
        bsr     get_char
        ldx     #sine_skip+1
        jsr     prog
        jmp     #$f800

nx5
        cmpa    #'U
        bne     rx_quit
        ldaa    #1
        ldx     #status
        jsr     prog
        jmp     #$f800              *restart
```

Figure 40 - Continued

```
rx_quit
        ldx     #$ffff          *delay for base unit
rxqd
        dex
        bne     rxqd
        rts

*-----------------------------------------------------------------

get_msg

* Gets string of chars from serial port
*and stores in memory (ram or eeprom). Called from base_serv routine.

        bsr     get_char
        jsr     prog
        inx
        dey
        bne     get_msg
        rts

*-----------------------------------------------------------------
get_char

* Waits til a char is received on serial port
*and returns that char in acca. Called from get_msg routine.

        jsr     reset_watchdog
        ldaa    scsr
        anda    #$20
        beq     get_char
        ldaa    scdr
        rts
```

Figure 40 - Continued

```
*-------------------------------------------------------------
send_msg

*Sends string of ascii chars to serial port. Called from base_serv
*routine.

sm1     ldaa    0,x
        bsr     send_char
        inx
        dey
        bne     sm1
        rts

*-------------------------------------------------------------
send_char

*Waits for serial tx ready and sends one char to serial port
*Called from clock_isr and base_serv routines.

        ldab    scsr
        andb    #$80
        beq     send_char
        staa    scdr
        jsr     reset_watchdog
        rts
*****************************************************************
*subroutine to sound beeper a user-specified # of times
flashb
        jsr     reset_watchdog
        ldaa    #$40
        staa    portc
        ldx     #20000
fldl
        dex
        bne     fldl
        clra
        staa    portc
        ldx     #45000
```

Figure 40 - Continued

```
fl2
        dex
        bne     fl2
        dey
        bne     flashb
        rts

*****************************************************************
*subroutine to power down system
power_down
        ldaa    #$c0
        staa    porta
        clra
        staa    portb
        staa    power_flag
        staa    tmsk1           *disable timer interrupt
        ldaa    #one_sec
        jsr     clockinit
        rts

*****************************************************************
*subroutine to power up system
power_up
        ldaa    #$40            *reenable timer interrupt
        staa    tmsk1
power_up_no_int
        ldaa    porta           *turn on sys power
        anda    #$7f
        staa    porta
        ldaa    #$ff
        staa    power_flag
        ldx     #16666                  *delay 100 msec (1 Mhz clock)
dpux
        dex
        bne     dpux
        ldaa    #one_min        *go to 1-min rtc interrupts
        jsr     clockinit

        rts
*****************************************************************
```

Figure 40 - Continued

```
*subroutine to enter time blocks in log
log_time_block
        ldaa    cum15_count  *put time block and break info in event_id
        beq     nolev
        lsla
        lsla
        lsla
        lsla
        ldab    break_count
        lslb
        lslb
        lslb
        lslb
        lslb
        std     event_id
log_event
        ldaa    log_full_flag
        bne     nolev
        ldd     log_ptr              *check if log full
        cpd     #$ffde
        blo     lev
        ldaa    #$ff
        staa    log_full_flag
        ldd     #end_log
        std     event_id
lev
        jsr     clockread     *read real time clock
        ldx     log_ptr
        ldaa    month10
        jsr     mult10
        adda    month1
        oraa    event_id
        jsr     prog          *program ms byte of log entry
        inx
        ldaa    day10
        jsr     mult10
        adda    day1
        oraa    event_id+1
        jsr     prog          *prog ls byte of log entry
```

Figure 40 - Continued

```
        inx
        xgdx
        ldx     #log_ptr
        jsr     prog
        tba
        inx
        jsr     prog
nolev
        rts

*****************************************************************************


*real-time clock subroutines


*************************************************************
*subroutine to init real-time clock control regs
clockinit
        psha
        jsr     select_clock
        clra
        ldab    #$d
        jsr     cwrite
        pula
        oraa    #2
        incb
        jsr     cwrite
        ldaa    #1
        incb
        jsr     cwrite
        ldaa    #5
        jsr     cwrite
        ldaa    #4
        jsr     cwrite
        jsr     deselect_clock
        rts

*************************************************************************8
```

Figure 40 - Continued

```
clockwrite
        stab    portb                   *adr of ones minutes reg
        jsr     select_clock
        ldy     #pclock_data
        bsr     check_busy
cllp    ldaa    0,y
        bsr     cwrite
        incb
        iny
        dex
        bne     cllp
        clra
        ldab    #$d
        bsr     cwrite
        jsr     deselect_clock
        rts

*****************************************************************************
*subroutine to wait til clock chip is not busy

check_busy
        pshb
        ldaa    #1
        ldab    #$0d
        bsr     cwrite
        bsr     cread
        bita    #busy
        beq     cbu2
        clra
        bsr     cwrite
        bra     check_busy
cbu2    pulb
        rts

*****************************************************************************
```

Figure 40 - Continued

```
*subroutine to pulse write signal of real time clock chip
cwrite
        pshb
        staa    portc
        ldaa    portb
        psha
        stab    portb
        ldaa    #writesel
        staa    portd
        ldaa    #$ff
        staa    portd
        pula
        staa    portb
        pulb
        rts


*************************************************************************
*subroutine to read clock data
clockread
        ldx     #clock_data
        clrb
        jsr     select_clock
        bsr     check_busy
crcr    bsr     cread
        staa    0,x
        incb
        inx
        cpx     #clock_data+10
        bne     crcr
        clra
        ldab    #$d
        bsr     cwrite
        jsr     deselect_clock
        rts

*************************************************************************8
```

Figure 40 - Continued

```
*subroutine to pulse read signal

cread   pshb
        ldaa    portb
        psha
        stab    portb
        clrb
        stab    ddrc
        ldaa    #readsel
        staa    portd
        ldaa    portc
        anda    #$0f
        ldab    #$ff
        stab    ddrc
        stab    portd
        pulb
        stab    portb
        pulb
        rts

*****************************************************************************
*subroutine to turn on real-time clock chip select
select_clock
        ldaa    porta
        anda    #clocksel
        staa    porta
        rts
*****************************************************************************
*subroutine to turn off real time clock chip select
deselect_clock
        ldaa    porta
        oraa    #notclock
        staa    porta
        rts

*****************************************************************************
```

Figure 40 - Continued

```
*subroutine to multiply acca contents by 10
mult10      pshb
        lsla
        psha
        lsla
        lsla
        pulb
        aba
        pulb
        rts

*****************************************************************
*subroutine to read field from a/d converter
a2d_in
        clra
        staa    adctl               ;start a/d converter
a2d     ldaa    adctl               ;wait til a/d conversion done
        anda    #$80
        beq     a2d
        clra
        ldab    adr2                ;get a/d result
        eorb    #$80            *invert ms bit for 2's comp
        rts
*****************************************************************
*****
*subroutine to output accd contents to dac

* update dac output
sine_out
        addd    filt_out
dac_out
        anda    #3
        lsla
        lsla
        lsla
        eora    #$70
        staa    porta
        stab    portb
        rts
```

Figure 40 - Continued

```
*************************************************************************
* sine wave interrupt service routine


sine1
*for ascending positive 1/4  of sine wave
*inc sine output
        ldd     sine
        addd    sine_skip
        std     sine
        jsr     sine_out

*at sine peak?
        ldd     sine
        cpd     sine_peak
        beq     spk1

*update sine table ptr and oc2 reg
iupoc2
        ldx     trans_ptr
        inx
        inx
upoc2
        ldd     toc2
        addd    0,x
        std     toc2
        xgdx
        std     trans_ptr
        jmp     squit

*if at pos peak call subrtn, change interr vector, reuse last transition time
spk1
        jsr     pos_peak
        ldd     #sine2
        std     oc2_vector+1
```

Figure 40 - Continued

```
nupoc2
        ldx     trans_ptr
        ldd     toc2
        addd    0,x
        std     toc2
        jmp     squit

*for descending positive 1/4 of sine wave
sine2
        ldd     sine
        subd    sine_skip
        std     sine
        jsr     sine_out

*at 0 value of sine wave?
        ldaa    sine+1
        beq     sz2

*update sine table ptr and oc2 reg
dupoc2
        ldx     trans_ptr
        dex
        dex
        jmp     upoc2

*change oc2 interr vector and update oc2 reg
sz2
        ldd     #sine3
        std     oc2_vector+1
        jmp     nupoc2


*for descending negative 1/4 of sine wave
sine3
        ldd     sine
        subd    sine_skip
        std     sine
        jsr     sine_out
```

Figure 40 - Continued

```
*at neg peak of sine?
        ldd     #0
        subd    sine_peak
        cpd     sine
        beq     spk3

*update sine table ptr and oc2 reg
        jmp     iupoc2

*if at neg peak, call subr, change interr vector, update oc2 reg
spk3
        jsr     neg_peak
        ldd     #sine4
        std     oc2_vector+1
        jmp     nupoc2

*for negative ascending /4 of sine wave
sine4
*inc sine
        ldd     sine
        addd    sine_skip
        std     sine
        jsr     sine_out

*at 0 sine value?
        ldaa    sine+1
        beq     sz4
        jmp     dupoc2

*if at sine 0, change interr vector, update oc2 reg
sz4
        ldd     #sine1
        std     oc2_vector+1
        jmp     nupoc2

*exit
squit
        ldaa    #$40
        staa    tflg1
        rti
```

Figure 40 - Continued

```
**************************************************************8
*subroutine to be performed at pos peak of sine wave
pos_peak

*run digital filter and control loop
        ldd     z_minus_1               ;update dig filt locs
        std     z_minus_2
        ldd     filt_in
        std     z_minus_1
        jsr     a2d_in                  *read field strength
        clra
        bitb    #$80
        beq     nng
        coma
nng
        std     ppeak           *store field strength in ppeak

        addd    npeak           *avg ppeak and npeak
        asra
        rorb
        std     feedback        *store avg in feedback
        ldd     ref                     ;subtract from desired ref
        subd    feedback
        addd    z_minus_1               ;run dig filt, tran func is=
*                                       ;1/8*(1+2*z_minus_1+z_minus_2)/
*                                       ;(1-z_minus_1)
        std     filt_in
        addd    z_minus_1
        addd    z_minus_1
        addd    z_minus_2
        asra
        rorb
        asra
        rorb
        asra
        rorb
        asra
        rorb
        std     filt_out
```

Figure 40 - Continued

```
        cpd     #perr_thresh
        blt     noper
        ldaa    #$ff
        staa    cerr_flag
noper
        cpd     #nerr_thresh
        bgt     noner
        ldaa    #$ff
        staa    cerr_flag
noner
        rts

*************************************************************88
*subroutine to be performed at neg peak of sine wave
neg_peak

*sample field and store

        jsr     a2d_in
        clra
        bitb    #$80
        beq     nng2
        coma
nng2
        std     npeak

*reset watchdog timer
noswmo
        jsr     reset_watchdog

*keep track of time
        ldaa    tflg1
        anda    #$20
        beq     nolyet
        staa    tflg1           *reset oc3 for next time
```

Figure 40 - Continued

```
*check if time to flash lights (flashed every 3 secs)
trlc
        inc     light_count
        ldaa    light_count
        cmpa    #45
        bne     chup
        ldaa    #$a0            *turn on green and yellow lights
        staa    portc

*check for out of calibration in last 3 sec period
        ldaa    cerr_flag
        beq     nolyet
        ldd     cal_out_count
        addd    #1
        std     cal_out_count
        clr     cerr_flag
chup
        cmpa    #46
        bne     nolyet
        clra
        staa    portc
        staa    light_count
nolyet
        rts


**********************************************************************
****


* subroutine to erase and program 1 byte of eeprom
progr   sei

        pshb
        pshy
        ldab    #$16                    ;erase eeprom byte
        stab    pprog
        stab    0,x
        ldab    #$17
        stab    pprog
```

Figure 40 - Continued

```
        ldy         #2860       ;delay 20 msec
ins     dey
        bne         ins
        clr         pprog
        ldab  #2                ;program byte
        stab  pprog
        staa  0,x
        ldab  #3
        stab  pprog
        ldy         #2860       ;delay 20 msec
ins1    dey
        bne         ins1
        clr         pprog
        puly
        pulb
endprogr    rts

*****************************************************************
*eeprom  data section

start_time          fcb   #0
id                  fcb   #'1,#'2,#'3,#'A,#'B,#'C
status              fcb   #1
sine_skip
sine_skip_high          fcb   #0
sine_skip_low           fcb   #13
log_ptr                 rmb   2
end24_flag          rmb   1

ref                     rmb       2
on_time_per_day     rmb       1
total_treat         rmb       1
sine_count          rmb       2
sineconsts          rmb       30


log                     rmb       255
endlog                  rmb       1
```

Figure 40 - Continued

APPENDIX C

SUMMARY OF YEAST EXPERIMENT RESULTS

Table 3. Results of yeast experiments

Exp #	B_{DC} (g)	B_{AC} (g pk)	Freq (Hz)	%	Ion	Tmp °F	YEP pH	$CaCl_2$ added	Comment
1	0	0	0	0	None	80	?	0	
2	.38	.2	29.1	-2.2	Ca	79	?	0	
3	.38	.2	29.0	+1.5	Ca	79	?	0	
4	.209	.2	16.0	0	Ca	75	?	0	
5	.407	.2	16.0	-2.1	K	73	?	0	
6	.307	.2	16.0	0	Co	74	?	0	
7	.209	.2	76.6	0	Ca5/ Mg3	74	?	0	
8	.38	.2	29.1	+17.5	Ca	64	?	0	
9	.38	.2	29.1	-5.0	Ca	66	?	0	
10	.38	.2	29.1	+6.9	Ca	66	?	0	
11	.38	.34	29.1	+6.4	Ca	66	?	0	
12	.38	.34	29.1	-3.8	Ca	66	?	0	
13	.2	.2	8.7	-4.8	Cl	67	?	0	
14	.2	.2	7.9	-2.9	K	68	?	0	
15	.2	.2	10.4	+3.6	Co	64	?	0	
16	.2	.2	13.4	-1.5	Na	68	?	0	
17	.2	.2	25.3	+9.3	Mg	65	?	0	
18	.2	.2	25.3	-8.0	Mg	65	?	0	
19	.2	.2	25.3	+4.2	Mg	67	?	0	
20	.594	.2	75	+3.0	Mg	69	?	0	
21	.594	.2	75	0	Mg	67	?	0	
22	.2	.2	25.3	+.8	Mg	67	?	0	
23	.4	.2	30.6	+5.9	Ca	71	?	0	
25	.4	.2	27.6	+5.4	--	71	?	0	

Table 3. Continued

Exp #	B_{DC} (g)	B_{AC} (g pk)	Freq (Hz)	%	Ion	Tmp °F	YEP pH	$CaCl_2$ added	Comment
26	.4	.2	27.6	-.7	--	71	?	0	
27	.4	.2	28.6	+3.4	--	71	?	0	
28	.4	.2	29.6	+5.6	--	70	?	0	
29	.4	.2	31.6	-1.0	Ca	75	?	0	
30	.4	.2	32.6	+3.0	--	71	?	0	
31	.209	.2	16	0	Ca	74	?	0	Phytone peptone, new YEP
32	.209	.2	16	+.9	Ca	75	?	0	B_{DC}=0 in ctl
33	.209	.2	16	+3.8	Ca	74	?	0	
34	.209	.2	16	-4.2	Ca	72	?	0	
35	.209	.2	16	+8.1	Ca	74	5.0	0	
36	.209	.2	16	0	Ca	72	5.57	0	
37	.209	.2	16	+7.6	Ca	74	4.5	0	
38	.209	.2	16	-3.9	Ca	73	4.00	0	
39	.209	.2	16	+4.8	Ca	76	4.93	0	
40	.209	.2	16	+8.2	Ca	76	5.99	0	
41	.209	.2	16	+4.3	Ca	76	6.5	0	
42	.209	.2	16	+8.3	Ca	79	7.02	0	
43	.209	.2	16	+18.4	Ca	75	7.00	0	
44	.209	.2	16	-1.3	Ca	76	7.00	0	
45	.209	.2	16	+3.8	Ca	75	7.5	0	
46	.209	.2	16	-1.4	Ca	?	7.04	0	
47	.209	.2	16	+1.1	Ca	?	3.00	0	Pressure sensors used
48	.209	.2	16	+2.1	Ca	?	6.86	0	

Table 3. Continued

Exp #	B_{DC} (g)	B_{AC} (g pk)	Freq (Hz)	%	Ion	Tmp °F	YEP pH	$CaCl_2$ added	Comment
49	.209	.2	16	+50	Ca	77	2.0	0	almost no growth
50	.209	.2	16	0	Ca	75	2.5	2 mM	
51	.209	.2	16	+14.5	Ca	75	2.48	0	
52	.209	.2	16	-1.5	Ca	76	2.48	2 mM	
53	.209	.2	16	-2.2	Ca	?	2.48	0	
54	.209	.2	16	0	Ca	75	2.49	0	
55	.209	.2	16	+1.4	Ca	75	2.17	0	
56	.209	.2	16	+8.0	Ca	76	2.18	.1 mM	
57	.209	.2	16	-6.5	Ca	76	2.18	.2 mM	
58	0	0	0	+7.7	--	75	6.86	.1 mM	
59	0	0	0	+3.9	--	78	6.87	2 mM	
60	0	0	0	+49.3	--	78	2.5	Ctl= 0, Trt= 2 mM	
61	0	0	0	+23.9	--	78	2.5	Ctl=0, Trt= .5 mM	
62	0	0	0	+12.1	--	78	2.5	Ctl=0, Trt= 3 mM	
63	0	0	0	+32.9	--	78	2.5	Ctl=0, Trt= 1 mM	
64	.209	.2	16	+7.4	Ca	78	2.0	.5 mM	.5 hr on, .5 hr off
65	.209	.2	16	-6.5	Ca	77	2.5	.5 mM	.5 hr on .5 hr off
66	0	0	0	+4.2	--	?	2.5	0	Calibrate

Table 3. Continued

Exp #	B_{DC} (g)	B_{AC} (g pk)	Freq (Hz)	%	Ion	Tmp °F	YEP pH	$CaCl_2$ added	Comment
67	.209	.2	16	-18.7	Ca	77	?	0	
68	.209	.2	16	-2.0	Ca	77	6.9	0	
69	.209	.2	16	-1.0	Ca	77	6.9	0	
70	0	0	0	+.8	--	76	6.83	Ctl=0, Trt= 1 mM	
71	.209	.2	16	-10.7	Ca	?	7.22	0	.1x yeast extract
72	.209	.2	16	+8.3	Ca	?	?	0	.1x yeast extract
73	.209	.2	16	-5.5	Ca	?	?	0	.1x peptone
74	.209	.2	16	0	Ca	?	?	0	.1x dextrose, no growth
75	.407	.2	16	0	K	?	?	0	.1x peptone
76	.209	.2	16	0	Ca	?	?	0	.1x yeast extract
77	.407	.2	16	+5.2	K	?	?	0	.1x yeast extract
78	.291	.2	16	+5.0	Fe	?	?	0	.1x yeast extract
79	.30	.2	10	-.5	--	?	?	0	Freq series
80	.30	.2	11	+3.0	--	?	?	0	
81	.20	.2	8	+.6	--	?	?	0	
82	.20	.2	10	+5.8	--	?	?	0	
83	.20	.2	10	-4.0	--	?	?	0	

Table 3. Continued

Exp #	B_{DC} (g)	B_{AC} (g pk)	Freq (Hz)	%	Ion	Tmp °F	YEP pH	$CaCl_2$ added	Comment
84	.20	.2	12	+4.3	--	?	?	0	
85	.20	.2	14	-.5	--	?	?	0	
86	.20	.2	18	0	--	?	?	0	
87	.20	.2	20	+2.1	--	?	?	0	
88	.209	.2	16	+12	Ca	?	?	0	37°C heat shock
89	.209	.2	16	+9.2	Ca	?	?	0	heat shock
90	.209	.2	16	-7.9	Ca	?	?	0	heat shock
91	.209	.2	16	+2.9	Ca	?	?	0	heat shock
92	.209	.2	16	+40	Ca	?	?	0	40°C heat shock
93	.209	.2	16	-9.6	Ca	?	?	0	40°C shock
94	.209	.29	16	-3.3	Ca	?	?	0	40°C shock
95	.2	.2	10	-6.1	--	81	?	0	Freq series
96	.2	.2	14	+5.5	--	70	?	0	
97	.2	.2	18	-7.0	--	?	?	0	
98	.2	.2	20	-16	--	?	?	0	
99	.209	.2	16	+6.0	Ca	?	?	0	
100	.209	.2	16	+4.9	Ca	?	?	0	
101	.209	.2	16	-1.3	Ca	?	?	0	

APPENDIX D

PLANT EXPERIMENT PROTOCOL

PLANT EXPERIMENT PROTOCOL (10/3/90)

EXPERIMENT_____
DATES_____

1.____Set up coils at control and experimental sites. Record conditions at the sites.

	CTL	EXP
Ion		
B_o (gauss)		
B_{ac} (g p-p)		
Freq (Hz)		
B_{60Hz} (g p-p)		
Light (Lux)		

2.____Record type and source of seeds used. Type:_____
Source:_____

3.____Pour vermiculite to a depth of 1.75" in each of the experimental pots. (Pots are 12"x9"x2.5" clear plastic containers with slots in bottom for water circulation). Compress vermiculite with flat-bottomed object. Place seeds on top of vermiculite in 3 symmetrical rows. Plant each seed with the hilum down. Add more vermiculite until .5" above the top of the seeds. Compress vermiculite again. Place pots inside larger plastic containers at experimental sites. Record number of seeds planted in each pot: _____.

4.____Pour 1 Liter of deionized water into the larger plastic container (not directly into the plant pot). On each day thereafter, water with 150 mL of deionized water.

5.____During experiment, daily record the stem height of each plant on the data sheet provided. Measure the height from the soil surface to the fork at which the leaf stems begin. Also record the lab temperature daily.

6.____At termination of experiment, record measurements of root and stem masses on the data sheet.

7.____Analyze data using student's t test to draw statistical conclusions.

PLANT EXPERIMENT DATA SHEET

EXPERIMENT_____
DATES_____

DAY	1	2	3	4	5	6	7	8
B_{DC} (mg)								
TMP (°F)								

	DAILY STEM HEIGHTS (CM)								END MASSES			
	DAY___ C / E		DAY__ C / E		DAY__ C / E		DAY__ C / E		ROOTS (gms)		PLANTS (gms)	
1												
2												
3												
4												
5												
6												
7												
8												
9												
10												
11												
12												
13												
14												
15												
16												
17												

APPENDIX E

MATLAB CODE TO CALCULATE SPHERICAL RESONANT SURFACES

```
%Matlab program to calculate areas on sphere covering resonance
%conditions for diff ions.


%Initialize
  clear
  conv=[221.4,126.35,80.86,76.67,66.81,55.94,55.02,52.36,52.13,47,...
        43.33,39.3,24.18,19.22]';
  shortstring=['Li','Mg','F ','Ca','Na','Mn','Fe','Ni','Co','Zn','Cl',...
        'K ','Cu','Br'];
  longstring=['Li+1','Mg+2','F-1 ','Ca+2','Na+1','Mn+2','Fe+2','Ni+2',...
        'Co+2','Zn+2','Cl-1','K+1 ','Cu+1','Br-1'];

  harm=[1,3,5,15];
  dp= input('Enter angle resolution (degrees):');
  dt=dp;
  bg=input('Enter geo field magnitude:');

%Choose resonant ion or magnetic field conditions
  phig= input('Enter geo field phi (degrees):');
  phig= phig*pi/180;
  thetag=input('Enter geo field theta (degrees):');
  thetag= thetag*pi/180;
  fprintf('\n\nResonant ion choices\n')
  fprintf('\n   1. Li+1')
  fprintf('\n   2. Mg+2')
  fprintf('\n   3. F-1')
  fprintf('\n   4. Ca+2')
  fprintf('\n   5. Na+1')
  fprintf('\n   6. Mn+2')
  fprintf('\n   7. Fe+2')
  fprintf('\n   8. Ni+2')
  fprintf('\n   9. Co+2')
  fprintf('\n  10. Zn+2')
  fprintf('\n  11. Cl-1')
  fprintf('\n  12. K+1')
  fprintf('\n  13. Cu+1')
  fprintf('\n  14. Br-1')
  fprintf('\n  15. Other\n\n')
  elem= input('Enter resonant ion: ');
```

Figure 41. MATLAB code to calculate resonant surface areas

```
  if elem==15
    rion=' '
    bdc= input('Enter DC field (Gauss): ');
    bac= input('Enter AC amplitude (Gauss): ');
    freq= input('Enter frequency (Hz): ');
  else
    rion= longstring((elem*4-3):elem*4)
    eharm= input('Enter harmonic: ');
    freq= input('Enter AC frequency (Hz):');
    bdc= freq/eharm/conv(elem)
    bac= input('Enter AC amplitude (gauss): ');
  end

%Calculate Bc, the field from coils necessary to produce b0 in the
%presence of the geomagnetic dc field.
  bcoil= bdc-bg*cos(phig)*cos(thetag);

%set up phi and theta vectors
  phi= pi/180*[0:dp:360]';
  theta= pi/180*[90:-dt:0];
  li=zeros(length(theta),length(phi));
  f=li;
  na=li;
  mg=li;
  cl=li;
  k=li;
  ca=li;
  mn=li;
  cu=li;
  zn=li;
  br=li;
  co=li;
  fe=li;
  ni=li;

%set up grids with dc and ac values of B
  btotdc= abs(bcoil*cos(phi)*cos(theta)+bg*(cos(phig-phi)*(cos(thetag)...
          .*cos(theta))+ones(length(phi),1)*(sin(thetag).*sin(theta))));
  btotac= abs(bac*cos(phi)*cos(theta));
```

Figure 41 - Continued

```
%set up grid of resonant conditions for diff ions
 bresdc=  conv.\1*freq*(harm.\1);
 bresac=  bdc;
 loac= .6*bresac;
 hiac= 1.4*bresac;
 btotac= (btotac>=loac)&(btotac<=hiac);

 for ion= 1:14
  ion
  for h= 1:4
   go= harm(h)*((btotdc>=.875*bresdc(ion,h))&(btotdc<=1.125*bresdc(ion,h))...
      &btotac)';
   go= harm(h)*.5*(sign(sign(btotdc-.875*bresdc(ion,h))...
              +sign(1.125*bresdc(ion,h)-btotdc)...
              +sign(btotac-.6*bresac(ion,h))...
              +sign(1.4*bresac(ion,h)-btotac)-3.5)+1)';
   harea(ion,h)= sum(cos(theta).*sum(go'/harm(h)));

        if ion==1
            li= li+go;
        elseif ion==2
            mg= mg+go;
        elseif ion==3
            f= f+go;
        elseif ion==4
            ca= ca+go;
        elseif ion==5
            na= na+go;
        elseif ion==6
            mn= mn+go;
        elseif ion==7
            fe= fe+go;
        elseif ion==8
            ni= ni+go;
        elseif ion==9
            co= co+go;
        elseif ion==10
            zn= zn+go;
        elseif ion==11
            cl= cl+go;
```

Figure 41 - Continued

```
            elseif ion==12
                k= k+go;
            elseif ion==13
                cu= cu+go;
            elseif ion==14
                br= br+go;
            end
          end
        end

  area= sum(harea');

  totarea= sum(length(phi)*cos(theta));
  area= 100*area/totarea;
  harea= 100*harea/totarea;
  barea
  pause
  end


%MATLAB subroutine to Plot results from sphere resonance program

%Make plot
  ep=.0001;
  ymax= (fix(max(area)/5)+2)*5;
  y= .96*ymax;
  dy=.035*y;
  av= [0 19 0 ymax];
  axis(av);
  bar(area);

%Put labels on plot
  xlabel('ION')
  ylabel('% TOTAL SURFACE AREA')

  x=15;
  text(x,y,['Ion= ',num2str(rion)])
  y=y-dy;
  text(x,y,['Bdc= ',num2str(bdc),' g'])
  y=y-dy;
```

Figure 41 - Continued

```
text(x,y,['Freq= ',num2str(freq),' Hz'])
y=y-dy;
text(x,y,['Bgeo= ',num2str(bg),' g'])
y=y-dy;
text(x,y,['Phi= ',num2str(phig*180/pi),' deg'])
y=y-dy;
text(x,y,['Theta=',num2str(thetag*180/pi),' deg'])
ydisp= .14;
text(.8,ydisp,'Li')
text(1.8,ydisp,'Mg')
text(2.8,ydisp,'F')
text(3.72,ydisp,'Ca')
text(4.8,ydisp,'Na')
text(5.8,ydisp,'Mn')
text(6.8,ydisp,'Fe')
text(7.8,ydisp,'Ni')
text(8.8,ydisp,'Co')
text(9.8,ydisp,'Zn')
text(10.8,ydisp,'Cl')
text(11.8,ydisp,'K')
text(12.8,ydisp,'Cu')
text(13.8,ydisp,'Br')

dy= ymax/102;
for ion=1:14
  cum=0;
  for h=1:4
   if harea(ion,h)>0
    cum= cum+harea(ion,h);
    if h==1
       if cum+ep < area(ion)
         text((ion-.4),cum-dy,'-')
         text(ion-.1,cum-1.8*dy,'1')
       else
         text(ion-.1,cum+dy/2,'1')
       end
    elseif h==2
       if cum+ep < area(ion)
         text((ion-.4),cum-dy,'-')
         text(ion-.1,cum-1.8*dy,'3')
       else
```

Figure 41 - Continued

```
        text(ion-.1,cum+dy/2,'3')
      end
    elseif h==3
      if cum+ep < area(ion)
        text((ion-.4),cum-dy,'-')
        text(ion-.1,cum-1.8*dy,'5')
      else
        text(ion-.1,cum+dy/2,'5')
      end
    elseif h==4
      text(ion-.2,cum+dy/2,'15')
    end
   end
  end
end
end
```

Figure 41 - Continued